Hochschule für Angewandte Wissenschaften Hamburg
Hamburg University of Applied Sciences

Masterarbeit

Anja Neusser

Development of an emission inventory methodology for air traffic on the basis of a flight schedule scenario for a fast subsequent climate impact analysis

Fakultät Technik und Informatik
Department Fahrzeugtechnik und Flugzeugbau

Faculty of Engineering and Computer Science
Department of Automotive and Aeronautical Engineering

Anja Neusser

Development of an emission inventory methodology for air traffic on the basis of a flight schedule scenario for a fast subsequent climate impact analysis

Masterarbeit eingereicht im Rahmen der Masterprüfung

im Studiengang Flugzeugbau
am Department Fahrzeugtechnik und Flugzeugbau
der Fakultät Technik und Informatik
der Hochschule für Angewandte Wissenschaften Hamburg

in Zusammenarbeit mit:
German Aerospace Center (DLR)
Aircraft Design and System Integration
Hein-Saß-Weg 22
21129 Hamburg

Erstprüfer/in: Prof. Dr. Martin Wagner
Zweitprüfer/in: Dr. Thomas Zill
Industrieller Betreuer: M. Sc. Benjamin Fröhler

Abgabedatum: 04.01.2023

Zusammenfassung

Name des Studierenden: Anja Neusser

Thema der Masterthesis

Entwicklung einer Emissionskataster-Methodik für den Flugverkehr auf Basis eines Flugplans für eine schnelle Analyse der Klimaauswirkungen

Stichworte

Flugzeugemissionen, Strahlungsantrieb, durchschnittliche Temperaturreaktion

Kurzzusammenfassung

Diese Arbeit umfasst ein Konzept, mit dem die Klimaauswirkungen für verschiedene Flugzeugdesigns und -technologien einfach bewertet und verglichen werden können. Dafür fasst die Metrik die zeitlich veränderlichen CO_2 und nicht-CO_2 Emissionen in eine aussagekräftige Größe für eine gesamte Flugzeugflotte zusammen, wobei die höhenabhängigen Einflüsse der NO_x Emissionen und der durch den Flugverkehr verursachten Bewölkung berücksichtigt werden. Außerdem wurde die Metrik weiterentwickelt, damit sie auf einen Flugplan basiert werden kann, indem jede einzelne Flugzeugtrajektorie auf der Großkreisdistanz abgebildet und berechnet werden kann. Letztendlich können auch die Klimaauswirkungen von herkömmlichem Jet A-1 Kerosin mit denen von nachhaltigen Flugkraftstoffen basierend auf einer vereinfachten Flotten-zusammensetzung und Flugnetzstruktur verglichen werden.

Name of Student: Anja Neusser

Title of the paper

Development of emission inventory methodology for air traffic on the basis of flight schedule scenarios for a fast subsequent climate impact analysis

Keywords

Aircraft Emissions, Radiative Forcing, Average Temperature Response

Abstract

This thesis presents an approach to assess and compare the climate impacts of different aircraft design and technology options. For this purpose, the metric condenses the time-varying CO_2 and non-CO_2 effects into a single meaningful quantity for an entire fleet of aircraft, considering the altitude-varying forcings by NO_x emissions and by aviation induced cloudiness. Moreover, this metric has been enhanced by basing it onto a flight schedule by implementing a method of mapping and calculating the trajectory of any individual aircraft mission on a great circle path. Lastly, the climate impact of conventional Jet A-1 fuel, a drop-in fuel blend and a 100% Sustainable Aviation Fuel was analysed and assessed based on a simplified global fleet composition and flight network structure.

Contents

List of Symbols

A	Radiative Efficiency	$\left[\frac{W/m^2}{kg\ Species}\right]$
ATR	Average Temperature Response	$[K]$
d	Distance	$[NM]$
E	Annual Emissions	$[kg]$
E_{ref}	Annual Emissions for a Reference Year	$[kg]$
e	Emissions per Flight	$[kg]$
EI	Emission Index	$\left[\frac{kg\ Species}{kg\ fuel}\right]$
f	Efficacy of the Emission Species	$[-]$
φ	Latitude	[°]
G	Decaying Function	$\left[\frac{W/m^2}{kg\ Species}\right]$
H	Aircraft's Operational Lifetime	$[yrs]$
h	Altitude	$[ft]$
h_0	Initial Cruising Altitude	$[ft]$
h_f	Final Cruising Altitude	$[ft]$
L	Distance flown per Year	$[NM]$
L_{Cruise}	Cruising Distance flown per Year	$[NM]$
L_{ref}	Distance flown for a Reference Year	$[NM]$
λ	Longitude	[°]
r	Devaluation Rate	[%]
RF	Radiative Forcing	$\left[\frac{W}{m^2}\right]$
RF_{ref}	Radiative Forcing for a Reference Year	$\left[\frac{W}{m^2}\right]$
RF^*	Normalized Radiative Forcing	$[-]$
S	Climate Sensitivity Parameter	$[K]$
s	Altitude-dependent Forcing Factor	$[-]$
$\bar{s}$	Mission averaged Forcing Factor	$[-]$
s_{low}	Forcing Factor at h_{low} = 17500ft	$[-]$
σ_H	Input Emission Scenario	$[-]$
t	Time	$[yrs]$
t_{max}	Years under Consideration	$[yrs]$
$t_{Mission}$	Mission Flight Time	$[s]$
τ	Adjustment Time	$[yrs]$
ΔT	Temperature Change	$[K]$
$\Delta T_{sust,H}$	Temperature Change for an arbitrary Aircraft Emission Scenario	$[K]$
U	Number of Missions flown in a Year	$[-]$
W_{fuel}	Total Mission Fuel Consumption	$[kg]$
w	Weighting Function	$[-]$

List of Abbreviations

ACT	Aircraft Climate Tool
AIC	Aviation Induced Cloudiness
AOGCM	Atmosphere – Ocean General Circulation Model
ASM	Available Seat Miles
ATJ	Alcohol-to-Jet
ATR	Average Temperature Response
BTS	Bureau of Transportation Statistics
CHJ	Catalytic Hydrothermolysis Jet
CO_2	Carbon Dioxide
CPACS	Common Parametric Aircraft Configuration Schema
DICE	Dynamic Integrated Model of Climate and Economy
DLR	Deutsches Zentrum für Luft- und Raumfahrt (German Aerospace Center)
EI	Emission Index
EMIC	Earth System Models of Intermediate Complexity
FT	Fischer-Tropsch
FUND	Framework for Uncertainty, Negotiation and Distribution
GCM	Global Climate Model
GTP	Global Temperature Potential
GWP	Global Warming Potential
HEFA	Hydroprocessed Esters and Fatty Acids
HFS	Hydroprocessed Fermented Sugar
HHC	Hydroprocessed Hydrocarbon
H_2O	Water Vapor
IAM	Integrated Assessment Model
ICAO	International Civil Aviation Organization
IPCC	International Panel on Climate Change
LTR	Linear Temperature Response
NO_x	Nitrogen Oxides
PAGE	Policy Analysis of the Greenhouse Effect
ppmv	parts per million by volume
PtL	Power to Liquid
RCE	Remote Component Environment
RF	Radiative Forcing
RH	Relative Humidity
SAF	Sustainable Aviation Fuel
SCM	Simple Climate Model
SIP	Systhesized Iso-Paraffins
SKA	Synthetic Kerosene with Aromatics
SO_x	Sulfur Oxides
SPK	Synthetic Paraffinic Kerosene

List of Figures

List of Tables

1 Introduction

Flying has become indispensable in today's world, and with it emissions from air travel. These emissions from aviation alter the composition of the atmosphere and therefore drive climate change and ozone depletion, which could also lead to an increased ocean temperature, rising sea levels and melting snow and ice (IPCC, 2007).

The aviation sector has grown rapidly in the last decades, from 1960 to 2018. For example, the revenue passenger kilometers increased from 109 to 8269 billion km per year and carbon dioxide (CO_2) emissions increased by a factor of 6.8 (Lee, et al., 2020). Thereby, the growth rate for 2013 to 2018 is significantly higher at 44 Tg CO_2 per year, which is equal to a growth rate of 5% per year. In comparison, the average growth rate for the period 1960 to 2018 was 15 Tg CO_2 per year with an annually averaged growth rate of 2,2% per year between 1970 and 2012 (Lee, et al., 2020). Therefore, approximately 50% of the CO_2 emissions were emitted in the last 20 years and in 2018 the global aviation CO_2 emissions exceeded 1000 million tons per year for the first time. This highlights the growing concern about the environmental impact of aircraft, and the effects are becoming more apparent and also increasingly threatening to social life and well-being.

Not only CO_2 emissions are warming the atmosphere, but also non-CO_2 emissions such as nitrogen oxides (NO_x), water vapor (H_2O), sulfur oxides (SO_x), soot, and the effects of altered cloudiness are responsible for climate change. Total aviation emissions are currently projected to warm the climate three times as much as aviation CO_2 emissions alone, with contrail-cirrus and NO_x driven changes being the largest positive climate forcing next to CO_2. In 2005, it was estimated that the sum of aviation CO_2 and non-CO_2 effects represented approximately 5% of the total anthropogenic forcing. Furthermore, aviation radiative forcing is expected to increase by a factor of three to four between 2000 and 2050. (Grewe, et al., 2009)

As fuel consumptions and aviation emissions have grown at a lesser rate than the revenue passenger kilometers, which are a measure of transport work, aircraft efficiency has increased due to technological changes, larger aircraft sizes, and increased passenger load factor (Lee, et al., 2009). However, these changes will not be sufficient to bring the climate impact in line with the Paris climate targets (ICAO, et al., 2018).

Hence, the aircraft emissions need to be further reduced and metrics are needed to easily assess the impacts of different design and technology options. Therefore, in this thesis an aircraft climate assessment tool for conceptual aircraft design is programmed that expresses the climate impacts in one value. The process from aircraft emissions to climate impacts generally consist of three parts: the Emission Modelling, the Climate Impact Modelling, and the Climate Change Metric. For each part, there are many models of varying complexity, quality, and computational effort. However, for aircraft design studies computationally efficient methods are needed. In a PhD by Dallara (Dallara, 2011) it was investigated which models are best suited for this purpose, and the programmed tool will be based on the formulas used therein. Thereby, the time-varying short- and long-term CO_2 and non-CO_2 effects are condensed into a single, meaningful quantity for a fleet of a particular aircraft. The altitude varying-forcings by NO_x emissions and aviation induced cloudiness are also considered.

As it will be explained in chapter 3.2, the metric developed by Dallara is based only on one typical mission, which is flown a specific number of times per year. To calculate the impacts on more realistic data, this metric needs to be enhanced so that the impacts of any aircraft trajectory can be calculated. This way, the metric can be based on a flight schedule and the climate impacts of different aircraft types can be assessed based on their typical routes.

There are also other possibilities to reduce the impact of the greenhouse gas emissions on the global climate. A promising short-term option introduced to address the aviation's environmental challenges are Sustainable Aviation Fuels (SAF), which are renewable biofuels. SAFs use the same fuel distribution network and the same aircraft engines already in use, as they can be blended with conventional kerosene. Since SAFs reduce CO_2 and soot emissions in particular, they offer a good opportunity to further limit the climate impacts (ICAO, et al., 2018). The effects of SAFs will be integrated in the tool so that the climate impacts of Jet A-1 fuel and SAFs can be easily compared.

This thesis first provides theoretical background information on aircraft emissions and their impact on climate, some general modelling approaches for emission modelling, climate impact modelling and climate change metric, and the different fuel types, Jet A-1 and SAF. Afterwards, the aircraft climate assessment tool is explained, which is based on the methodology developed by Dallara (Dallara, 2011). It condenses CO_2 and non-CO_2 effects into one quantity, taking into account the altitude dependency of NO_x emissions and aviation induced cloudiness. In a next step this metric is enhanced so that it can be based on a flight schedule and the necessary modifications for the different fuel types are implemented. The calculation of climate impacts requires some external input files, a global flight schedule on which the climate assessment tool can be based, and different aircraft types with their calculated trajectories, which are explained in the next chapter. Finally, the results of the interpolations needed to base the tool on a flight schedule and the results of the climate assessment tool are shown and the climate impact of Jet A-1 fuel and SAF are compared.

2 Theoretical Background

As concern about the earth's climate has increased significantly in recent decades, it has become even more important to understand, measure, and mitigate the environmental impacts of aviation. The interest and the assessments of aviation's impact on climate began already in the late 1990s, culminating with the IPCC Special Report, Aviation and the Global Atmosphere (IPCC, et al., 1999), and many reports and research programs have followed since (Dallara, 2011).

Aircraft affect the climate by emitting gases and particles directly into the troposphere and lower stratosphere, which alters the concentration of the greenhouse gases and triggers the formation of contrails and cirrus clouds ((IPCC), 1999). These greenhouse gases are responsible for keeping the earth warmer than it would be without them: The sun's energy reaches the earth mainly as light, but that same energy leaves the earth as infrared radiation, which is perceived as heat. The greenhouse gases now reflect this infrared radiation, so that some of the heat returns to the earth's surface. Without this so-called 'greenhouse effect' the earth would be too cold to live on. However, if the concentration of the greenhouse gases increases, the strength of the greenhouse effect also increases, causing more heat to be trapped in the earth's atmosphere and therefore warming of the earth's surface. (Chandler, 2020)

In order that the effects of the future aircraft's emissions can be determined, models which estimate the climate impacts are needed. So, this chapter first discusses the effects of aircraft emissions on climate and presents some general modelling approaches afterwards. Then the great circle distance is explained, which is needed for the first step to base the models on a flight schedule. Finally, different possible fuel types for the reduction of the climate impacts are considered.

2.1 Aircraft Emissions and Climate

In order to model the climate impacts, it is important to understand the relationship between the aircraft emissions and the climate impacts. This relationship can be seen in Figure 1.

Figure 1: Relationship between aircraft emissions and climate impacts (Lee, et al., 2009)

Aircraft engines are powered by the combustion of hydrocarbon fuel, which leads to combustion products. For an ideal combustion these combustion products are: CO_2, H_2O, sulfur dioxide (SO_2), nitrogen (N_2) and dioxygen (O_2). But for a real combustion additionally to the ideal combustion products trace amounts of unburned hydrocarbons (UHC), carbon monoxide (CO), soot, NO_x and SO_x are also released (Lee, et al., 2009). Of these combustion products, CO_2, H_2O, NO_x, SO_x

and soot each alter the concentration of greenhouse gases and particles. How each of these products affect the climate is presented in the next sections (see chapter 2.1.1 to 2.1.6). Altering the concentration of the greenhouse gases and particles changes the balance between incoming solar and outgoing infrared radiation, resulting in Radiative Forcing (RF). This RF influences many climate properties such as changes in temperature, sea level, ice or snow cover, precipitation, and extreme weather events (Lee, et al., 2009). These climate changes then affect many systems including the agriculture and forestry, ecosystems, energy production and consumption, social effects and the availability of food, water, and energy (Lee, et al., 2009). Eventually, these climate impacts can be translated into damages to societal welfare and costs.

To limit these impacts and damages due to climate change, the environmental impacts of aircraft must be reduced. To do this, the impacts of each direct emissions must be known and a framework for quantifying and comparing the climate performance of future aircraft configurations must be developed.

2.1.1 Carbon Dioxide (CO_2)

Carbon dioxide is a greenhouse gas, an unavoidable end product of the hydrocarbon fuel combustion process, and its behavior in the atmosphere is well understood. Thus, CO_2 directly affects the climate change, and the impact simply depends on its atmospheric concentration. CO_2 molecules absorb infrared radiation emitted from the earth's surface and lower atmosphere, so an increase in CO_2 concentration leads to warming and increased surface temperatures. ((IPCC), 1999)

CO_2 has a long residence time in the atmosphere. Following a pulse of CO_2 emissions, approximately 50% of the emissions remain in the atmosphere after 30 years and 30% after 200 years, according to a model from IPCC (IPCC, 2007)(Dallara, 2011). Because of its long residence time, it is well mixed throughout the atmosphere. Therefore, CO_2 emissions from aircraft are indistinguishable from the same quantity of CO_2 emitted from other sources, and the impact on climate is the same ((IPCC), 1999).

2.1.2 Nitrogen Oxides (NO_x)

Nitrogen oxide refers to nitrogen monoxide (NO) and nitrogen dioxide (NO_2). They form in the primary zone of a gas turbine combustor, where the gas temperatures are highest, and are therefore also an end product of the combustion process (Heywood, et al., 1973). NO_x emissions indirectly affect the climate change through chemical reactions in the atmosphere that alter the concentration of the greenhouse gases ozone (O_3) and methane (CH_4) (Dallara, 2011). If the concentration of either of these greenhouse gases increases, the RF is positive and vice versa. Therefore, the RF caused by NO_x emissions is composed of three components: First, the production of tropospheric O_3, which causes a warming effect; second, the longer-term reduction in ambient CH_4, which causes a cooling effect; and third, the longer-term small decrease in O_3, which also causes a cooling effect (Lee, et al., 2009).

The tropospheric ozone produced has an atmospheric lifetime of several weeks, and the production rate depends in particular on location and altitude. The production rate of NO_x emissions to O_3 is most effective in the mid-latitude upper troposphere and lower stratosphere. At higher altitudes, in the stratosphere, NO_x emissions transition from net O_3 production to O_3 destruction. This is thought to occur at an altitude of about 16 km or 52000 feet. Because of the short atmospheric lifetime, short-term ozone production is concentrated near flight routes. The longer-term destruction of CH_4 and the longer-term decrease of O_3 are well mixed throughout the atmosphere due to their long atmospheric lifetimes. (Dallara, 2011)

It should be noted that NO_x emissions also affect climate through the formation of particular nitrate, but since the resulting negative RF is highly uncertain, it is not considered in this thesis (Dallara, 2011).

2.1.3 Water Vapor (H_2O)

As with carbon dioxide, water vapor is an end product of the hydrocarbon fuel combustion process and a greenhouse gas. An increase in the concentration of H_2O leads to warming of the earth's surface and thus to increased surface temperatures. However, the direct effect of H_2O is small compared to other aircraft emissions such as CO_2 or NO_x. This is because H_2O has a short atmospheric lifetime of only one to two weeks in the troposphere ((IPCC), 1999). In the stratosphere, H_2O has a longer lifetime, ranging from months to years, and can build up to larger concentrations, which can therefore have a greater impact on climate. Water vapor also plays a role in the formation of aerosol particles and clouds, as it will be discussed in chapter 2.1.6.

2.1.4 Sulfur Oxides (SO_x)

Sulfur oxides refer to SO_2, sulfur trioxide (SO_3) and sulfuric acid (H_2SO_4) and are formed through oxidation processes of the sulfur contained in the fuel in the combustor and engine (Dallara, 2011). Also, liquid particles are formed by homogenous nucleation and are growing in size due to coagulation and condensation processes. These processes lead to an increased sulfate aerosol number, which scatter incoming solar radiation and absorb very little outgoing infrared radiation, resulting in a cooling impact (Dallara, 2011). Because of the short residence times of SO_x of up to four days, the increase in sulfate aerosol number is concentrated only near flight routes, and the direct impact of SO_x emissions is small. Nevertheless, they also play a role in the formation of contrails and cirrus clouds.

2.1.5 Soot

Carbon soot particles form in combustor of turbine engines, with emission rates depending on operating conditions and combustor design, but generally increasing with throttle setting (Dopelheuer, et al., 1998). Soot absorbs solar radiation and causes a warming effect. Because of its short atmospheric lifetime of about one week, its direct impact on climate is small, as with water vapor and sulfur oxides, but it also plays a role in the formation of contrail and cirrus clouds.

2.1.6 Aviation Induced Cloudiness (AIC)

As already discussed, water vapor, sulfur oxides, and soot have small direct climate impacts mainly because of their short residence times, but they play a role in the formation of contrail and cirrus clouds, collectively referred to as Aviation Induced Cloudiness (AIC). AIC includes the formation of linear contrails, aged contrail-cirrus clouds, and soot-cirrus clouds. These clouds trap the outgoing longwave radiation emitted by the earth and atmosphere, causing a warming effect that is partially compensated by their reflection of incoming solar radiation, resulting in a cooling effect (Stuber, et al., 2006). On average, the longwave, warming effect predominates, so the net RF is expected to be positive, leading to a temperature increase. However, quantifying RF for contrail-cirrus and soot-cirrus clouds is subject to large uncertainties because cirrus modelling and prediction are in their beginning stages and are difficult to define. There are also large uncertainties in estimating the RF of contrails that depend on models of contrail coverage and optical depth, which are not as accurate and need to be revised as more knowledge about contrail RF is gained (Dallara, 2011).

Contrails form when hot and humid exhaust gases mix with cold, dry ambient air. This increases the relative humidity (RH) and possibly leads to water saturation if the ambient air is below a critical temperature Tc, which is given by the Schmidt-Appleman criterion and depends on ambient pressure, humidity and temperature as well as engine-dependent parameters. If the ambient air is dry (RH below saturation over an ice surface), the ice particles that form in the contrail evoporate, the contrails are short-lived, and dissappear after seconds to minutes. However, if the ambient humidity is higher than the saturation humidity over ice surfaces, the air masses become ice-supersaturated, and the ice particles in the contrails grow by depositing water vapor molecules from the ambient air, resulting in contrails that persist as long as the ambient air in which the contrail forms remains ice-supersaturated (often several hours). (Schumann, 2005)

But the RF of contrails also changes, among others, with season and time. A study by Stuber et al. (Stuber, et al., 2006) revealed that night-time flights (between 18:00 and 06:00 GMT) are responsible for most of the daily RF: Although they account for only 25% of the air traffic, they contribute to 60 to 80% of the net RF. In addition, contrails are twice as likely to form in the winter months as in the summer months and contribute 50% of the annual mean RF, even though winter air traffic accounts for only 22% of air traffic (Stuber, et al., 2006). The AIC RF also shows a dependence on altitude. Most contrails occur at an altitude of about 10 km, which is also where most of the air traffic occurs, but there is also a seasonal shift in coverage to lower altitudes in the winter months (Radel, et al., 2008).

Cirrus clouds can form via two processes: First, by the spreading of linear contrails, known as contrail-cirrus; second, by combustion particles contained in the engine exhaust (mainly soot and small volatile particles) acting as condensation nuclei, known as soot-cirrus (Dallara, 2011). Although highly uncertain, it is estimated that contrail-cirrus increases contrail coverage by a factor of 1.8, while the uncertainties for soot-cirrus are even larger and it is currently unknown whether the net soot-cirrus RF is positive or negative (Dallara, 2011). Nevertheless, these impacts are included in this thesis.

2.2 General Modelling Approaches for Aircraft Climate Assessment

In the last section the relationship between aircraft emissions and climate impacts and how each of the combustion products contributes to climate change was shown. These relationships and the resulting climate impacts must now be modelled.

Generally, the process for determining climate impacts resulting from aircraft emissions is divided into three sections: First, Emission Modelling; second, Climate Impact Modelling; and third, Climate Change Metric (Dallara, 2011). This process and possible metrics for each section can be seen in Figure 2 and are discussed in more detail below. Out of these an appropriate metric will be selected for each section for an aircraft climate assessment for conceptual design, as will be shown in chapter 3.2.

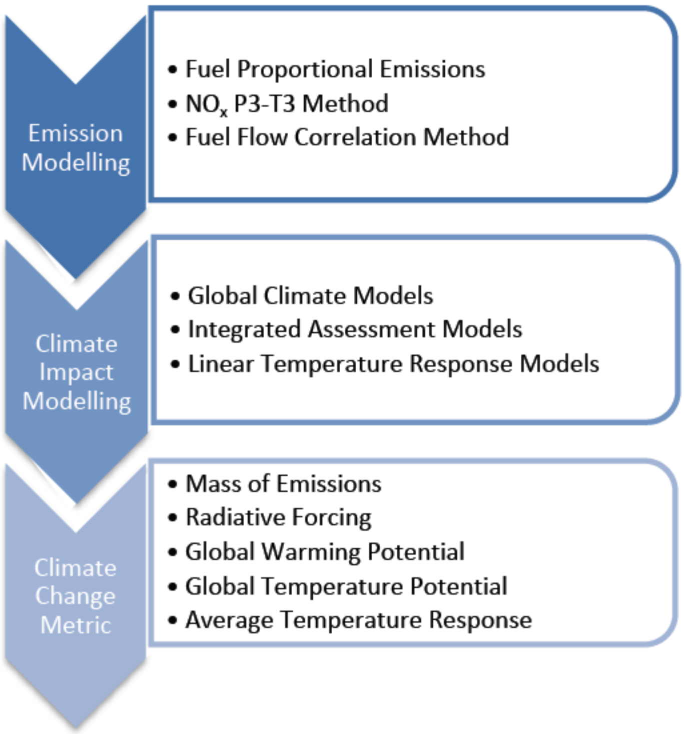

Figure 2: General modelling approach – Possible metrics

2.2.1 Emissions Modelling

In order to determine the climate impact, aircraft emissions must be modelled over the entire flight mission. This can be done by different models with varying complexity. For the conceptual aircraft design, computationally efficient methods are needed, which is why the Fuel Proportional Emissions approach, the NO_x P3-T3 methods and the Fuel Flow Correlation Methods are presented below.

Fuel Proportional Emissions:

The Fuel Proportional Emissions can be calculated very easily, as the total emissions are simply proportional to fuel consumption. The more fuel is consumed, the higher the total emissions. Of the direct emissions presented in chapter 2.1, the emissions of the species CO_2, H_2O and SO_x are proportional to the fuel consumption. The mass of the different species released per fuel burned is determined based on the composition of the fuel. The emission rates are described by the emission indices (EIs), which are constant between different designs and under all operating conditions. (Dallara, 2011)

NO_x P3-T3 Method:

Unlike the EI of CO_2, H_2O, and SO_x, the EI of NO_x varies and depends on engine design characteristics and operating conditions such as throttle setting, flight speed, and altitude. Since the formation of NO_x depends on transient physical processes and non-equilibrium chemical reactions, analytical modelling is difficult. Therefore, empirical methods have been developed that simplify emission rates and are based on experimental data (Dallara, 2011). Studies by Lefebvre have shown that the following variables are proportional to EI and therefore have the greatest impact on the NO_x emissions: The mean residence time in the combustor zone, which depends on combustor length and flow velocity; chemical reaction rates, which depend on combustor temperature and pressure; and mixing rates, which depend on the pressure drop through the combustor (Lefebvre, 1984).

For a fixed combustor design, the EI can be made dependent only on the combustor inlet temperature and pressure, which are referred as P3-T3 models. The values of the constants for the combustor design are determined by regression analysis of emissions data or by full-scale engine test (Dallara, 2011). They are valid only for that combustor design and lose accuracy when applied more generally. Therefore, various P3-T3 models for different combustor designs exist.

Fuel Flow Correlation Methods:

In order to apply the P3-T3 methods just explained, proprietary information or accurate engine designs are required, as they rely on knowledge of inlet temperature and pressure. However, since this information might not always be available, simpler methods have been developed, such as the fuel flow correlation methods. The most commonly used methods are those developed by

Boeing (DuBois, et al., 2006) and the German Aerospace Center (DLR) (Deidewig, et al., 1996). For the calculation of the NO_x engine emissions, these methods rely on the following input data: The actual engine fuel flow, the thrust-dependent reference EIs, the fuel flows for sea-level static conditions found in the ICAO engine emission databank, the actual ambient conditions including temperature and pressure, and the flight speed (Schaefer, et al., 2013). Therefore, no internal engine parameters are required since these methods are based on the assumption that in-flight EIs can be transferred to EIs at reference sea-level static conditions and vice versa. For the calculation of the EIs, the in-flight fuel flow must first be reduced to the reference conditions, and then the reference EI is calculated based on the reference fuel flow. In the last step, the calculated reference EI is transferred back to the actual in-flight EI (Schaefer, et al., 2013). Both, the DLR and Boeing fuel flow correlation methods are based on the same principle just mentioned but differ in the input parameters required: The Boeing method needs ambient air pressure and Mach number as input, the DLR method requires total pressure and temperature. However, the simpler method is also associated with less accuracy. The Boeing and DLR methods are expected to predict the NO_x emissions during cruise flight with an average accuracy of +/- 10% ((IPCC), 1999).

Fuel flow correlation methods for cruise soot EI are also available but calculating soot emissions is more difficult because reference data for soot EI are not available from the ICAO database (Schaefer, et al., 2013). Therefore, since the soot climate impacts are small compared to the other species' impacts, soot EI is usually assumed to be constant across all operating conditions.

2.2.2 Climate Impact Modelling

After the emission modelling is implemented, the next step is to model the climate impact. Again, there are many different models for predicting climate impacts, varying in complexity, quality, and computational effort. Three different types of models, Global Climate Models (GCMs), Integrated Assessment Models (IAMs), and Linear Temperature Response Models (LTRs), and their respective characteristics are presented below.

Global Climate Models:

The GCMs are complex mathematical representations of the major components of the climate system, such as the atmosphere, land surface, ocean, sea ice, and their interactions. These models predict the impact of anthropogenic emissions on climate and several models with various complexities have been developed (GFDL). The simplest version of the GCMs is called Simple Climate Models (SCMs). They represent the ocean-atmosphere system as a set of global or hemispheric boxes and predict global surface temperature with energy balance equations, a specified value of climate sensitivity, and a basic representation of ocean heat uptake (IPCC, 2007). More complex GCMs are the Earth System Models of Intermediate Complexity (EMICs). They include some dynamics of atmospheric and oceanic circulations and can include models of biochemical cycles. However, they often have a lower spatial resolution (IPCC, 2007). The most complex models are the Atmosphere – Ocean General Circulation Models (AOGCMs). They include dynamical processes that describe atmospheric, oceanic, and land surface processes, as well as sea, ice, and other components. Over 20 models from different centers were applied for climate simulations in the fourth IPCC assessment report. The models have improved considerably in recent decades, and the models are believed to provide reliable estimates of future climate change (IPCC, 2007). However, GCMs are very complex and computationally intensive, requiring a computational time of weeks or months on a high-performance computer (Lim, et al., 2006).

Integrated Assessment Models:

Due to the high complexity of the GCMs, simplified climate response models have been developed, which reflect the main characteristic responses of the GCMs. One of these simplified models are the IAMs. IAMs combine climate processes, economic growth, and feedbacks between climate and the global economy into a single modelling framework. However, they are based on less detailed representations of the underlying climatic and economic systems. The most commonly used IAMs are the FUND (Framework for Uncertainty, Negotiation and Distribution) (Tol, 2006), DICE (Dynamic Integrated Model of Climate and Economy) (Nordhaus, 1992), and PAGE (Policy Analysis of the Greenhouse Effect) (Hope, et al., 1993) models. They convert the emissions into changes in greenhouse gas concentrations in the atmosphere, changes in temperature, and ultimately into economic damages. Converting economic damages over time into a single value requires judgement about how to discount them, and each of the models mentioned calculates slightly differently how emissions lead to economic damages. To translate climate changes into net economic losses, damage functions are used. These functions are based on the best judgement of IAM modellers, but these representations are incomplete and highly uncertain. IAMs are used primarily for climate change policy decisions. (United States Government, 2010)

Linear Temperature Response Models:

LTR models are simplified representations of the climate system and are based on the results of the GCMs. Unlike GCMs, the RF or temperature change is not calculated on a time-varying three-dimensional grid, but as globally and annually averaged values (Dallara, 2011). Linearized response functions based on carbon cycles and climate models have been developed in several research studies. For example, Sausen et al. (Sausen, et al., 2000) developed a linear model based on the response functions formulated by Hasselmann et al. (Hasselmann, et al., 1997) to analyze the impacts of CO_2 and NO_x emissions. One of the most recent LTR models is the DLR's in-house software AirClim, developed by Grewe et al. (Grewe, et al., 2008), which calculates the impacts for four latitude regions and six pressure (altitude) levels (Wuebbles, et al., 2009). On the one hand, the LTR models are less accurate than the GCM. In addition, the choice of the model needs to be further evaluated because the simplified models can only be as good as the scientific models on which they are based, and therefore the LTR models need to be updated as newer versions of the carbon cycle and climate models are developed. On the other hand, LTR models have the major advantage that they significantly reduce the complexity and computational costs of determining the climate impacts of aviation and are therefore a useful tool for conceptual design optimization studies where many emission scenarios must be considered (Wuebbles, et al., 2009). They are also transparent and have the flexibility to incorporate new knowledge.

2.2.3 Climate Change Metric

Once the climate impacts have been modelled, a method is needed to quantify these impacts from climate change. Several different metrics have been developed for this purpose, of which five common ones are identified: Mass of Emissions, Radiative Forcing, Global Warming Potential (GWP), Global Temperature Potential (GTP) and Average Temperature Response (ATR) are described below.

Mass of Emissions:

The metric mass of emissions quantifies the climate impacts by calculating the total mass of each emission. This metric is mostly used for CO_2 because its impacts are well understood, it has a long atmospheric lifetime, and total masses can be quickly compared. However, for many different types of species with different lifetimes and intensities, this metric is not useful. (Dallara, 2011)

Radiative Forcing:

The RF quantifies the change in net irradiance at the tropopause due to an alteration in atmospheric concentration of the greenhouse gases or particles. Therefore, it does not directly measure the change in climate behavior but quantifies the change in energy that leads to changes in climate properties (Dallara, 2011). RF is usually a snapshot at a particular point in time, but an integral of RF over a period of time or its mean value can also be used (IPCC, 2009). The RF could also be linearly related to the change in global equilibrium mean surface temperature under certain circumstances.

The advantages of RF are that it requires little additional information and is well suited for comparing the effects of different radiation sources. Nevertheless, more attention needs to be paid to the use of RF in the evaluation of sustainable agents and to the development of individual or cumulative systems for RF. (IPCC, 2009)

Global Warming Potential:

The GWP compares the integrated RF of a pulse emission of radiatively active species or its precursors for a specific time horizon and is therefore based on the concept of RF (Fuglestvedt, et al., 2003). It is a relative measure and defined as the time integrated commitment to climate RF from the instantaneous release of a fixed amount of a trace gas expressed relative to the same fixed amount of the reference gas CO_2 (EPA, 2020). The larger the GWP, the more a given gas warms the earth relative to CO_2 over a given time period. Various time horizons can be used, but the most common is 100 years, as this is the time frame specified in the Kyoto Protocol (EPA, 2020).

A negative aspect of the GWP is that it may not be properly understood as an integrated RF over a chosen time horizon, as the name may lead to the conclusion that it expresses equivalence in terms of the contribution of different gases to temperature increase. In addition, because of the different lifetimes of greenhouse gases, it does not give a clear indication of the effect of pulse emissions on temperature. Although a strong greenhouse gas with a short lifetime could have the same GWP as a weaker greenhouse gas with a longer lifetime, identical (in mass terms) pulse emissions from the two gases at a given time could cause a different temperature change. Moreover, the GWP is not often applied to the climate impact of very short-lived greenhouse gases due to the inhomogeneous concentration changes. Nevertheless, it is widely used, mainly because of the simplicity of its definition, the small number of input parameters required, and the relative ease of calculation. (Shine, et al., 2005)

Global Temperature Potential:

The GTP is the ratio of changes in global mean temperature resulting from emissions of CO_2 and other species of the same mass at a given time t (Shine, et al., 2005). Therefore, the GTP is an extension of the GWP, as the GTP explicitly represents the impact of an emission change on temperature. However, unlike the GWP, which integrates the RF along a time path, the GTP focuses on a specific point in time and indicates the temperature effect at that point in time relative to CO_2 (IPCC, 2009). There are two different types of GTPs: the GTP_P is based on the temperature effect of pulse emissions and the GTP_s on the effect of persistent emission changes.

The drawbacks of the GTP are that the simple analytical expressions derived for the GTP_P perform poorly compared to an energy balance model and are therefore not suitable for policy consideration, but rather for comparing the temperature impact of pulse emissions. It could also be calculated with any other more detailed climate model. However, the results are strongly influenced by specific model assumptions and uncertainties. The advantages of the GTP are similar to those of the GWP, such as the transparent formulation and the reliance on relatively few parameters and required inputs. However, the GTP has the further advantage of representing an actual climate impact. Furthermore, the climate impact of short-lived greenhouse gases could also be studied, but since the GTP for such gases would be very small for any time horizon beyond a year, this is often not considered. (Shine, et al., 2005)

Average Temperature Response:

The ATR is based on temperature change and therefore indicates a change in climate behavior directly, but also with more uncertainty. To calculate the ATR, the time-varying global mean temperature change caused by H years of continuous operation and subsequent zero emissions is first calculated. For the parameter H typical lifetime values of aircraft, about 25 to 35 years, should be used. This temperature change is then weighted, integrated, and divided by H to obtain an average temperature response. Weighting functions can include integration windows, which only consider impacts within a specified time frame, and discounted metrics, which weight future impacts with an exponentially decaying function. The purpose of the ATR metric is to quantify, for a given aircraft, the climate impacts that result from emissions during operation, as well as the climate impacts that result from perturbations that remain in the earth-atmosphere system after the aircraft's operating lifetime has ended (Dallara, 2011).

2.2.4 Desired Metric Properties

Before a metric can be selected, the desired properties of the metric must be determined. Some of these properties are explained below for the climate assessment for conceptual aircraft design.

The first question is what quantity, mass of emissions, RF, or temperature change, should be measured. The mass of emissions is often not useful because it is usually used for CO_2 emissions and there is a wide variety of species with different lifetimes and impacts. Therefore, the same mass of, for example, CO_2 and NO_x emissions, will have different impacts on climate. RF does not directly measure the change in climate behavior as does the temperature change, so the temperature change is often more relevant than the RF. However, the greater relevance of the temperature change is also accompanied by greater scientific uncertainty compared to RF. It is also important to consider that RF is mostly a snapshot at a single point in time and time-integrated metrics are rarely used. However, both RF and temperature change could be used as measured quantity.

Second, the emission case must be considered. Different time horizons can be used for the GWP, with 100 years being the most commonly used. But there is a difference between the sustained 100 years GWP, where the GWP is calculated assuming emissions for 100 years, and the pulse 100 years GWP, where the GWP is calculated assuming emissions for only one year and zero emissions thereafter. However, for comparing different aircraft designs and technology options, it may be more favorable to compute climate impacts using an emission case that is representative of the likely operation of the aircraft (Dallara, 2011). Since the operational lifetime of aircraft typically varies between 25 and 35 years, a suitable emission case might be 30 years of continuous operation, resulting in constant emissions, and zero emissions after the aircraft is retired from service.

The metrics can either be a snapshot at a point in time, as is mostly the case with RF and GTP, or an integrated impact, such as GWP. Snapshot metrics can be practically used to quantify, for instance, a climate target or the climate impacts at the end of an aircraft's operational lifetime. However, in comparative studies, snapshot metrics are very sensitive to timing. Integrated impacts metrics are less sensitive to timing and lifetime as they quantify mean impacts over an integration period. Therefore, lifetime-averaged metrics are preferred for comparing aircraft designs because components of RF and temperature vary annually. (Dallara, 2011)

The next aspect to consider is temporal weighting, where the relative importance of short-lived and long-lived impacts can be altered. Weighting factors and integration windows are mostly used. Weighting factors specify the relative importance of present and future impacts. Integration windows also influence the importance between the two by setting a maximum time horizon for the inclusion of impacts. A weighting function can be used to combine the two aspects of weighting factors and integration windows, and it can be useful for the user to be able to specify which impacts he wants to focus on. (Dallara, 2011)

2.3 Great Circle Distance

In order to assess the impacts based on a global flight network, the distance between the city pairs specified in the flight schedule must be calculated. For this purpose, the great circle distance is used. A great circle is defined as the line of intersection of a sphere and a plane through the center of the sphere as can be seen on the left side in Figure 3 (Lufthansa Aviation Training, 2016). For navigational purposes, it is common to refer to a great circle, even if only an arc of that great circle is considered. Therefore, the red, solid line on both sides in Figure 3 represents a great circle.

If there are two antipodal locations on the earth, for example the poles, then any desired number of great circles can be passed through these two points. However, all other locations can only be connected by one great circle, since there is only one plane that passes through both locations and the center of the earth. The resulting great circle represents the shortest connection and therefore also the shortest flight path between two locations on the earth's surface.

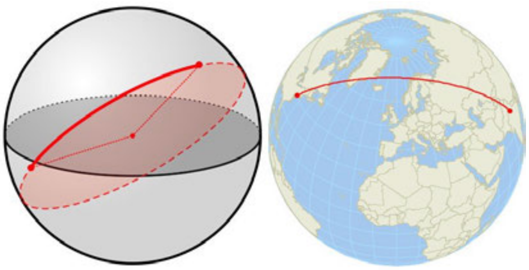

Figure 3: Great circle distance (Lufthansa Aviation Training, 2016)

2.4 Fuel Types

The modelling approaches described in section 2.2 also offer the possibility to assess the climate impact of different energy carriers. Nowadays, aircraft are mostly powered by liquid aviation fuel such as Jet A/A-1, which is mainly produced from fossil fuel sources. However, due to increasing annual travel growth, emissions are expected to rise. Therefore, measures need to be taken to reduce the impact of aviation emissions on local air quality and to align climate impacts with the Paris climate targets (ICAO, et al., 2018). Possibilities to reduce the impact of the greenhouse gas emissions on the global climate include 'zero-emission' options or switching the energy carrier to renewably generated variants. However, the proposed 'zero-emission' options such as electrification, direct usage of hydrogen (H_2), or cryogenic fuels are not relevant options in the short-term because they are not yet technically mature, have a limited range, and require new energy supply networks (Stephen, et al., 2022). Furthermore, the gas turbines in use today are reliable, economically competitive, have a great power-to-weight ratio, and an excellent range due to the high energy density of liquids (ICAO, et al., 2018). Also, the current and near-term aircraft, which will remain in operation for decades, are designed around aviation kerosene such as Jet A/A-1. Regarding those aspects, switching the energy carrier to renewably produced variants such as SAF is a promising short-term option. In the following, only the short-term option is considered and the commonly used aviation jet fuel and the renewable product variant SAF are explained.

2.4.1 Aviation Jet Fuel

Aviation jet fuel is considered the optimum fuel for most modern aircraft. It consists of light petroleum that goes through modern refinery processes such as distillation, hydrotreatment and catalytic reforming. After refining, small amounts of additives are added to prevent, for example, the formation of deposits in the turbine, electrical charging of the fuel or uncontrolled ignition of the fuel. However, the exact composition varies greatly depending on the petroleum source and the manufacturing process, so it is not possible to define jet fuel as a ratio of specific hydrocarbons. For this reason, jet fuel is defined as a performance specification rather than a chemical compound. (Ariyan)

The most commonly used kerosene-based fuels are Jet A and Jet A-1 fuels. They are essentially the same product, with the main difference being the freezing point, which is <-40°C for Jet A and <-47°C for Jet A-1, as well as some other minor differences. Jet A-1 Is primarily used around the world, while Jet A is only available in the United States and in Canada, although Canada also mainly uses Jet A-1. (Arnot, 2019)

Due to the high consumption of aviation jet fuel, the commercial aviation industry has set strict safety and quality standards for this fuel. For example, the volatility, the combustion, the thermal stability, the flash and freezing point, the density, the lubricity, the composition, and other parameters are strictly defined for Jet A/A-1 fuel (Ariyan). However, due to the huge growth of the aviation sector and the expected further growth, the energy demand and the emissions of aviation jet fuels are also increasing, so research has shifted from the commonly used jet fuel to renewable production options such as SAF.

2.4.2 Sustainable Aviation Fuel (SAF)

The renewable production variant SAF is produced from a variety of feedstocks and waste and is often referred to as ‘next generation biofuels’ or ‘advanced biofuels’. Nevertheless, SAFs are different from standard biofuels. The term ‘biofuels’ refers only to fuels produced from biological resources, the production of which need not be sustainable and may cause additional environmental damage, such as competition with food and water and deforestation. In contrast, SAFs may only be produced from feedstocks that can be grown or produced without the risk of unintended environmental and social damage. SAFs use the same fuel distribution network and the same aircraft engines already in use, as they can be blended with conventional kerosene. (Aviation Benefits beyond Borders)

The amount of CO_2 produced when SAF is burned is comparable to the amount produced when conventional aircraft fuel is used. However, compared on a life cycle basis, SAF shows great CO_2 emission reductions: when municipal solid waste or industrial waste gases are used to produce SAF, the reductions result from the multiple use of fossil carbon, and when biomass is used to produce SAF, the reductions result from the plants absorbing CO_2 during growth (ICAO, et al., 2018). The amount of CO_2 absorbed during the plant growth is approximately equivalent to the amount of CO_2 produced, when the fuel is burned in the engine. With this consideration, SAFs can be identified as carbon neutral. However, this does not consider that CO_2 is also emitted, for example, during the production and the transportation process of SAF. Therefore, the emission reductions vary depending on the feedstocks used, the conversion process and the logistics. Nevertheless, even if all these processes are considered, SAFs can still achieve significant reductions, up to 80%, in the overall CO_2 lifecycle emissions (Stephen, et al., 2022). SAF also reduces the soot emissions. The reduced number of soot particles emitted also influences the contrail properties.

Figure 4 illustrates the process for the production of SAF. The production generally consists of the feedstock, its pretreatment, which creates the conditions for the conversion process, and the conversion process, which transform the pretreated feedstock into aviation fuel (ICAO, et al., 2018).

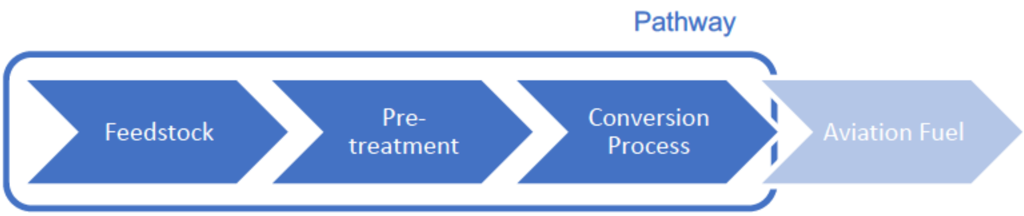

Figure 4: SAF pathway concept (ICAO, et al., 2018)

Currently SAFs can be produced through seven internationally approved conversion processes, which can be seen in Table 1. The best known and most used processes for the production of SAF are the Hydroprocessed Esters and Fatty Acids (HEFA) process and the Fischer-Tropsch (FT) process. In the HEFA process, oils are hydrotreated, i.e., the oils are reacted with hydrogen and catalysts under high pressure to produce aviation fuel (ICAO, et al., 2018). For the FT process, the solid biomass if first gasified, producing a mixture of gases, mainly CO and H_2. This mixture is purified and then synthesized into a mixture of liquids and gases, which contain hydrocarbon chains of different sizes (ICAO, et al., 2018). This catalytic reaction is called FT process, and products with similar characteristics to aviation fuel can be obtained. It is expected that additional process pathways are qualified in the coming years, which are shown in Table 1 as well. The feedstocks that can be used for these conversion processes are mostly municipal solid waste such as product packaging, clothing, and food waste; cellulosic waste such as excess wood and forestry residues; waste cooking oil; and plants such as camelina, jatropha, halophytes, and algae (ICAO, et al., 2018). There are also non-biological SAFs, such as 'power-to-liquid' (PtL) or 'sun-to-liquid'. PtL uses renewable energy to produce green hydrogen through electrolysis, which is then synthesized with carbon feedstock in the FT process to produce SAF. In the 'Sun-to-liquid' process concentrated sunlight is used to produce a so-called synthesis gas - a mixture of hydrogen and carbon monoxide - from water and CO_2 through a thermochemical redox reaction (ATAG, 2017). This synthesis gas is then transformed in SAF via the FT process.

The synthesized components may lack certain chemical components required to meet the strict quality safety standards for aviation fuel, such as aromatics, or may have other characteristics outside the acceptable ranges. Therefore, to date, SAFs may only be used in commercial aviation if they are blended up to approved limits (Kramer, et al., 2022). This so called 'drop-in jet fuel blend' is a substitute for conventional jet fuel that is completely interchangeable and compatible with conventional jet fuel. Therefore, it can be handled in the same way as any other aviation fuel and no adaptions to the engine fuel system and the fuel distribution network are necessary (ICAO, et al., 2018). The blending limit varies between 10% and 50% depending on the process pathway, as can be seen in Table 1. Setting a blend limit ensures that the blended fuel is a true drop-in fuel and does not require additional infrastructure for its use (BP, 2022). Additional testing and evaluation are required before it can be assured that blends with higher blend limits are still drop-in capable.

Nevertheless, the goal is to achieve 100% utilization of SAF. These fuels must be appropriately developed, assessed, and deployed. There are two options that could be considered in short-term and implemented within the next two years: First, all Jet A/ A-1 fuel properties are replicated in a single fuel, or second, the properties are replicated in a blended fuel, and as many synthetic blends as necessary could be used to replace the properties of Jet A/A-1. A third option, which requires more time, could be to redefine the jet fuel requirements, since not all current Jet A/ A-1 specifications may be necessary for engine and aircraft performance. Changing, removing, or adding requirements could facilitate SAF production. Table 1 also shows the ability of the process pathways to be used as 100% drop-in fuel in the future. Here, the green box indicates that it is identical to Jet A/ A-1, meaning that it is compatible with the current infrastructure and aircraft engines and therefore 100% SAF could be achieved with a single fuel (option 1). The yellow box means it is similar, but not identical, to Jet A/ A-1, allowing it to be used in some existing aircraft, but would require a modification to existing specifications and infrastructure. The red box signals that it is not comparable to Jet A/ A-1 and cannot be used as stand-alone jet fuel in the current infrastructure or equipment. However, 100% SAF could be reached if the blend components of, for example, the yellow and the red boxes are mixed (option 2). (Kramer, et al., 2022)

Table 1: SAF process pathways, their blending limit, and their ability to be future 100% Drop-In (Kramer, et al., 2022)

Sustainable Aviation Fuel			
Process Pathway	**Qualified Today**	**Blend Limit (%)**	**Future 100% Drop-In**
FT-SPK, Fischer-Tropsch Synthetic Paraffinic Kerosene	yes	50	no
HEFA-SPK, Hydroprocessed Esters and Fatty Acids Synthetic Paraffinic Kerosene	yes	50	no
HFS-SIP, Hydroprocessed Fermented Sugar Synthesized Iso-Paraffins	yes	10	no
FT-SKA, Fisher-Tropsch Synthetic Kerosene with Aromatics	yes	50	yes
ATJ-SPK, Alcohol-to-Jet Synthetic Paraffinic Kerosene	yes	50	no no
CHJ, Catalytic Hydrothermolysis Jet	yes	50	yes
HHC-SPK, Hydroprocessed Hydrocarbon Synthetic Paraffinic Kerosene	yes	10	no
ATJ-SKA, Alcohol-to-Jet Synthetic Kerosene with Aromatics	no	50	yes
HEFA-SKA, Hydroprocessed Esters and Fatty Acids Synthetic Kerosene with Aromatics	no	50	yes
HDO-SAK, Hydrodeoxygenerated Aromatic Kerosene	no	20	no
CPK-0 Cycloparaffinic Kerosene	no	50	yes yes
HFP-HEFA-SPK, High Freeze Point Hydroprocessed Esters and Fatty Acids Synthetic Paraffinic Kerosene	no	15-30	no

3 Aircraft Climate Assessment for Conceptual Aircraft Design

Since the background information about the effects of aircraft emissions on climate, the general modelling approach, the calculation of great circle distances and different fuel types were shown, this chapter now deals with the selection of the most appropriate models for aircraft design studies and the implementation of the theoretical models in a mathematical environment.

The following sections, first, provide a general overview of the aircraft design environment. Second, the development of the Aircraft Climate Tool (ACT) is shown, a metric that can be used to calculate the climate impact of various aircraft emissions, based on Dallara's PhD (Dallara, 2011). Subsequently, the generation of the Emission Inventory Generation Methodology is presented, which allows the trajectories for each specific mission in the flight schedule to be interpolated between the existing aircraft trajectories. Finally, it is explained what changes are required for the calculation with SAF.

3.1 General Overview of the Design Environment

The design environment established by DLR is based on the open-source Remote Component Environment (RCE) integration framework, which enables to connect and manage standalone tools of different disciplines and varying fidelity (Seider, et al., 2012). Therefore, the individual tools can be published and distributed remotely between different DLR sites, and they can be easily integrated into the design environment. The Common Parametric Aircraft Configuration Schema (CPACS) supports the exchange of information and is used for import and export. CPACS is a standardized data model for aviation systems, a central data source, and ensures consistent data transfer between domains by defining a common language for aircraft design (Alder, et al.). As a data model, CPACS organizes the data elements and standardizes how they relate to each other.

A generic design environment can be seen in Figure 5 for the conceptual aircraft design. The design environment is divided into Level-0 and Level-1 based on the level of fidelity. To start the workflow, at least a minimum set of top-level aircraft requirements, such as design range, cruise altitude and payload definition, and design parameters, such as the engines' location and the wing vertical position, must be specified (Wöhler, et al., 2020). With these parameters, the aircraft design process begins in the Level-0 segment, where the tool derives an initial design such as the geometrical layout, aerodynamics, and mission performance. In the Level-1 section, disciplinary tools are used to improve the quality and refine the accuracy of the design studies (Wöhler, et al., 2020). When convergence is reached in the Level-1 section, the design is complete and post-processing, such as mission and climate impact analysis, can follow. This is where the climate assessment tool developed within in this thesis is integrated, as shown by the red rectangle in Figure 5.

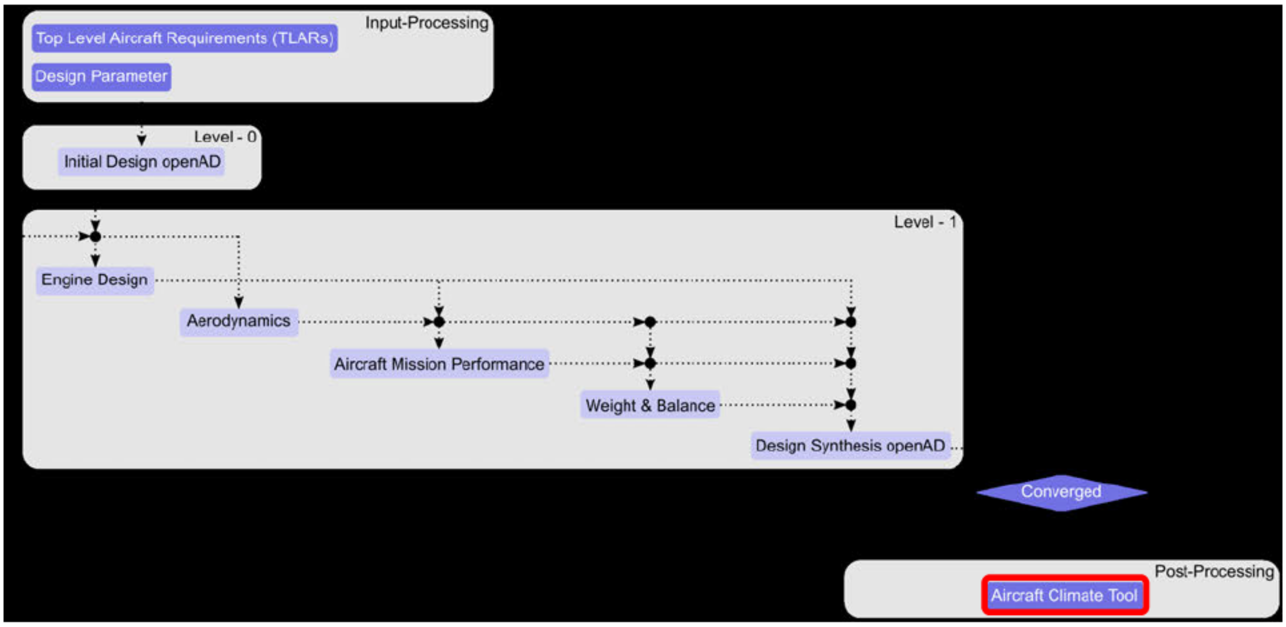

Figure 5: Flowchart of a design environment (Wöhler, et al., 2020)

The DLR tool OpenAD, with which conceptual aircraft designs are calculated, is based on well-understood handbook methods (Torenbeek, 2013) (Raymer, 2018) and some own methods, where no adequate methods could be found in literature. It can interpret CPACS tool specifics data as input in order to specify calculation settings and change calculation parameter. OpenAD generates a CPACS output file with all relevant data. (Wöhler, et al., 2020)

3.2 Aircraft Climate Tool (ACT)

The Aircraft Climate Tool (ACT) programmed herein is a metric for quantifying and comparing the climate performance of aircraft configurations and is based on the methodology developed by Dallara (Dallara, 2011). For implementing the tool, Python, an interpreted, object-oriented, high-level programming language, was used. The required inputs for the tools, such as different CPACS files for different aircraft calculated with the OpenAD tool and a flight schedule, on which the tool can be based, are described in chapter 4. ACT consists of three sections: The Emission Modelling, the Climate Impact Modelling and the Climate Change Metric as can be seen in Figure 6. For each of these sections different possible models were already presented (see chapter 2.2).

For the Emission Modelling there was no need to use the P3-T3 method or the Fuel Flow Correlation Methods because the emission flows in kg/s for different species, including NO_x, were already given in this thesis. Therefore, the use of Fuel Proportional Emissions, where the EI is proportional to fuel consumption, was sufficient.

For the Climate Impact Modelling simplified computationally efficient models are important. GCMs are assumed to be highly capable of reproducing observations of past and present climate changes and providing reliable values. But they are also computationally expensive, and therefore not desirable for conceptual design studies that require numerous calculations. IAMs are less accurate than the GCMs but provide information on regional and global economic impacts and are therefore rather used to inform climate change policy decisions. LTR Models estimate globally- and annually-averaged conditions and are therefore also less accurate than the GCMs. However, they unite the advantages of computational efficiency, transparency, and ease of incorporating new knowledge, making them an important tool for evaluating many different emissions scenarios. Therefore, they are perfect for aviation and conceptual design studies and are used in this thesis by translating the aircraft emissions into RF and temperature change.

For the Climate Change Metric, a lot of different metric properties are important. With respect to the already described target metrics for comparative aircraft design (see chapter 2.2.4), it can be seen that the ATR metric fulfills almost all requirements and therefore appears to be a suitable metric for this purpose. As described, ATR is based on temperature change because it is commonly used, because it is understood by non-experts, and because it directly shows a change in climate behavior. Furthermore, as the purpose of this metric is to quantify the climate impact resulting from aircraft emissions during operation and from emissions that remain in the atmosphere after the end of the aircraft's service life, the metric quantifies an integrated temperature change. The emission case used is representative of the likely operation of an aircraft, as the global mean temperature change is calculated assuming constant emissions during the first H years of operation and zero emissions thereafter. Thereby, H is the operational lifetime of the aircraft. Lastly, also a weighting function can be included to vary the importance of the long-lived and the short-lived impacts.

Each model with the formulas used is presented separately below. The values for modelling the emissions are initially based on Jet A-1 fuel and are later adjusted for SAF.

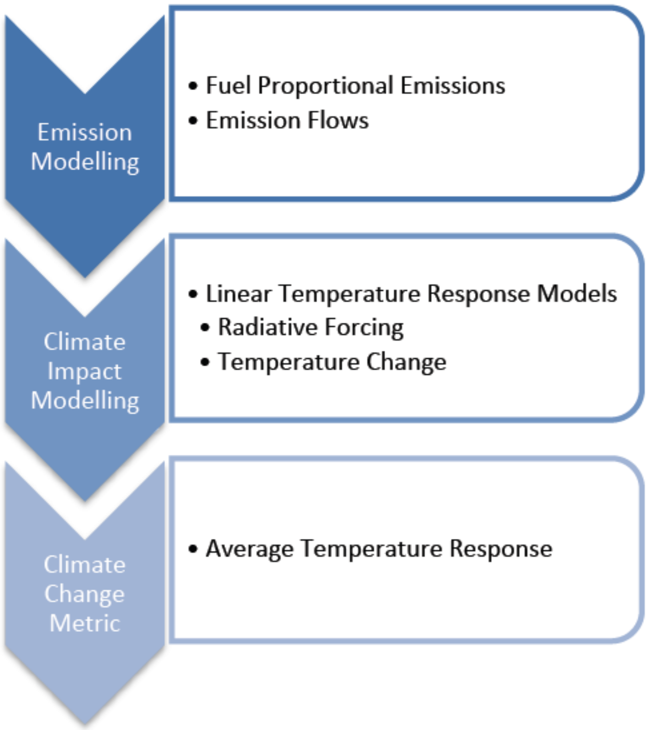

Figure 6: Modelling approach and chosen metrics

3.2.1 Emission Modelling

The first step in calculating the climate impacts of aircraft emissions is to develop a construct that indicates the future emissions of a particular aircraft. This is done by assuming that the aircraft completes a typical mission a specified number of times per year. $U(t)$ thus, refers to the number of missions flown in a year. The emissions per flight, e_i, refer to the total amount of species i released during a typical mission, where i represents CO_2, H_2O, SO_4, soot and NO_x. Therefore, the annual emissions of each species, $E_i(t)$, can be calculated with equation (3.1). (Dallara, 2011)

$$E_i(t) = e_i * U(t) \quad (3.1)$$

$U(t)$ is a variable input parameter, so only the emissions per flight need to be calculated. In the calculated trajectories in CPACS, which were given as input parameters, the emission flows in $\left[\frac{kg}{s}\right]$ were already computed for CO_2, H_2O, NO_x and partly also for soot. Therefore, for these species, the emissions per flight can be calculated by multiplying the total mission emission flow, $EmissionFlow_i$, with the mission flight time, $t_{Mission}$, as shown in equation (3.2).

$$e_i = EmissionFlow_i * t_{Mission} \quad for\ CO_2, H_2O, NO_x, (soot) \quad (3.2)$$

For the other species, SO_4 and sometimes soot, the emissions per flight are related to fuel consumption by the emission index. The Emissions Index, EI_i, is a key parameter that determines the total mass of emissions. For many species, including SO_4, EI is a property of the fuel that cannot be changed and is therefore taken to be constant (Dallara, 2011). As already described (see chapter 2.1.5), the EI of soot can vary with the operating condition of the engine. In this thesis, however, it is assumed to be constant without significant loss of accuracy, since soot accounts for only a small part of the total climate impacts. The EIs of SO_4 and soot according to IPCC (IPCC, et al., 1999) are shown in Table 2.

Table 2: Emission Indices (IPCC, et al., 1999)

Species	Emission Index
SO_4	$2.0 * 10^{-4} \frac{kg\ S}{kg\ fuel}$
$soot$	$4.0 * 10^{-5} \frac{kg\ soot}{kg\ fuel}$

Since the EIs are constant, the emissions per flight, e_i, for SO_4 (and soot) are simply the product of Emission Index, EI_i, and total mission fuel consumption, W_{fuel}, as shown in equation (3.3). The total mission fuel consumption was already calculated in the given aircraft trajectories.

$$e_i = EI_i * W_{fuel} \quad for\ SO_4, (soot) \quad (3.3)$$

The given aircraft trajectories sometimes include the $SootFlow$ and sometimes do not. If they contain a $SootFlow$, the soot emissions per flight are calculated with equation (3.2), if not, the soot emissions per flight are calculated with equation (3.3).

3.2.2 Climate Impact Modelling

The next step is to compute the climate impact of the calculated annual emissions. This requires different models for long-lived gases, short-lived pollutants, and aviation induced cloudiness. But before this can be done, the altitude variation must first be considered. A major difference between ground-level emission sources and aircraft emissions is that aircraft emissions are deposited directly in the upper troposphere and lower stratosphere. Especially the climate impact of NO_x emissions and AIC vary significantly with emission altitude. To account for this variation, altitude-dependent forcing factors, $s_i(h)$, were developed. These are based on normalized data from perturbational aircraft emissions studies by Kohler et al. (Kohler, et al., 2008) and Radel et al. (Radel, et al., 2008) for NO_x RF per emission and AIC RF per distance flown as function of altitude (Dallara, 2011). This data is normalized by the distance-weighted average RF per emission to define $s_i(h)$. The resulting RF factor data for NO_x emissions and AIC can be seen in Figure 7.

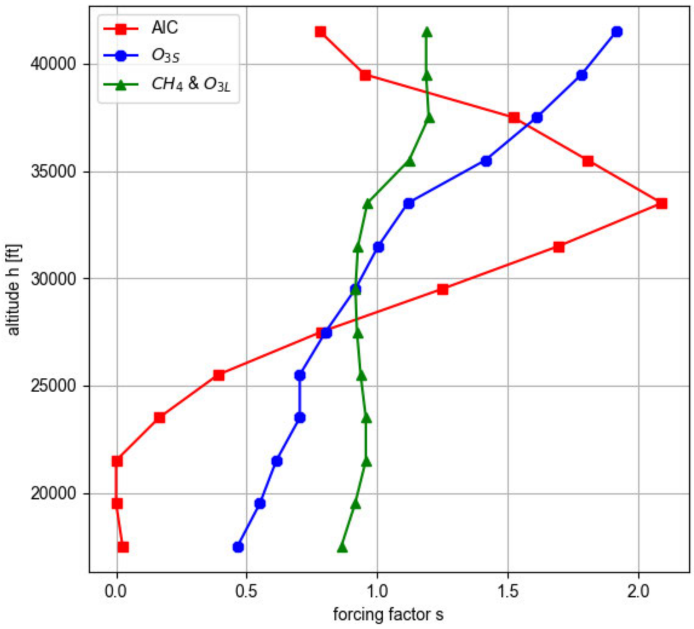

Figure 7: Radiative forcing factor data for NO_x impacts and AIC (Dallara, 2011)

As shown in Figure 7, the NO_x emissions are composed of two components: the short-term production of O_3, which produces a warming effect (referred to as O_{3S}) and the long-term destruction of CH_4 and O_3, which produces a cooling effect (referred to as O_{3L}) (see chapter 2.1.2). Therefore, two different NO_x RF functions are defined, one for the short-term and one for the long-term effect.

During the development of the altitude-dependent forcing factors shown in Figure 7, some assumptions had to be made. The first concerns the AIC. Since many studies consider only the impacts of contrails because of the large uncertainties accompanying the impacts of cirrus clouds, data on the altitude sensitivity of cloud impacts were published only for contrails (Radel, et al., 2008). However, contrail-cirrus clouds form from aging contrails and the radiative properties of contrail-cirrus are currently estimated to be similar to those of linear contrails. Therefore, the RF factors for contrails are extended to AIC RF, which includes the effects of both contrail and cirrus clouds. As can be seen in Figure 7, no data were available for NO_x RF per emission below 17500ft, but even in this range the forcing factor is not zero. Therefore, it is assumed that the data for the range below 17500ft is constant and corresponds to h = 17500ft. This assumption has only a minor effect on the magnitude of the forcing factor, since the forcing factors at these altitudes are comparatively low and only a small portion of distance is flown below this altitude (Dallara, 2011). Lastly, the direct effects of water vapor also vary with emission altitude (see chapter 2.1.3). However, water vapor has a very short lifetime of one to two weeks in the troposphere and lower stratosphere, where subsonic aircraft generally fly. Because of the short lifetime, the climate impact of water vapor is rather small compared to CO_2, NO_x, or AIC, and therefore the variation of H_2O with altitude can be neglected (Dallara, 2011).

3.2.2.1 Radiative Forcing

RF quantifies the change in net irradiance at the tropopause due to a disturbance, such as aircraft emissions. A positive RF causes warming, while a negative RF causes cooling. With the altitude-dependent forcing factors the time-varying RF as a function of altitude and mass of aircraft emissions can be calculated. The different models for long-lived gases, short-lived pollutants and AIC are shown below.

Carbon Dioxide (CO_2):

CO_2 has a long lifetime and is well mixed within the atmosphere (see chapter 2.1.1), and therefore CO_2 impacts do not depend on altitude. The IPCC estimates the RF caused by small perturbing CO_2 emissions using equations (3.4) and (3.5), which assume a constant CO_2 background concentration of 378 parts per million by volume (ppmv) ((IPCC), 1999):

$$RF_{CO_2}(t) = \int_0^t G_{CO_2}(t-\tau)\, E_{CO_2}(\tau)\, d\tau \quad (3.4)$$

$$G_{CO_2}(t) = A_{CO_2}\left[1 + \sum_{j=1}^{3} \alpha_{cj}\ \left(exp\left(\frac{-t}{\tau_{cj}}\right) - 1\right)\right] \quad (3.5)$$

$G_{CO_2}(t)$ represents the decay of RF caused by a pulse emission of CO_2; thus, the bracketed part in equation (3.5) describes the fraction of CO_2 emitted at t = 0 that remains in the atmosphere at time t (Dallara, 2011). The values of the parameters A_{CO_2}, τ_{cj} and α_{cj} are shown in Table 3 according to the IPCC fourth assessment report (IPCC, 2007) and are based on best estimates. The response function, $G_{CO_2}(t)$, multiplied by the annual emissions of CO_2, E_{CO_2}, and integrated over the time t yields the RF of CO_2 as shown in equation (3.4).

Table 3: Best estimates for CO_2 parameter values (IPCC, 2007)

CO_2 Parameter	Best Estimates
A_{CO_2}	$1.8 * 10^{-15} \frac{W/m^2}{kg\ CO_2}$
α_{c1}	0.259
α_{c2}	0.338
α_{c3}	0.186
τ_{c1}	$172.9\ yrs$
τ_{c2}	$18.51\ yrs$
τ_{c3}	$1.186\ yrs$

Methane (CH_4) and long-lived Ozone (O_{3L}):

For the NO_x emissions, different models for the short-term production of O_3 (O_{3S}) and the long-term destruction of CH_4 and O_3 (O_{3L}) are needed. First, the long-term effects (CH_4 and O_{3L}) will be considered. The RF caused by small perturbational emissions of NO_x is estimated with the equations (3.6) and (3.7) (Dallara, 2011).

$$RF_i(t,h) = s_i(h) \int_0^t G_i(t-\tau)\, E_{NO_x}(\tau)\, d\tau \quad for\ i = CH_4,\ O_{3L} \quad (3.6)$$

$$Gi(t) = Ai * exp\left(\frac{-t}{\tau_{CH4}}\right)\ for\ i = CH_4,\ O_{3L} \quad (3.7)$$

The response functions $G_i(t)$ are derived from fleetwide emissions and altitude and represent the decay of RF caused by a pulse emission of NO_x. The values of the parameters $A_{CH_4}, A_{O_{3L}}$ and the adjustment time of methane τ_{CH_4} are shown in Table 4 and are based on best estimates. Using the altitude-dependent forcing factors (see chapter 3.2.2), the RF are calculated as altitude-specific values. The response function, $G_i(t)$, multiplied by the annual emissions of NO_x, E_{NO_x}, integrated over the time t, and multiplied by the altitude-depended forcing factor, $s_i(h)$, yields the RF of CH_4 and O_{3L}, as shown in equation (3.6).

Table 4: Best estimates for NO_x parameter values

NO_x Parameter	Best Estimates
A_{CH_4}	$-5.16 * 10^{-13} \frac{W/m^2}{kg\ NO_x}$ (Marais, et al., 2008)

$A_{O_{3L}}$	$-1.21 * 10^{-13} \frac{W/m^2}{kg\ NO_x}$ (Marais, et al., 2008)
τ_{CH_4}	$12\ yrs$ (IPCC, 2007)

Short-lived Species (H_2O, $NO_x - O_{3S}$, soot, SO_4):

The short-lived species, including H_2O, $NO_x - O_{3S}$, soot, and SO_4, have lifetimes of less than a year and therefore cause RF for only a short time after emission. For these short-lived species, the RF is assumed to be directly proportional to the RF per emission for a reference year based on IPCC (IPCC, et al., 1999) and subsequent studies (Dallara, 2011). Therefore, the RF for these species can be calculated by multiplying the annual emissions of the emission species, $E_i(t)$, by the RF per emission for a reference year according to equation (3.8).

$$RF_i(t,h) = s_i(h)\left(\frac{RF_{ref}}{E_{ref}}\right)_i E_i(t) \quad for\ i = H_2O,\ NO_x - O_{3S},\ soot,\ SO_4 \quad (3.8)$$

With the altitude-dependent forcing factor for O_{3S} (see chapter 3.2.2), the RF for short-lived ozone is computed as altitude-specific value. The forcing factors for the other short-lived species are equal to one. The values of the short-lived species parameters are shown in Table 5 and are based on best estimates.

Table 5: Best estimates for short-lived species parameter values (Dallara, 2011)

Short-lived Species Parameter	Best Estimates
$\left(\frac{RF_{ref}}{E_{ref}}\right)_{H_2O}$	$7.43 * 10^{-15} \frac{W/m^2}{kg\ H_2O}$
$\left(\frac{RF_{ref}}{E_{ref}}\right)_{O_{3S}}$	$1.01 * 10^{-11} \frac{W/m^2}{kg\ NO_x}$
$\left(\frac{RF_{ref}}{E_{ref}}\right)_{SO_4}$	$-1.0 * 10^{-10} \frac{W/m^2}{kg\ SO_4}$
$\left(\frac{RF_{ref}}{E_{ref}}\right)_{soot}$	$5.0 * 10^{-10} \frac{W/m^2}{kg\ soot}$
$\left(\frac{RF_{ref}}{L_{ref}}\right)_{AIC}$	$2.21 * 10^{-12} \frac{W/m^2}{nmi}$

Aviation Induced Cloudiness (AIC):

Contrails and cirrus clouds are also short-lived effects. The linear model used to calculate the RF of AIC is based on the assumption of Stordal et al. (Stordal, et al., 2005). This model assumes that a change in cloud cover over an area is proportional to a change in aircraft flight distance and, furthermore, that the RF scales linearly with cloud coverage. Thus, it is suggested that the RF of the AIC is directly proportional to a reference RF per distance traveled (Dallara, 2011). Therefore, the RF of AIC can be calculated by multiplying the distance flown per year, $L(t)$, with the reference RF per distance travelled as shown in equation (3.9). Using the altitude-dependent forcing factor for AIC (see chapter 3.2.2), the RF of AIC is computed as altitude-specific value. The distance flown per year, $L(t)$, is a variable input parameter. The best estimate of the value $\left(\frac{RF_{ref}}{L_{ref}}\right)_{AIC}$ is given in Table 5.

$$RF_{AIC}(t,h) = s_{AIC}(h)\left(\frac{RF_{ref}}{L_{ref}}\right)_{AIC} L(t) \quad (3.9)$$

3.2.2.2 Temperature Change

The RFs calculated by the above mentioned methods, are linearly related to the change in global mean equilibrium surface temperature. The calculated RF can therefore be converted into temperature change. But before doing so, the RF for each species must be normalized. To do this, the RF of each species is multiplied by the species' efficacy, f_i, and divided by the RF that would result if CO_2 emissions were doubled, as shown in equation (3.10) (Dallara, 2011).

$$RF_i^*(t,h) = f_i \frac{RF_i(t,h)}{RF_{2xCO_2}} \quad for\ i = CO_2,\ CH_4,\ O_{3L},\ O_{3S},\ H_2O,\ soot,\ SO_4,\ AIC \quad (3.10)$$

The values for RF_{2xCO_2} and for the efficacies, which are unitless parameters comparing the change in surface temperature for equal RF of species i and CO_2, are given in Table 6. The efficacy of CO_2 must be one.

Table 6: Best estimates for RF normalized model parameter values (Dallara, 2011)

Normalized RF Model Parameter	Best Estimates
f_{CH_4}	1.18
f_{H_2O}	1.14
f_{O_3}	1.37
f_{SO_4}	0.9
f_{soot}	0.7
f_{AIC}	0.59
RF_{2xCO_2}	$3.7\ W/m^2$

In the next step, all normalized RFs, RF_i^*, are summed and applied to a climate impulse response function, $G_T(t)$. This term integrated over the time t yields the time-varying global mean temperature change, $\Delta T(t)$, as seen in equation (3.11).

$$\Delta T(t) = \int_0^t G_T(t-\tau)\left(\sum RF_i^*(\tau)\right) d\tau \;\; for\; i = CO_2, CH_4, O_{3L}, O_{3S}, H_2O, soot, SO_4, AIC \quad (3.11)$$

The impulse response function used is the two-mode impulse response function developed by Boucher et al. (Boucher, et al., 2008), which is shown in equation (3.12) (Dallara, 2011).

$$G_T(t) = S\left[\frac{\alpha_t}{\tau_{t1}} exp\left(\frac{-t}{\tau_{t1}}\right) + \frac{1-\alpha_t}{\tau_{t2}} exp\left(\frac{-t}{\tau_{t2}}\right)\right] \quad (3.12)$$

The values for the parameters $\alpha_t, \tau_{t1}, \tau_{t2}$ and the climate sensitivity parameter, S, which represents the steady-state temperature change that would result from a constant annual RF of RF_{2xCO_2}, are given in Table 7.

Table 7: Best estimates for temperature model parameter values (Dallara, 2011)

Temperature Model Parameter	Best Estimates
S	$3.0\ K$
α_t	0.595
τ_{t1}	$8.4\ yrs$
τ_{t2}	$409.5\ yrs$

3.2.3 Climate Change Metric

In the final step, a metric is needed to quantify the impact of climate change. For this purpose, the Average Temperature Response metric is used in this thesis. To calculate the ATR, the global mean temperature change must be calculated as shown in equations (3.1) to (3.12), but with the scenario of constant emissions during the first H years of operation and zero emissions thereafter. This leads to the time-varying temperature change calculated for an arbitrary aircraft emission scenario, $\Delta T_{sust,H}$ defined in equation (3.13) (Dallara, 2011).

$$\Delta T_{sust,H} = \Delta T|_{s_i=\bar{s}_i,\; E_i(t)=e_i U_{sust\sigma_H(t)}} \qquad \sigma_H(t) = \begin{cases} 1 & t \leq H \\ 0 & H < t \leq t_{max} \end{cases} \quad (3.13)$$

In this equation, the parameter H defines the operational lifetime, which is a variable input parameter. In this thesis, H is assumed to be 30 years. The parameter t_{max} defines the years under consideration, is also a variable input parameter, and is assumed to be 100 years. The parameter $\sigma_H(t)$ characterizes the input emission scenario. $\Delta T_{sust,H}$ is calculated with the mission averaged forcing-factors, $\bar{s}_i$, defined in the equations (3.14) and (3.15) (Dallara, 2011).

$$\bar{s}_i = \frac{E_{NO_{x},Cruise}}{E_{NO_x}}\left(\frac{1}{h_f - h_0}\int_{h_0}^{h_f} s_i(h)\,dh\right) + \left(1 - \frac{E_{NO_{x},Cruise}}{E_{NO_x}}\right) s_{i,low} \quad for\ i = CH_4,\ O_{3L},\ O_{3S} \qquad (3.14)$$

$$\bar{s}_{AIC} = \frac{L_{cruise}}{L}\left(\frac{1}{h_f - h_0}\int_{h_0}^{h_f} s_{AIC}(h)\,dh\right) \qquad (3.15)$$

These equations yield weighted averages of the forcing factors during cruise, takeoff-landing, and climb-descent phases of the mission. Thereby, the weighted averages for the NO_x forcing factors are based on the proportion of emissions and the averages for AIC forcing factors are based on the proportion of flight distance in each flight segment (Dallara, 2011). Since there is no function given for the calculation of the forcing factors, but only different points between which interpolation is possible (see chapter 3.2.2), the term $\int_{h_0}^{h_f} s_i(h)\,dh$ is calculated by integrating the forcing factors and the equivalent altitudes from the initial cruise altitude h_0 to the final cruise altitude h_f using the trapezoidal rule. Another problem arises when the initial cruise altitude is equal to the final cruise altitude (no step climbs), because then the first part of the term $\frac{1}{h_f - h_0}\int_{h_0}^{h_f} s_i(h)\,dh$ would be divided by zero. However, since the term defines the average forcing factor, only one forcing factor is considered as they are all equal, and this one value defines the average. NO_x forcing factors during takeoff, climb, descent and landing are denoted $s_{i,low}$ and are based on the forcing factors at $h_{low} = 17500ft$ (Dallara, 2011). AIC forcing factors outside of cruise are considered to be zero.

The last step that is missing in the calculation of the ATR is the determination of a weighting function. The function used in this thesis is given in equation (3.16).

$$w_r(t) = \begin{cases} 1 & t \le H \\ 0 & \\ \dfrac{1}{(1+r)^{t-H}} & H < t \le t_{max} \\ 0 & \\ 0 & t > t_{max} \end{cases} \qquad (3.16)$$

In this function, the temperature change during the operational lifetime of the aircraft is weighted by one unity $(t \le H)$ and an exponential devaluation rate is applied to temperature change occurring after the end of the operational lifetime of the aircraft $(H < t)$ (Dallara, 2011). The devaluation rate r is a variable input parameter. A devaluation rate of zero means that climate impacts during the operation and climate impacts after the operation are equally important, and a devaluation rate of infinity means that climate impacts occurring after the operation of the aircraft are of no importance. A maximum integration window is also applied, defined by t_{max}, because a fraction of CO_2 emissions remains in the atmosphere for many thousands of years and therefore most models for CO_2 -induced temperature change do not decay to zero (Dallara, 2011).

Once $\Delta T_{sust,H}$ is known and metric parameters, i.e., devaluation rate r and operating lifetime H, are specified, the ATR can be calculated according to equation (3.17) (Dallara, 2011). As shown in this equation, the weighted temperature change per year is integrated and divided by H to obtain an average temperature response.

$$ATR_H = \frac{1}{H}\int_0^{\infty} \Delta T_{sust,H}(t)\, w_r(t)\, dt \qquad (3.17)$$

Different devaluation rates, operating lifetimes and integration windows may be used. However, it is important that the same rates, lifetimes, and windows are used to compare different aircraft designs. The ATR condenses the lifetime impact of aircraft into a single, meaningful quantity, so that the lifetime temperature change of different aircraft designs and technologies can now be compared.

3.2.4 Implementation of ACT in CPACS

The DLR, as well as many other institutions, uses CPACS to combine different tools and to ensure consistent data transfer between domains by defining a common language for aircraft design (see chapter 3.1). Therefore, to integrate ACT into the DLR's processes and tool landscapes, the tool's inputs and outputs had to utilize CPACS. The inputs required by the aircraft trajectories calculated with OpenAD (see chaper 3.1) are the altitude [m], the flight time [s], the flight distance [m] and the fuel and the different emission flows $\left[\frac{kg}{s}\right]$, as shown in Table 8.

Table 8: Input parameters of the aircraft trajectories

Input parameters of the aircraft trajectories	
Parameter	**Unit**
Altitude	m
Flight Time	s
Fuel Flow	kg/s
CO_2 Flow	kg/s
H_2O Flow	kg/s
NO_x Flow	kg/s
Soot Flow	kg/s
Flight Distance	m
Segment UID	-

Other inputs needed for the metric shown, which can be specified via CPACS, are the devaluation rate r $[-]$, the missions flown per year U $[-]$, the distance flown per year L $[NM]$, the emission index of SO_4 EI_{SO_4} $\left[\frac{kg\ S}{kg\ fuel}\right]$, the emission index of soot EI_{soot} $\left[\frac{kg\ soot}{kg\ fuel}\right]$, the considered years t_{max} $[yrs]$ as an integer and the aircraft's operational lifetime H $[yrs]$ as an integer, as shown in Table 9. With these inputs, the metric explained in chapter 3.2 can be implemented in Python. Python Version 3.7 is used for this purpose. The tool is similar in structure to the shown metric. First, the input parameters are imported and the constants for the metrics presented are defined. Then, the total quantities of species released during each mission and the mission averaged forcing factors can be calculated. With these data, the annual emissions, the RF, the mean temperature change and the ATRs can be computed. A weighting function is also defined for the

ATRs. The main part is calculated in ‚mode0‘, while calculations that are the same for some of the emission species and occur more than once are specified in ‚methods‘.

Table 9: Input parameters for the metric

Input parameters of the metric	
Parameter	**Unit**
Devaluation Rate	-
Number of missions flown per year	-
Distance flown per year	NM
EI of SO_4	kg S / kg fuel
EI of soot	kg soot/ kg fuel
Considered years	yrs
Aircraft's operational lifetime	yrs

The CPACS outputs consist of the RFs, the mean temperature changes for H years of sustained operation $\Delta T_{sust,H}(t)$ and the ATRs, for CO_2, $NO_{x\ cooling}$, $NO_{x\ warming}$, H_2O, SO_4 & soot, AIC, and total, as shown in Table 10.

Table 10: Output parameters of the ACT

Output parameters of the ACT	
Parameter	**Unit**
RF	W / m^2
Mean Temperature Change	K
ATR	K

In addition, a plot of the ATRs and a plot of the mean temperature change for H years of sustained operation for CO_2, NO_x cooling, NO_x warming, H_2O, SO_4 & soot, AIC, and total are given, as will be shown in the results (chapter 6).

3.2.5 Limitations of the Climate Model

The linear climate model used in this thesis, RF and temperature change, offers many advantages over more complex models, including lower computational costs. However, to take advantage of these benefits, many assumptions had to be made, so the climate model has some limitations, which are described below.

First, the temperature change computed here (see chapter 3.2.2.2) is a global mean temperature respond to RF, which can be generated both globally and regionally. For long-lived gases such as CO_2 and CH_4, this distinction between global or regional is not particularly important because their long lifetimes mean that they mix throughout the atmosphere and are therefore independent of the emission location. Short-lived species, however, cause RF only near flight routes, so the short-lived RFs are greatest in the northern mid-latitudes, where air traffic is most dense. This means that the global mean RF can produce strong positive and negative temperature responses regionally, but these varying impacts are not accounted for by the linear temperature response model as it focuses on the climate response averaged over the earth's surface. (Dallara, 2011)

A further limitation arises from the fact that the models used in this thesis are based on average impact of fleetwide routing in a single year within the last decade. Therefore, the models quantify the average RF caused by emission distributed spatially and temporally according to a routing that corresponds to current traffic. This routing is largely concentrated in the mid-latitudes of the Northern Hemisphere. As a result, the best estimates of the model parameter values become less accurate when the flight route distribution differs significantly from the current routing. (Dallara, 2011)

In addition, the linear temperature response models do not capture as many sensitivities as the global climate model. For example, emissions from sources other than aviation could alter the climate parameters, and the effects of some aviation emissions are also chemically coupled but are considered independent in this thesis (Dallara, 2011).

The linear model applied by IPCC to calculate the CO_2 RF is based on constant background CO_2 concentrations of 378ppmv (see chapter 3.2.2.1). However, this assumed background concentration is a likely underestimate of actual short-term concentrations and therefore the climate impact of the CO_2 emissions is slightly overestimated (Dallara, 2011).

Moreover, NO_x and AIC climate impacts rest upon complex processes and effects that are highly simplified in the models used in this thesis, leading to large uncertainties. The models for ozone formation are complicated because the production rates are nonlinear and depend on background composition and meteorological conditions. Furthermore, the temperature change due to equal ozone production RFs may change with latitude and altitude. However, the model used herein only attempts to capture the effects of different altitudes via the forcing factors. Nevertheless, it should also be mentioned that studies by Lee et al. (Lee, et al., 2009) have demonstrated a linear relationship between the RF of ozone production and the NO_x emissions as used in the applied models (Dallara, 2011). In addition, the AIC RF models do not capture differential impacts due to changing particle and water vapor emissions or exhaust temperature, but only scale with flight distance (Dallara, 2011). Also, the AIC RF models are based on the results of the GCMs. However, the scientific understanding of AIC impacts is still incomplete, suggesting that the AIC RF models will be refined in the future, as the models used here are limited by the accuracy of the underlying GCM.

3.3 Emission Inventory Generation Methodology

The Emission modelling approach described in chapter 3.2.1 is based only on one typical mission, which is flown a certain number of flights per year. However, in order to base the lifetime climate impact of aircraft not just on one typical mission, but on more realistic data such as a flight schedule, the ACT needs to be further developed. This is done through the Emission Inventory

Generation Methodology, which can be used to calculate the climate impact of each mission in the flight schedule.

The further development of the ACT to the Emission Inventory Generation Methodology is carried out in two steps:

1. The great circle distance between city pairs specified in the given global flight network is calculated (see chapter 2.3)
2. The trajectory of an individual aircraft type must be determined for each city pair based on great circle distance and payload.

Once all the aircraft type missions are known for each city pair in the flight schedule, the lifetime climate impact of each mission can be calculated using the ACT, and the total lifetime climate impact of the aircraft type is the sum of the lifetime impact of each mission. The two steps required for the further development are outlined below.

3.3.1 Great Circle Distance Calculation

To calculate the great circle distance d between two locations on the earth's surface, equation (3.18) is used (Lufthansa Aviation Training, 2016),

$$cos(d) = sin(\varphi_A) * sin(\varphi_B) + cos(\varphi_A) * cos(\varphi_B) * cos(\Delta\lambda) \quad (3.18)$$

where φ is the latitude of point A or B and λ is the longitude. In addition, the following rules regarding the signs must be observed: North latitude is positive, south latitude is negative, east longitude is positive, and west longitude is negative. If the latitude and longitude of both points A and B are in radians, the result of the equation must be converted to degrees in the next step.

Practically, 1NM equals one minute of arc on a great circle. Due to the shape of the earth, this is not quite correct, since on a reference ellipsoid the length of one minute on a meridian varies depending on the latitude. Therefore, one minute of arc is slightly shorter than 1NM in equatorial latitudes and slightly longer in polar regions. However, the deviations are insignificant enough to be neglected for most practical applications (Lufthansa Aviation Training, 2016). Thus, to obtain the distance in nautical miles, the distance in degrees must be multiplied by 60, which yields the distance in minutes of angle, which at the same time corresponds to the distance in nautical miles (1° = 60‘ = 60NM).

3.3.2 Interpolation of the Aircraft Trajectories

Next, the aircraft trajectories must be interpolated for each city pair in the flight schedule. Since it is no longer only one typical mission that is considered, it is no longer possible to use only one typical trajectory of an aircraft type, but all existing trajectories of a specific aircraft type in which a complete mission is flown. For example, Figure 8 shows the payload-range diagram where each point represents an existing trajectory between which each individual aircraft mission can be interpolated. For one trajectory, the individual parameters needed for the calculation of the ATRs are each combined in one vector. If all the available aircraft trajectories are now used, the vectors of the individual trajectories are combined into one large vector. This vector with the individual vectors of each trajectory forms the basis for the interpolations of the Emission Inventory Generation Methodology.

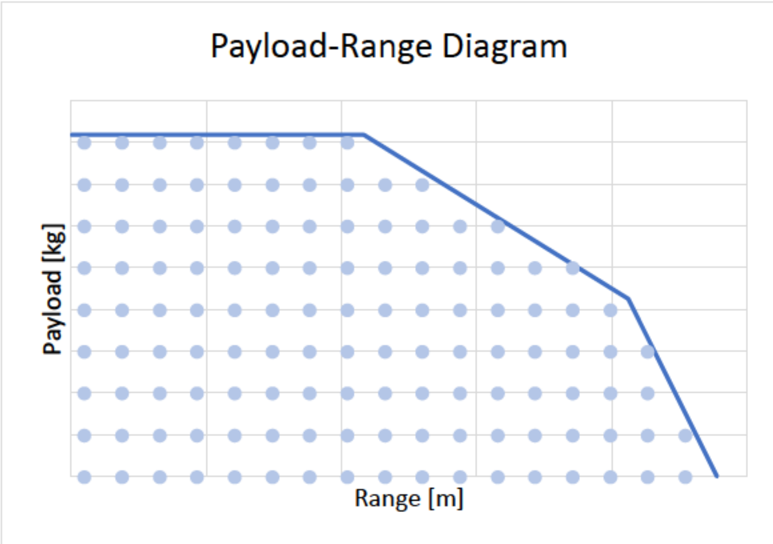

Figure 8: Example of a payload-range diagram with additional payload and range combination for interpolation

To calculate the lifetime climate impact of a given mission of the flight schedule with the ACT, the released species (e_i) of CO_2, H_2O, NO_x, SO_4 and soot throughout the mission, the cruising distance, the released amount of NO_x during cruise, and the cruising altitudes are needed. Therefore, these values must be interpolated between the existing trajectories. The interpolations are divided into the interpolation of the released species and the interpolation of the cruising altitudes, which are explained below.

3.3.2.1 Interpolation of the released emission species

The interpolations for the released emission species of CO_2, H_2O, NO_x, SO_4 and soot, for the cruising distance (L_{cruise}) and the released amount of NO_x during cruise ($e_{NOx\ cruise}$) can be performed in the same way. Before these mentioned values can be interpolated for each mission of the flight schedule, they must first be calculated for each existing trajectory (see chapter 3.2.1). Since the required values must be interpolated based on the great circle distance and based on the payload, the interpolations are again subdivided into interpolation for the different great circle distances and into interpolation for the different payloads.

For the interpolation of the different great circle distances, all payloads appearing in the existing trajectories in which a complete mission is flown were determined and counted how often each payload occurs. In the payload range diagram example shown in Figure 9, there are eight trajectories with a payload of 40000kg, ten with a payload of 35000kg, and so forth. Based on these numbers, the vector with the individual vectors of each trajectory were segmented into vectors of the different payloads and then each vector was interpolated with the great circle distance of a particular mission. The result are the interpolated values based on the great circle distance for a particular mission for each payload, as shown, for example, by the red points in Figure 9.

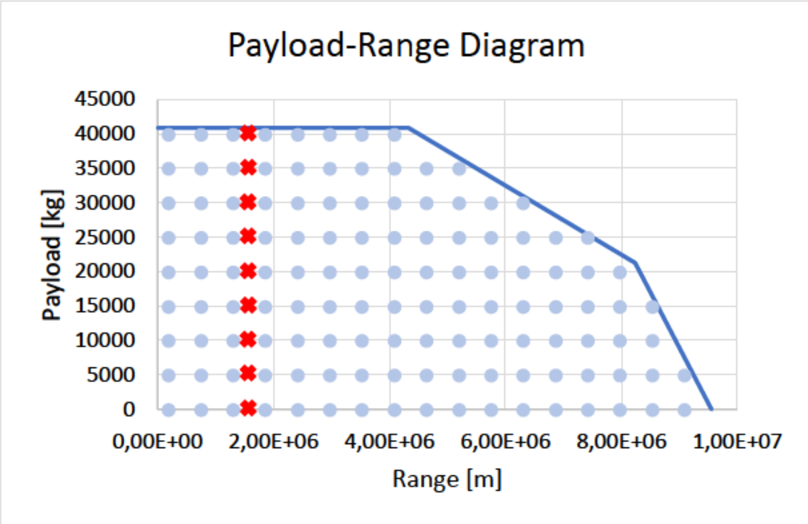

Figure 9: Results of the interpolations based on great circle distance

For the interpolations of the different payloads, the vector of the last interpolation must be rearranged to obtain a vector for each great circle distance with all interpolated payloads based on the great circle distance; so basically, the red points in Figure 9 in a vector. With this rearranged vector, the payloads can be interpolated. The results are the released emission species of CO_2, H_2O, NO_x, SO_4 and soot, the cruising distance, and the released amount of NO_x during cruise, interpolated based on the great circle distance and payload for each specific mission.

3.3.2.2 Interpolation of the cruising altitudes

The cruising altitudes must also be interpolated. The cruising altitudes of the individual trajectories consist of a vector. For the understanding of the interpolation of the cruising altitudes it is important how this vector is constructed. Each trajectory consists of different time steps, and for each time step the equations of motion are solved and the aircraft performance data are calculated. Therefore, a specific altitude is calculated for each time step. However, since the ACT only requires the cruising altitudes as input, only these are considered. A certain cruising altitude, for example 37000ft, is then flown for a specific number of time steps. This is often followed by a step climb to the next higher cruising altitude, for example 39000ft, which is also flown for a specific number of time steps. For example, if an aircraft performs a step climb from 37000ft to 39000ft during the cruise segment, the cruising altitude of 37000ft could occur 156 times and 39000ft 170 times. Therefore, the basic idea for the cruising altitude interpolations was to count how many time steps are flown at each cruising altitude for each trajectory and interpolate between these time step numbers. As with the interpolation of the released species, the interpolations of the cruising altitudes are divided into interpolations for the different great circle distances and interpolations for the different payloads.

For the interpolation of the different great circle distances, all cruising altitudes that occur multiple times in the existing trajectories were determined. The result is a vector of all cruising altitudes occurring in all trajectories where a complete mission is flown, neglecting intermediate altitudes during climb or descent towards a new cruising altitude. Then, for each trajectory, it is counted how many times each cruising altitude occurs. This generates a vector where for the first cruising altitude it is counted how often this altitude occurs in each trajectory, then for the second cruising altitude and so on. This vector must now be divided into the different cruising altitudes and then into the different payloads. The different payloads and their number of occurrences have already been determined for the interpolations of the released species. In this way, the interpolations can be performed for the different great circle distances.

For the interpolations of the different payloads, the vectors of the last interpolation must be rearranged again to obtain a vector for each great circle distance and for each cruising altitude with all the interpolated payloads based on the great circle distance. With this rearranged vector the payloads can be interpolated. As a result, one receives how often each cruising altitude occurs after the interpolation of the great circle distance and the payload. An example of the result of the interpolations for a particular mission is shown in Table 11. The first number represents the cruising altitude of 21000ft, the second one for 31000ft, and so forth.

Table 11: Example of a result of the cruising altitude interpolations based on great circle distance and payload

[0, 0, 0, 0, 61, 58]
[21000‘, 31000‘, 33000‘, 37000‘, 39000‘, 41000‘]

Based on these numbers a vector of the cruising altitudes can be created for a specific mission at a given great circle distance and payload. For the example in Table 11, the vector of the cruising altitudes would consist of 61 times 39000ft and 58 times 41000ft.

3.4 Needed modifications for the calculation with SAF

The programmed ACT also provides the opportunity to assess the climate impact of different fuel types. However, since the use of SAF changes the amount of some emission, modifications need to be made to the Python tool to obtain the results of the ATR for drop-in fuel blend and 100% SAF. Silberhorn et al. (Silberhorn, et al., 2022) provided the data needed for the conversion from Jet A-1 to drop-in fuel blend and 100% SAF. Thereby, a drop-in fuel blend, a 50% blend of HEFA and Jet A-1, and a 100% SAF, a PtL synthetic fuel without aromatics, are used (see chapter 2.4.2). The drop-in fuel blend applies to the strict fuel standardizations, while the 100% SAF is outside of current fuel specifications. Mainly due to the reduced amount of aromatics in fuel for the drop-in fuel blend and the zero amount of aromatics in fuel for the PtL, the hydrogen content is increased and the carbon content is decreased, which can also be seen by the EIs of CO_2 and

H_2O shown in Table 12 (Silberhorn, et al., 2022).

Table 12: Emission Indices of Drop-In and PtL Kerosene (Silberhorn, et al., 2022)

	Jet-A1	Drop-In	PtL
EI CO_2 [kg_{CO2}/kg_{Fuel}]	3.164	3.132	3.101
EI H_2O [kg_{H2O}/kg_{Fuel}]	1.220	1.297	1.374

Due to the different EIs of CO_2 and H_2O, the emission impact of CO_2 decreases to 98.989% (drop-in) and to 98.009% (PtL) and the emission impact of H_2O increases to 106.315% (drop-in) and to 112.623% (PtL) compared to Jet A-1 fuel.

The drop-in fuel blend and the 100% SAF are assumed to be produced from renewable carbon sources, so the production process is considered carbon neutral (Silberhorn, et al., 2022). Therefore, the in-flight CO_2 emissions from these fuel portions have no impact on the climate and are reduced to 50% for the 50% drop-in fuel blend, while they disappear for the 100% SAF. The soot emissions for the 50% drop-in fuel blend are reduced to 69% and for the PtL kerosene to 38%. These values are based on the results of the DLR in-flight measurement campaign 'Emission and Climate Impact of Alternative Fuels' (ECLIF) (Silberhorn, et al., 2022). Since soot particles play a role in the formation of contrail and cirrus clouds, reduced soot emissions practically influence the contrail properties. If the number of soot particles is reduced, the AIC climate impacts is also reduced. However, for the simplified climate assessment methods, such as the ACT, there is no direct dependence between soot and AIC. Therefore, the AIC climate impacts for drop-in fuel blend and the PtL kerosene are not modified. At the same time, the uncertainties of a low soot combustion are quite high anyway, since the effects of reduced soot emissions on the contrail impacts are not totally understood.

The overall emission adjustments for the 50% drop-in fuel blend and the PtL kerosene are summarized in Table 13.

Table 13: Emission impacts for 50% Drop-In and PtL Kerosene compared to Jet A-1 fuel (Silberhorn, et al., 2022)

	CO_2	Soot	H_2O
50% Drop-In	50% * 98.989% = 49.495%	69%	106.315%
PtL	0%	38%	112.623%

To implement these values in the Python ACT, another CPACS input parameter (see chapter 3.2.4) is added where the fuel type, Jet A-1, Drop-in or SAF (i.e. 100% SAF), can be selected. If Jet A-1 is selected, the calculations do not change as the values used in the methods shown in chapter 3.2 are based on Jet A-1 fuel. If Drop-in or SAF is selected, the calculated emissions are adjusted according to the values in Table 13. Apart from these modifications, the other calculations for the ATRs remain unchanged.

4 Required Input Files for the Aircraft Climate Assessment

In the last chapter, the methods of the ACT and the Emission Inventory Generation Methodology were explained. To obtain the results of these tools, further input files are required, such as the flight schedule on which the Emission Inventory Generation Methodology can be based, and the aircraft types, from which the calculated trajectories are needed. These two required inputs are explained in the following.

4.1 Flight Schedule

The flight schedule used for this thesis is from the Bureau of Transportation Statistics (BTS) (BTS, 2019), which is part of the United States Department of Transportation. The BTS is a federal statistical agency and a preeminent source of commercial aviation statistics that provides context for decision makers and the public. The data used are monthly, domestic, and international data reported by certificated U.S. and foreign air carriers on passenger, freight, and mail transported. Flights with both origin and destination in a foreign country are not included. A flight plan from the United States was chosen because the parameters used in the ACT are also based on values from the United States and therefore it is more accurate to use similar flight paths and emission hotspots. The year 2019 was chosen for the study of the ATRs because it was important to take as late a year as possible due to the annual increase in air traffic. However, in 2020, the Covid pandemic began, which led to a collapse of the aviation sector that has not been fully cured to this day, which is why the data from these last years are not representative.

The database contains a variety of parameters such as flight time, available capacity, seats, and service class. Table 14 shows some selected parameters needed for the calculation of the ATRs, namely: the number of performed departures, the payload, the origin and the destination city and the aircraft type.

Table 14: Section of the flight plan by BTS (BTS, 2019)

Flight Plan				
Departures Performed	Payload	Origin	Destination	Aircraft Type
2	69200	PNS (Pensacola, FL)	MSY (New Orleans, LA)	612
2	69200	RDG (Reading, PA)	MCO (Orlando, FL)	612
3	103800	RIC (Richmond, VA)	BWI (Baltimore, MD)	612
1	43400	RSW (Fort Myers, FL)	FLL (Fort Lauderdale, FL)	614
1	43400	SAN (San Diego, CA)	RIC (Richmond, VA)	614

The payload is provided as the accumulated payload in pounds, which means that, for example, in row three, the payload of 69200lbs is the total payload for both departures performed. It is assumed that the payload is distributed evenly among the flights. A different table is given to identify the aircraft types, with each code listed in Table 14 corresponding to a specific aircraft type, e.g., aircraft type code 612 corresponds to a Boeing 737-700/700LR/Max 7.

4.2 Aircraft Types

The table with the aircraft types includes over 50 different common aircraft types. In order to limit the calculation time, the common aircraft types found in the given flight schedule were divided into short-, medium-, and long- range aircraft according to payload and range. Table 15, Table 16 and Table 17 show the classification of the aircraft types into short-, medium-, and long-range, with the corresponding aircraft code used in the flight schedule, as well as the maximum payload and range of each aircraft type. For each range, one typical aircraft type was defined and calculated using OpenAD (see chapter 3.1).

Table 15: Short-range aircraft types (Airbus, 2022) (Boeing, 2022)

Short-Range			
Aircraft Type	**Aircraft Code**	**Max. Payload [kg]**	**Max. Range [NM]**
A319	698	17690	3750
A320-100/200	694	19958	3300
A321-200	699	25401	3200
A319-200NEO	719	17690	3750
A320-200NEO	722	20003	3500
A321-200NEO	721	25492	3650
A220-100	723	15105	3450
A220-300	724	18688	3600
B737-100/200	620	15700	2600
B737-300	619	16892	2255
B737-400	617	18253	2060
B737-500	616	14769	2375
B737-600	615	14380	3235
B737-700	612	16505	3445
B737-800	614	20540	3085
B737-900	888	20240	3235

Table 16: Medium-range aircraft types (Airbus, 2022) (Boeing, 2022)

Medium-Range			
Aircraft Type	**Aircraft Code**	**Max. Payload [kg]**	**Max. Range [NM]**
B767-200	625	33271	3850
B767-200ER	625	35557	6385
B767-300	626	40030	4260
B767-300ER	626	43799	5990
B767-400ER	624	45813	5620
B757-200	622	21346	3900
B757-300	623	30686	3395
A330-300	687	45586	6350
A330-200	696	49396	8150
A330-900NEO	824	45813	7200
B787-8	887	41050	7305
B787-9	889	52617	7565
B787-10	837	57289	6330

Table 17: Long-range aircraft types (Airbus, 2022) (Boeing, 2022)

Long-Range			
Aircraft Type	**Aircraft Code**	**Max. Payload [kg]**	**Max. Range [NM]**
A350-900	359	53524	8100
A350-1000	836	68039	8700
A340-300	871	52163	7300
A340-500	872	53977	9000
A340-200	873	50802	6700
A340-600	874	66224	7800
A380-800	882	83915	8000
B747-100	816	76800	4620
B747-200/300	817	76360	6560
B747-400	819	70620	7260
B747-8	821	76067	7730
B777-200LR	627	63957	8555
B777-300	637	64047	6006
B777-300ER	637	69853	7370

Figure 10 shows the Available Seat Miles (ASM) over the distance for the flight data by the BTS for the year 2019. ASM is a measure of the airplane's carrying capacity and is calculated by multiplying the number of miles that a given airplane will be flying by the number of seats available for a given flight (Kagan, 2020).

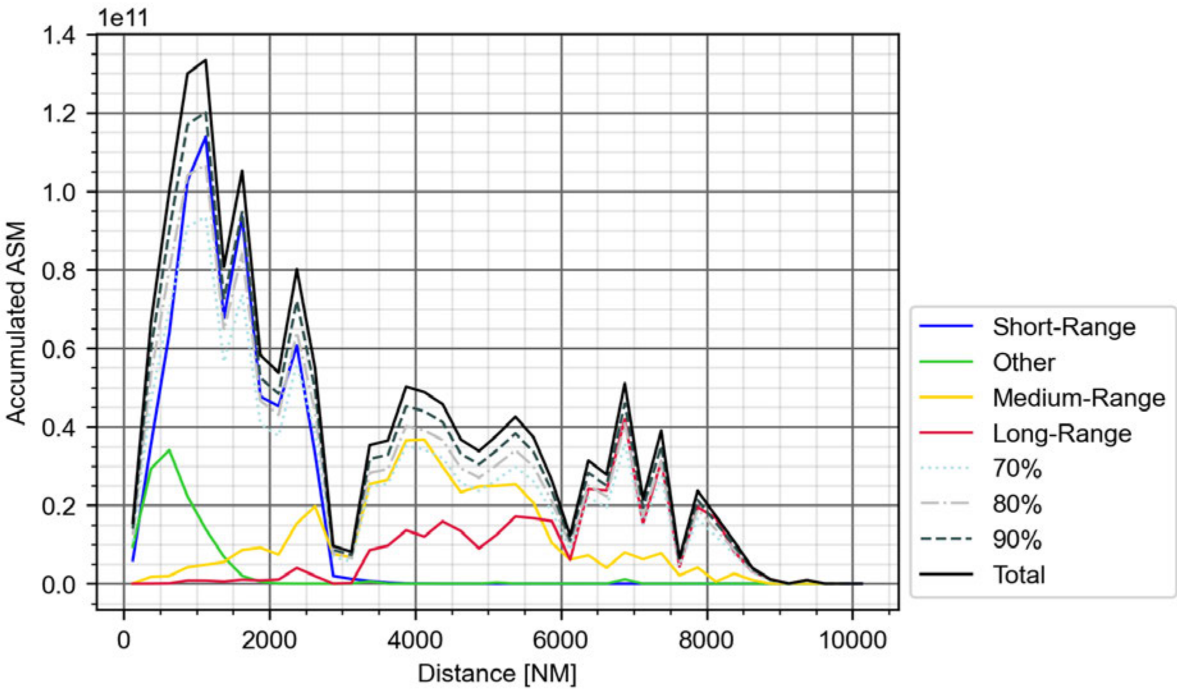

Figure 10: Available seat miles (ASM) for the flight data by BTS

The solid black line in Figure 10 corresponds to the total ASM. The first part of this solid black line from a range of 0NM to a range of about 3000NM corresponds to the short-range, the second part from about 3000NM to 6000NM corresponds to the medium-range and the third part from about 6000NM onwards corresponds to the long-range sector. The blue line represents the ASM for short-range, the yellow line represents the ASM for medium-range, and red line represents the ASM for long-range aircraft types according to the division in Table 15, Table 16 and Table 17. The black dashed line corresponds to 90%, the grey dot-dashed line corresponds to 80% and the light blue dotted line corresponds to 70% of the total ASM. It can be seen that the ASM of the short- and the long-range aircraft types account for about 80%, sometimes even up to 90%, of the total ASM. This is not quite true for the ASM of the medium-range aircraft types, whose ASM accounts for 60% to 70% of the total ASM, since some long-range aircraft types such as the A380 and the A340 also fly missions in the medium-range sector. The green line for the 'Other' aircraft types corresponds to propeller-driven aircraft and General Aviation aircraft. These aircraft types are not considered because flight times and ranges are mostly short and altitudes are low, so their climate impact is neglectable. Nevertheless, in Figure 10 it can be observed that the most important aircraft types are considered in the assessment of the climate impact.

The aircraft designed by DLR are based on the Airbus and Boeing Aircraft Manuals (Airbus, 2022) (Boeing, 2021). The short-range aircraft type is based on an A320 similar aircraft type, the medium-range on a B767 similar aircraft type and the long-range on an A350 similar aircraft type. In Table 18 the key aircraft characteristics, aircraft performance and mass estimates for the used aircraft types are shown.

Table 18: Key aircraft characteristics (Airbus, 2022) (Boeing, 2021)

Key Aircraft Characteristics				
Parameter	**Unit**	**Short-Range**	**Medium-Range**	**Long-Range**
Design Mission Range	NM	2935	3900	8207
Design Cruise Mach Number	-	0.78	0.8	0.85
Service Ceiling	ft	40000	41000	43000
Number of Passengers	-	180	261	315
Design Mission Payload	t	17.1	26.1	29.925
Max. Take-Off Mass	t	78.7	159.8	280
Max. Landing Mass	t	67.2	135.5	207
Max. Zero Fuel Mass	t	64.2	127	195.7
Operating Empty Mass	t	44.9	86.1	141.7
Max. Payload	t	19.3	40.9	54
Block Fuel (Design Mission)	t	19	40.56	113.68
Wing Span	m	35.8	47.57	64.75
Overall Length	m	37.57	54.94	66.8
Engine Type	-	Turbofan	Turbofan	Turbofan
Thrust (Sea Level Static, ISA)	kN	119.49	229.36	375.03
Thrust Specific Fuel Consumption	g/kN/s	54.06	65.94	53.1
Bypass Ratio	-	12.5	5.1	9.6

As can be seen in Table 18, the service ceiling increases from 40000ft for the short-range aircraft to 41000ft for the medium-range aircraft to 43000ft for the long-range aircraft, and so does the number of passenger from 180 for the short-range to 261 for the medium-range to 315 for the long-range aircraft. The maximum masses, the operating empty mass and the maximum payload are about twice as high for the medium-range aircraft and about three times as high for the long-range aircraft compared to the short-range aricraft. Wing span and overall length are about 17 m greater for the medium-range aircraft than for the short-range aircraft, while wing span and overall length increase by another 12 m for the long-range aircraft. All three aircraft have turbofan engines, and the thrust is twice as high on the medium-range aircraft and three times as high on the long-range aircraft as on the short-range aircraft. The two Airbus similar aircraft, short-, and long-range aircraft, have a much larger bypass ratio than the Boeing similar aircraft, medium-range aircraft. All performance data are calibrated for the design mission.

In Figure 11 the three used aircraft types, the short-range (see Figure 11(a)), the medium-range (see Figure 11(b)), and the long-range (see Figure 11(c)) with their approximate relation in size can be seen.

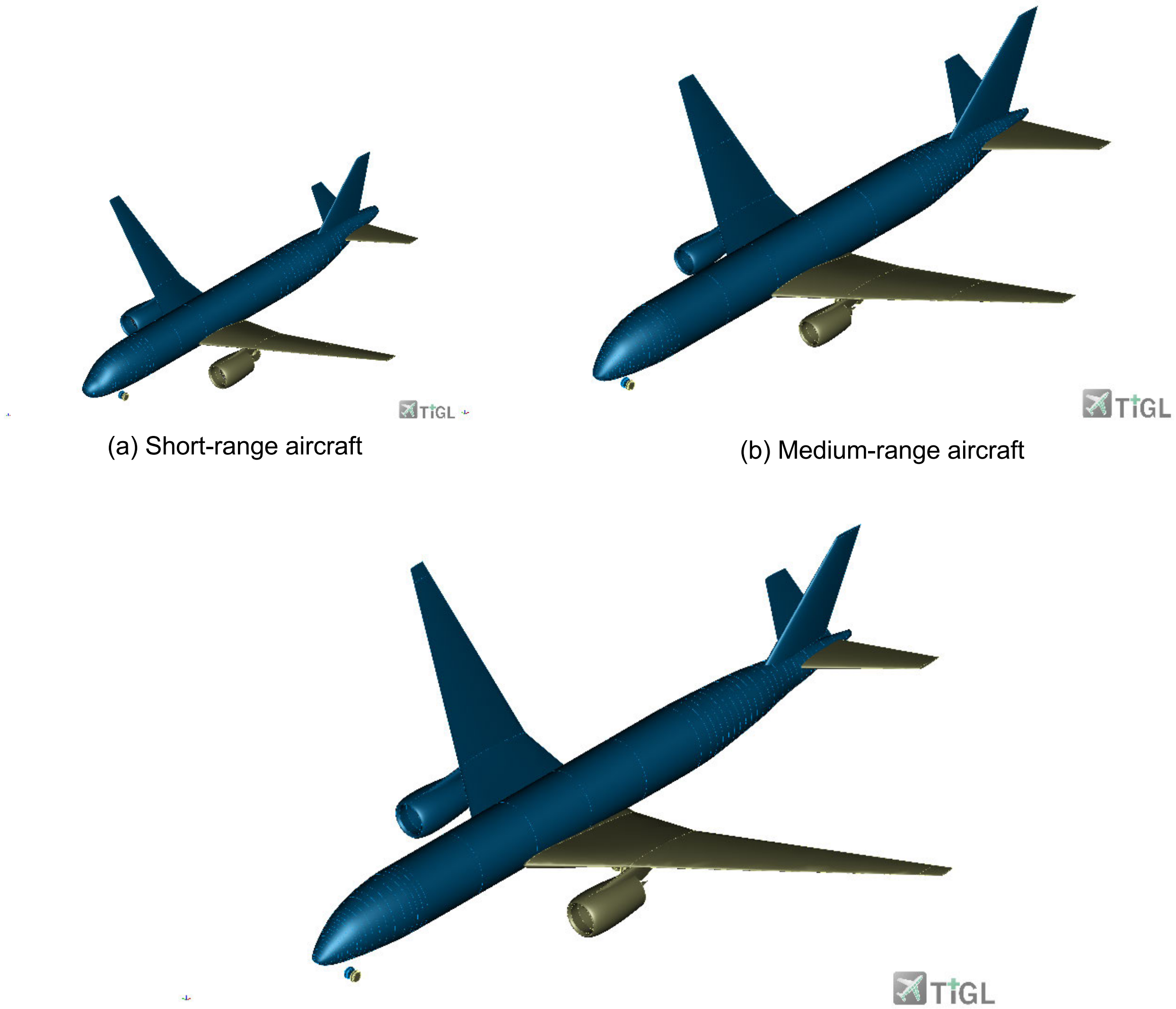

(a) Short-range aircraft

(b) Medium-range aircraft

(c) Long-range aircraft

Figure 11: View of the reference aircraft

Figure 12 shows the payload-range diagrams of the respective aircraft types. The short-range aircraft has a maximum payload of 19300kg and a maximum range of 8026.43km, the medium-range aircraft has a maximum payload of 40900kg and a maximum range of 9554.2km, and the long-range aircraft has a maximum payload of 54000kg and a maximum range of 17991.9km. Each light blue dot corresponds to a calculated trajectory of the respective aircraft, between which the missions of the flight schedule can be interpolated. The short-range aircraft type consists of

98 trajectories, the medium-range aircraft type of 125 trajectories, and the long-range aircraft type of 95 trajectories. It took approximately 9 hours to calculate the trajectories for each aircraft. This long calculation time shows the necessity of the interpolations. The considered aircraft types of the flight schedule consist of more than 260000 missions, and if each mission of the flight schedule would be calculated separately, it would take over a year.

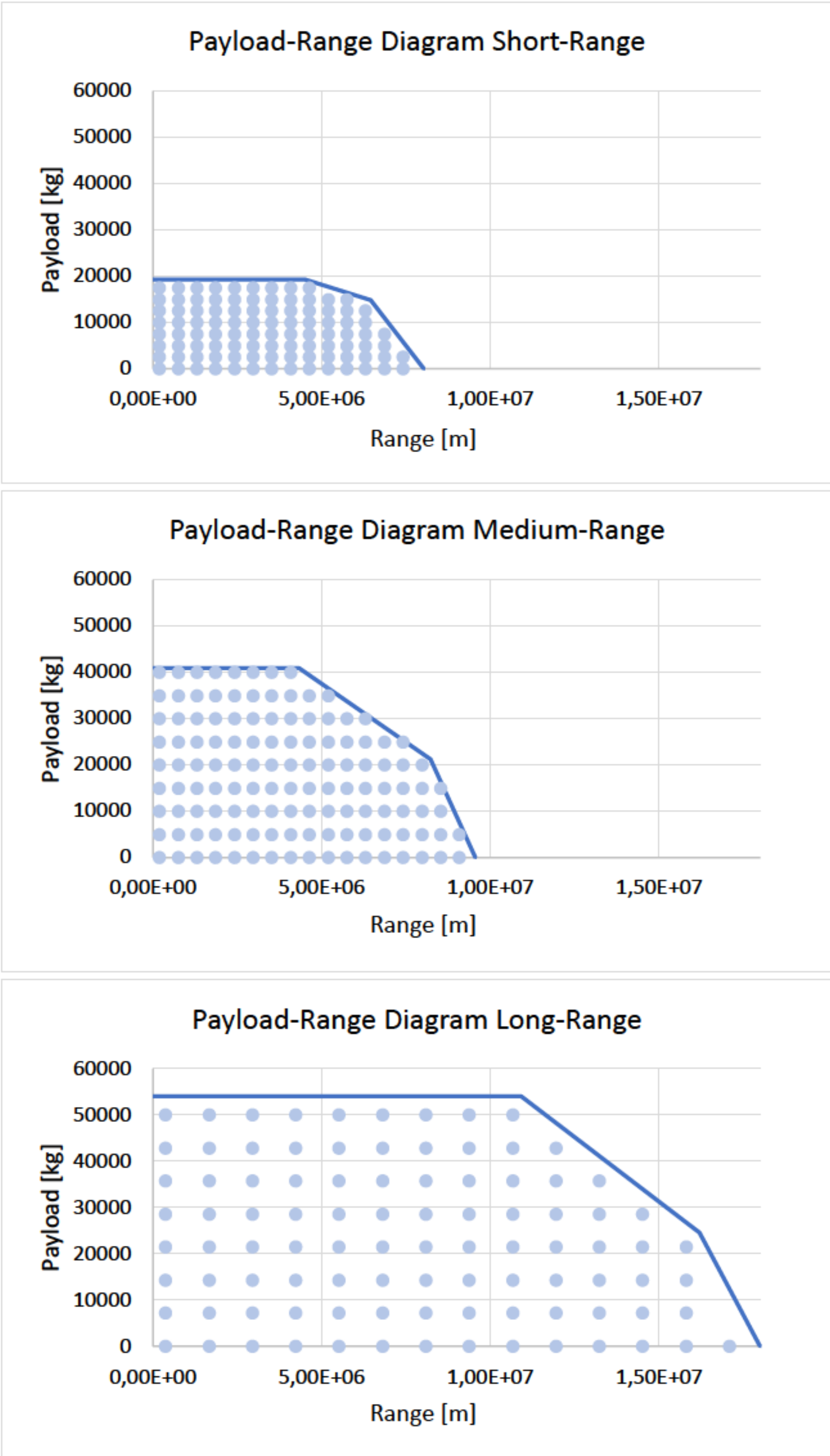

Figure 12: Payload-range diagram of the reference aircraft

5 Integration of the Flight Schedule and the Emission Inventories to ACT

Now that the different parts needed, the ACT and the Emission Inventory Generation methodology, are available, they can be combined into one Python tool and based on a flight schedule.

The process for calculating the ATRs from the flight schedule can be seen in Figure 13. First, the great circle distance (gc distance), the departures performed (U) and the payload of each mission of the aircraft types considered in the flight schedule must be determined, which are the inputs for the interpolations of the Emission Inventory Generation Methodology. The outputs of the Emission Inventory Generation Methodology, which are also some of the inputs required for the ACT are: the released species (e_i) of CO_2, H_2O, NO_x, SO_4, soot and $NO_{x\ cruise}$, the cruising range (L_{cruise}), and the vector with the cruising altitude time steps (cruise altitude). Finally, the outputs of the ACT are the RFs, the mean temperature change (mean TC) and the ATRs.

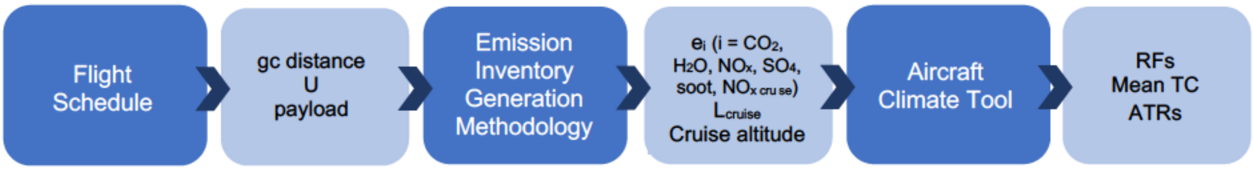

Figure 13: Path for the calculation of the ATRs

For the determination of the great circle distance, the performed departures, and the payload, first the flight schedule is imported into Python as csv-file. Then the aircraft type, the three letter codes of the origin and the destination cities, the payload and the departures performed are read out (see Figure 11). Subsequently, the corresponding row numbers in the flight schedule are determined for all considered aircraft types. Since the short-, medium- and long-range aircraft types have different payloads and ranges, they must be examined separately. Therefore, the aircraft types are divided into short-, medium- and long-range according to chapter 4.2 and the flight schedule row numbers of the corresponding aircraft types are merged into one list. In order to select whether the short-, medium- or long-range aircraft are considered, a new CPACS input parameter has been added (see chapter 3.2.4). This CPACS input parameter is called 'aircraft type' and allows the selection of 'short-range', 'medium-range' and 'long-range'.

With the help of the list, which summarizes the row numbers of the flight schedule of the short-, medium- and long-range aircraft under consideration, it is possible to determine the corresponding origin and destination cities, the performed departures and the payload of the aircraft types considered. These performed departures can already be used as input to the Emission Inventory Generation Methodology. Since the payloads are cumulative and expressed in pounds (see chapter 4.1), they must be divided by the departures performed and converted into kilograms and then serve as input. To calculate the great circle distance, the three letter codes of the origin and the destination cities of the flight schedule must be converted into coordinates. For this purpose, a database called 'airportcoordinates' has been created, in which coordinates are assigned to the three letter codes for most of the commercial airports. These coordinates can be used to calculate the great circle distances (see chapter 3.3.1), which then serve as input to the Emission Inventory Generation Methodology. Since the flight schedule contained some rows where the departures performed were zero or the origin and the destination city were the same, meaning that the great circle distance was zero, these rows had to be excluded from further calculations.

With the outputs of the flight schedule, the interpolations of the Emission Inventory Generation Methodology can be performed. Thereby, the released species of CO_2, H_2O, NO_x, SO_4, soot and $NO_{x\ cruise}$, the cruising distance, and the cruising altitudes are interpolated according to the payload and range, as shown in chapter 3.3.2. These interpolated values serve as input to ACT. In the ACT the RFs, the mean average temperature change and finally the ATRs are calculated according to the methodology presented in chapter 3.2.

6 Results

Since the ACT and the Emission Inventory Generation Methodology Tool are programmed and based on a flight schedule and any modifications required for the SAF are made, the results can be analyzed and compared. First, the results of the interpolations of the released emission species and of the cruising altitudes used in the Emission Inventory Generation Methodology to obtain a trajectory for each individual aircraft mission are regarded. Then, the results of the ACT, where only one mission is considered, and finally the results of the entire process based on a flight schedule for Jet A-1 fuel, 50% drop-in fuel blend, and 100% SAF are presented.

6.1 Results of the Interpolations

In order to base the ACT on a flight schedule, the interpolations of the released species (see chapter 3.3.2.1) and of the cruising altitudes (see chapter 3.3.2.2) were implemented. This enables each mission of the flight schedule to be interpolated between the existing trajectories. To evaluate these programmed interpolations, five trajectories with different ranges and payloads were selected in the payload-range diagram of the medium-range aircraft type, as shown by the red points in Figure 14. For these five trajectories, the results were first considered with the existing trajectories. Then the five trajectories were deleted and thus had to be interpolated between the existing trajectories. The two different results, of the existing trajectories and the deleted and thus interpolated trajectories, were compared.

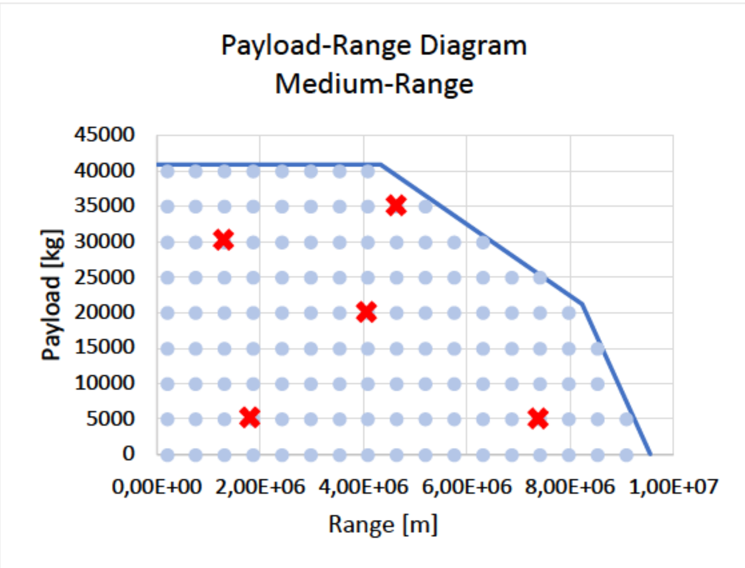

Number	Payload [kg]	Range [NM]
1	35000	2500
2	30000	700
3	20000	2200
4	10000	1000
5	5000	4000

Figure 14: Selected points to assess the interpolations

For the interpolations an already defined method in a Python package was used. It interpolates a 1-D function and takes arrays of values such as x and y to approximate a function y = f(x) (Kareko). This function can then be used to interpolate unknown y values with given x values. The type of the function, e.g. linear, quadratic and cubic, can also be specified. The interpolations of the released species were performed using three different interpolation methods: linear, quadratic, and cubic. These three interpolation methods were then assessed and compared to find the interpolation method with the least deviations. In the following, the deviations between the results of the existing trajectories and the results of the deleted trajectories for each interpolation method are shown.

Figure 15(a) shows the deviations of the released fuel corresponding to the released species of CO_2, H_2O, NO_x, SO_4 and soot, as the released fuel is simply multiplied by a certain factor to obtain the released amount of the other species mentioned. For all five points, the linear interpolation method has higher deviations than the quadratic and cubic methods, ranging from 0.1% to 0.38%. The deviations of the quadratic and cubic interpolation methods are all below 0.1%. For the first, third and fifth points, the deviations for the quadratic and cubic interpolation methods are the same, while for the second and fourth points, the quadratic interpolation method results in slightly less deviations than the cubic interpolation method.

A similar trend can be seen in Figure 15(b), where the deviations of the released amount of NO_x are shown. Again, the linear interpolation method has larger deviations than the quadratic and cubic interpolation methods for all five points, ranging from about 0.15% to 0.62%. The deviations of the cubic interpolation method for points one, three, four and five are less than 0.1%, with the second point having a deviation of 0.32%. The deviations of the quadradic interpolation method are all below 0.1%, but the cubic interpolation method for point one yields slightly smaller deviations than the quadratic one (0.03% to 0.01%). For the second, third and fourth points, the quadratic interpolation method has smaller deviations than the cubic method, and for the fifth point the deviations of the quadratic and the cubic interpolation methods are equal. For the interpolations of the released species, the quadratic interpolation method shows the least deviations overall.

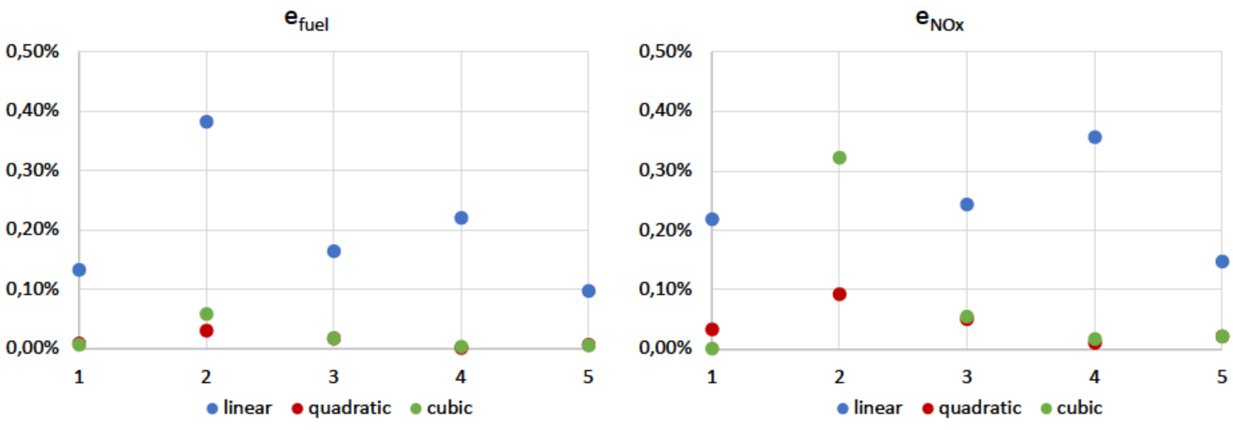

(a) Results for e_{fuel} (b) Results for e_{NOx}

Figure 15: Results of the interpolations for e_i (i = CO_2, H_2O, NO_x, SO_4, soot)

Next, the results of the interpolations of the cruising altitudes are compared. Since the equations of motion are solved and the performance data of the aircraft are calculated for each time step of the trajectories of the aircraft, a specific cruising altitude is calculated for each cruise time step. For the interpolations, it is counted how many time steps are flown at each cruising altitude, and then interpolated between these values (see chapter 3.3.2.2). Table 19 shows the results for the existing trajectories. Here, the second row shows all the cruising altitudes that occur in all the trajectories. Rows three through seven then show how many cruise time steps are flown at each cruising altitude for the given trajectories. These trajectories are then deleted, and Table 20 shows the number of cruise time steps at each cruising altitude for the deleted trajectories interpolated between the cruise time steps of the existing trajectories.

Table 19: Number of cruising altitude time steps with the existing trajectories

Results with existing trajectories						
Number	21000ft	31000ft	33000ft	37000ft	39000ft	41000ft
1	0	0	0	149	342	98
2	0	0	0	0	0	46
3	0	0	0	0	0	435
4	0	0	0	0	0	176
5	0	0	0	0	0	799

Table 20: Number of cruising altitude time steps with the deleted trajectories

Results with deleted trajectories						
Number	21000ft	31000ft	33000ft	37000ft	39000ft	41000ft
1	0	0	0	149	342	102
2	0	0	0	0	0	56
3	0	0	0	0	23	439
4	0	0	0	0	0	167
5	0	0	0	0	16	787

As can be seen in Table 19 and Table 20, the interpolations of the first, second and forth trajectory agree quite well with the existing trajectories, and only the cruising altitudes found in the existing trajectories appear in the results of the interpolations. However, in the interpolations of the third and fifth trajectories, time steps at the cruising altitude of 39000ft also appear, although only time steps at the cruising altitude of 41000ft occur in the existing trajectories. This is the case when, in the direction of the payload or in the direction of the range, the trajectory before or after the current trajectory has a step climb, but the current trajectory does not. This can be seen, for example, in Figure 16 for trajectory number five. Figure 16(a) shows the altitude profile of the existing trajectory with a range of 4000NM and a payload of 5000kg: There is only one cruising altitude of 41000ft. The same is true for the trajectory with the same payload of 5000kg, but with the next smaller range of 3700NM (Figure 16(b)) – only the cruising altitude of 41000ft occurs. However, for the trajectory with the same payload but with the next higher range of 4300NM (Figure 16(c)), there is a small cruising segment at an altitude of 39000ft. Thus, if the trajectory in Figure 16(a) with a range of 4000NM is deleted and must be interpolated between the two lower trajectories with ranges of 3700NM (Figure 16(b)) and 4300NM (Figure 16(c)), a few time steps result with a cruising altitude of 39000ft. The same is applicable for the third trajectory.

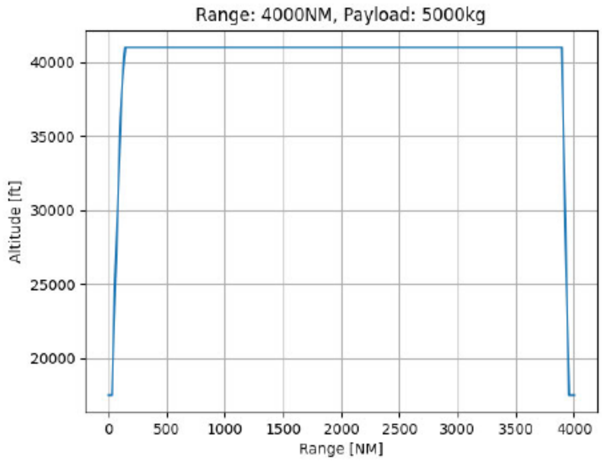

(a) Altitude profile for a range of 4000NM and a payload of 5000kg

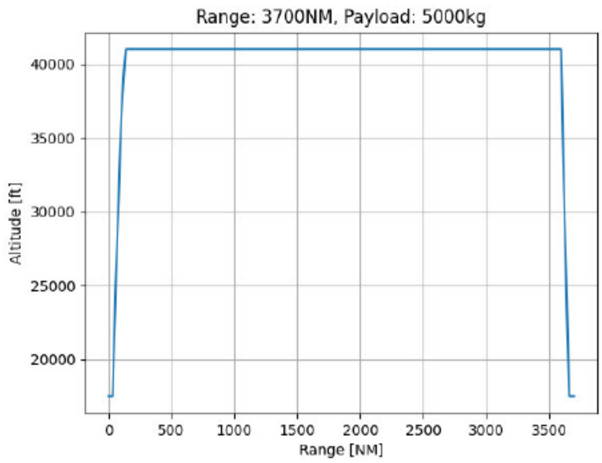

(b) Altitude profile for a range of 3700NM and a payload of 5000kg

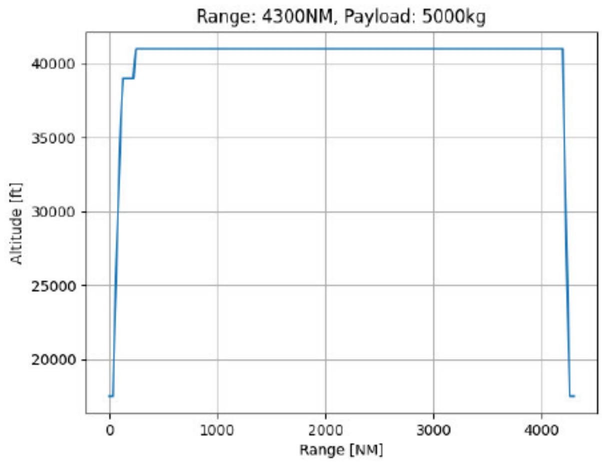

(c) Altitude profile for a range of 4300NM and a payload of 5000kg

Figure 16: Altitude profiles of the existing trajectories

The number of time steps during cruise also affects the results of the interpolations of the cruising distance (L_{Cruise}) and the released amount of NO_x during cruise ($e_{NOx\ Cruise}$). The deviations of the results for L_{Cruise} and $e_{NOx\ Cruise}$ can be seen in Figure 17. Except of point five, the cubic interpolation method shows larger deviations than the linear and quadratic interpolation methods, for point number two even up to 3.17% for L_{Cruise} and up to 4.05% for $e_{NOx\ Cruise}$. The linear interpolation method mostly achieves lower deviations than the quadratic method: Only for point one and five of the results for $e_{NOx\ Cruise}$ (Figure 17(b)) does the quadratic method achieve slightly lower deviations than the linear (0.07% to 0.22% for point one and 0.58% to 0.72% for point five). For the quadratic and the linear interpolation methods, point three shows the largest deviations of about 1.2% for L_{Cruise} and 2.14% for $e_{NOx\ Cruise}$ for the linear method. The reason why the deviations are the largest for point three is the larger total number of cruise time steps after the interpolation compared to the existing trajectory – there are 27 more cruise time steps after the interpolation, to be exact (see Table 19 and Table 20) Therefore, the cruising distance and the amount of NO_x released during cruise are larger, resulting in greater divergence. For the other four trajectories, the maximum spread between the number of the existing cruise time steps and the number of the interpolated cruise time steps is ten (see Table 19 and Table 20). Therefore, the deviation of the cruising distance and the amount of NO_x released during cruise between the existing and the interpolated values is smaller for the other four points and the deviations of the linear and the quadratic methods for these points are all below 1%.

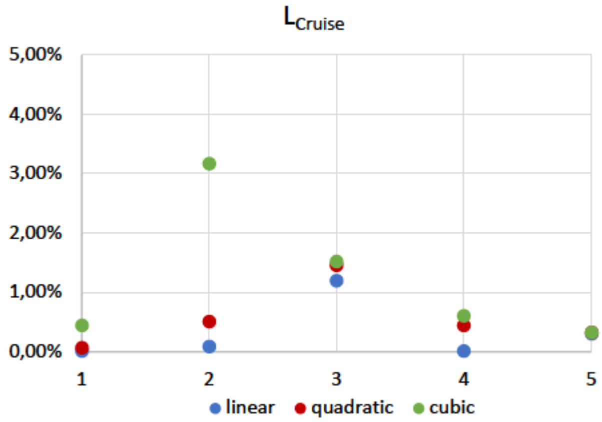

(a) Results for L_{Cruise}

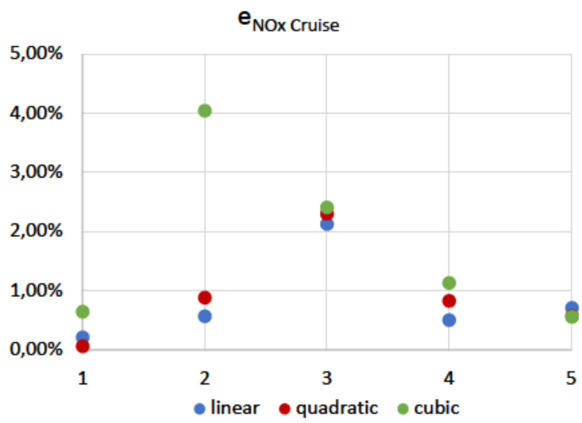

(b) Results for $e_{NOx\ cruise}$

Figure 17: Results of the interpolations for L_{cruise} and $e_{NOx\ cruise}$

The results shown in the previous tables and figures (Figure 15, Table 19, Table 20, Figure 17) represent the divergence between the existing and the interpolated trajectories for the ACT input parameters. Figure 18 now shows the influence of the deviations of the input parameters on the output parameter ATR.

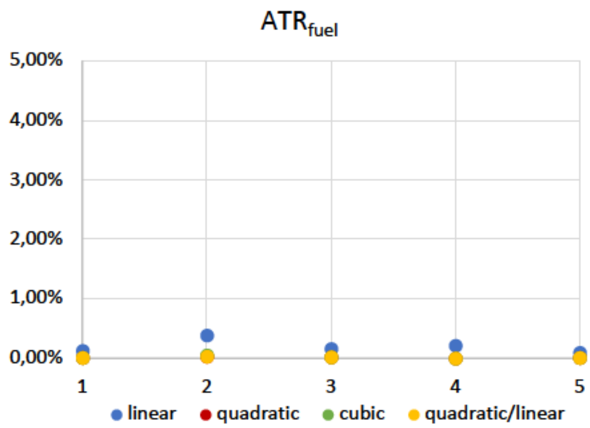

(a) Results for the ATR of fuel

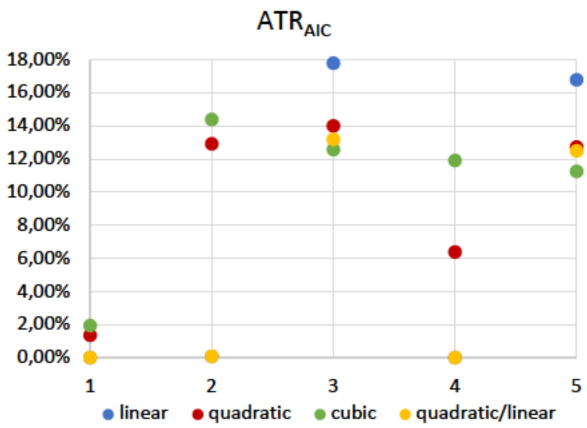

(b) Results for the ATR of AIC

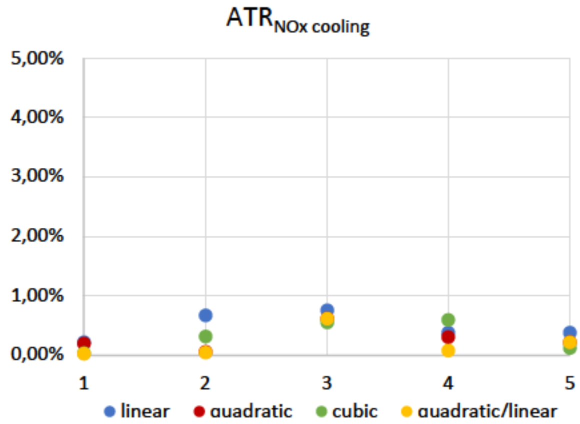

(c) Results for the ATR of $NO_{x\ cooling}$

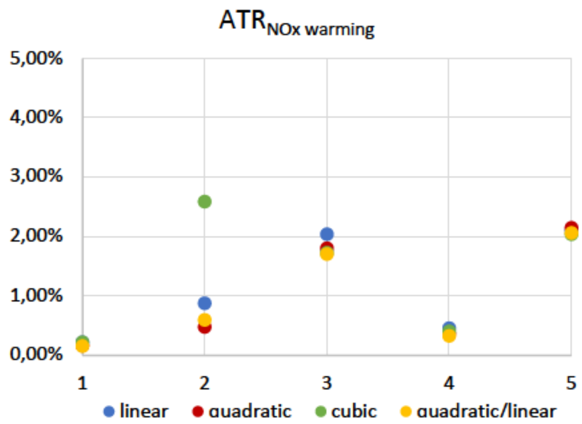

(d) Results for the ATR of $NO_{x\ warming}$

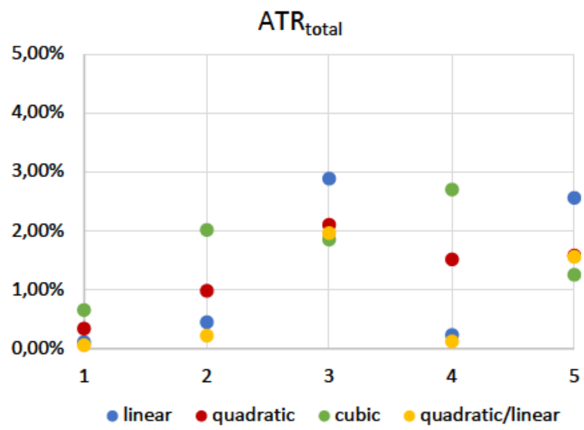

(e) Results for the total ATR

Figure 18: Results of the interpolations for the ATRs

In addition to the linear, quadratic, and cubic interpolation methods, there is now a fourth, linear and quadratic. This fourth method means that the released species of CO_2, H_2O, NO_x, SO_4 and soot are interpolated quadratically, since these results show the least deviation. The cruising altitude, the cruising distance, and the amount of NO_x released during cruise are linearly interpolated.

Figure 18(a) shows the deviations of the ATR of fuel, which corresponds to the deviations of the ATR of CO_2, H_2O, NO_x, SO_4 and soot. Since the linearly interpolated parameters are not relevant for the calculation of the ATR_{fuel}, quadratic/linear is equivalent to quadratic. The quadratic/ linear interpolation method shows the smallest deviations, less than 0.3%. The ATR calculation of $NO_{x\ cooling}$ (Figure 18(c)) and of $NO_{x\ warming}$ (Figure 18(d)) includes the cruising altitudes and the amount of NO_x released during cruise. These two input parameters have larger deviations after the interpolations than the released fuel, which is needed to calculate ATR_{fuel}. Therefore, the deviations of $ATR_{NOx\ warming/\ cooling}$ are larger than the deviations of ATR_{fuel}. Nevertheless, the deviations of $ATR_{NOx\ cooling}$ are still less than 1% and the deviations of $NO_{x\ warming}$ are less than 3%. For points three and five in Figure 18(c), the cubic interpolation method shows slightly smaller deviations than the quadratic/ linear method (0.62% to 0.56% for point three and 0.22% to 0.12%

for point five). For the other three points the quadratic/ linear interpolation method shows the smallest deviations. In Figure 18(d), the quadratic method has a slightly smaller deviation than the quadratic/ linear method for the second point (0.6% to 0.48%), and the cubic method has a smaller deviation than the quadratic/ linear method for the fifth point (2.04% to 2.07%). For the other three points, the quadratic/ linear method again achieves the lowest deviations. Figure 18(b) shows the deviations of the ATR of AIC, in whose calculation the cruising altitudes and the cruising distance are included. The quadratic/ linear method achieves small deviations of less than 0.1% for points one, two, and five. However, the deviations for points three and five, which are on the edge of a step climb, are high, reaching about 18%. For those two points the quadratic/ linear method achieves the second smallest deviations, and the cubic method achieves the smallest deviations. In Figure 18(e), all the ATRs are combined to form the total ATR. For points one, two and five, the smallest deviations are again obtained using the quadratic/ linear method and they are less than 0.3%. Points three and five have larger deviations, with the cubic method achieving the smallest deviations of 1.86% (point three) and 1.25% (point five). The quadratic/ linear interpolation method reaches slightly higher deviations of 1.96% (point three) and 1.56% (point five). Since, except of points three and five of the ATR_{AIC} (Figure 18(b)), all the deviations of the results are below 3%, with the deviations for $ATR_{NOx\ cooling}$ and ATR_{fuel} even below 1%, the interpolations are considered sufficient for the climate assessment for conceptual aircraft design.

6.2 Results of the ACT

To compare the results of the ACT, a medium-range aircraft type mission was used as a reference. The flight profile of this mission is shown in Figure 19. It has a range of d = 1900NM, an initial cruising altitude of h_0 = 39000ft, and a final cruising altitude of h_f = 41000ft. The total mission fuel consumption is W_{fuel} = 19306.7kg and the payload is payload = 26100kg. An operational lifetime of H = 30 years, a maximum integration window of t_{max} = 100 years, a number of flown missions per year of U = 10000, a distance flown per year of L = 37e6NM, and a devaluation rate of r = 0% were used as input parameters for this mission. To analyze the impact of the different input parameters, the payload and the range, only one parameter was changed at a time and the effects on the ATRs were considered.

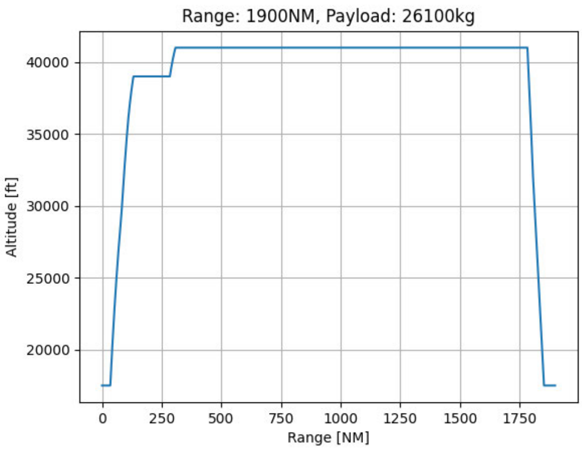

Figure 19: Altitude profile of the reference mission

The flight profile shown in Figure 19 leads to the results shown in Figure 20. On the left side, the temperature change over the time is shown. It can be seen that the short-lived impacts, SO_4, soot, H_2O, NO_x warming and AIC, decline rapidly after the end of the aircraft's operational life. The long-lived impacts, CO_2 and CH_4 and O_{3L}, which are combined in $NO_{x\ cooling}$, remain in the atmosphere longer and decline more slowly. The right side in Figure 20 shows the total ATR and the ATR of the different emissions.

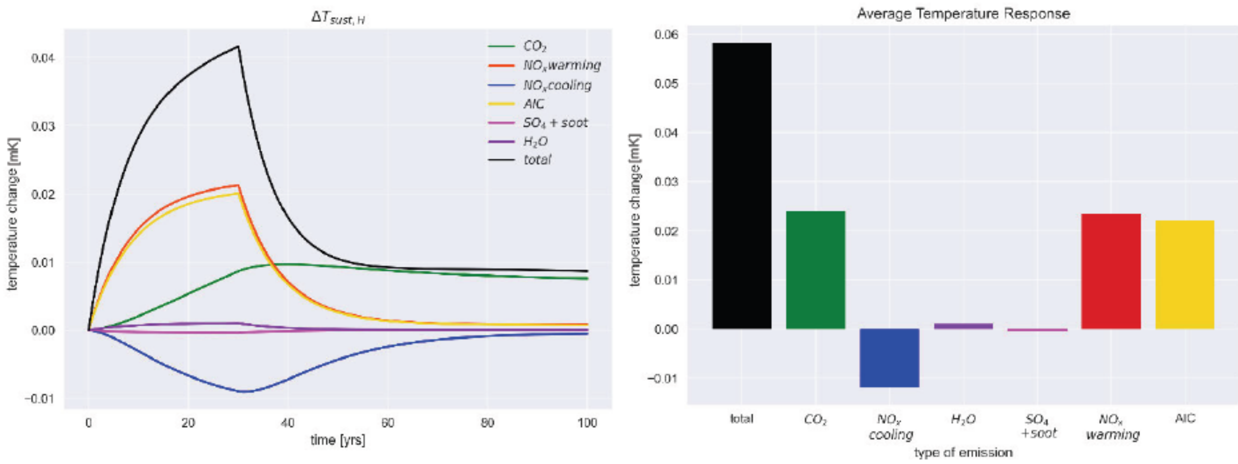

Figure 20: Temperature change and ATR of the reference mission

First, it is analyzed how the ATR responds when the flight distance is changed from 1900NM to 3800NM and 1000NM. The flight profiles for these two new missions are shown in Figure 21. The flight profile for the 3800NM (Figure 21(a)) has an initial cruising altitude of h_0 = 37000ft, followed by two step climbs to the final cruising altitude of h_f = 41000ft. The total mission fuel consumption is W_{fuel} = 39423.9kg, which is slightly more than double the reference mission. The flight profile for 1000NM (Figure 21(b)) has one only cruising altitude of h_0 = h_f = 41000ft and a total mission fuel consumption of W_{fuel} = 10696.1kg, which is slightly more than half of the reference mission.

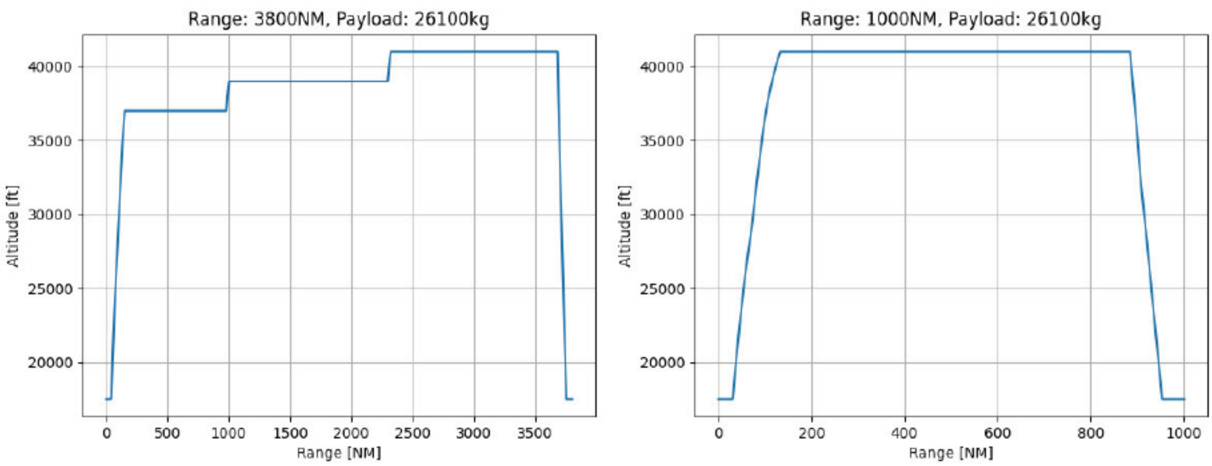

(a) Altitude profile for a range of 3800NM and a payload of 26100kg

(b) Altitude profile for a range of 1000NM and a payload of 26100kg

Figure 21: Altitude profile of two missions with different ranges

The ATRs for these three different ranges can be seen in Figure 22. First, onto the 3800NM mission. Since the total mission fuel consumption is approximately twice the total mission fuel consumption of the reference mission, the ATRs of CO_2, H_2O, SO_4, and soot are also approximately twice as high. This is due to the fact that the emissions, and therefore the climate impacts, are proportional to the fuel consumed. However, the ATR of AIC is not proportional to the fuel consumed, but to the total distance flown per year, L. This parameter was not changed, but the ATR of AIC still increased. This is because the model used here includes the altitude variations for AIC implemented by the altitude-dependent forcing factors. As can be seen in Figure 7, AIC has a greater climate impact between the altitudes of 28000ft and 39000ft. In the reference mission, the initial cruising altitude is 39000ft, which is in a sector where the climate impact of AIC is no longer as large. In the 3800NM mission, the initial cruising altitude is 37000ft and thus in a sector where the climate impact of AIC is greater, increasing the ATR of AIC. Another reason for the increase of the AIC's ATR is that the ratio between the cruising distance and the total distance is higher, which means that the cruising segment has a larger share in the total mission. This ratio is used to calculate the AIC average forcing factor, and the forcing factor, and thus the climate impact, increases as this ratio increases (see chapter 3.2.3). The $NO_{x\ cooling}$ and $NO_{x\ warming}$ climate impacts also increase with increasing fuel consumption, but because of the altitude-dependent forcing factors that account for the altitude variation of NO_x, this increase of ATR_{NOx} is not proportional to the fuel consumption. The NO_x average forcing factor increases as the proportion of the NO_x emissions during cruise to the NO_x emission during the whole mission increases. Nevertheless, the general trend of the NO_x average forcing factors is that they increase with altitude.

Compared to the 1000NM mission, where the total mission fuel consumption is about 55% of the reference mission, the ATRs of CO_2, H_2O, SO_4, and soot are also about 55% of the reference mission, as these emissions are again proportional to the fuel consumed. The ATR of AIC decreases because, first, the cruising altitude is now 41000ft and in this segment the impact of AIC is lower, and second, the ratio between the cruising distance and the total distance used to calculate the forcing factor is lower compared to the reference mission. $NO_{x\ warming}$ and $NO_{x\ cooling}$ decreases mainly due to the lower fuel consumption, but again not proportionally because of the forcing factors.

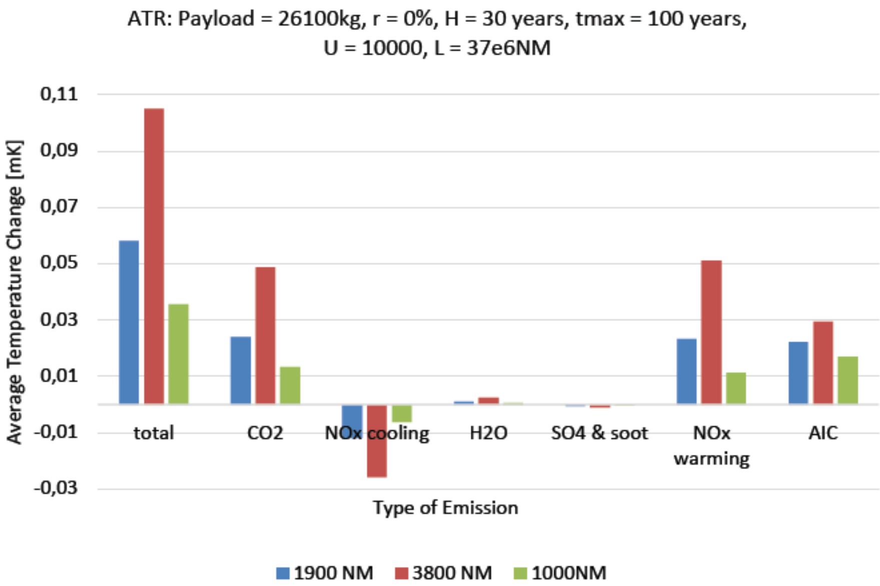

Figure 22: ATRs of different ranges

The second parameter changed is the devaluation rate r, which is applied to the temperature change at the end of the aircraft's operational lifetime. Increasing the devaluation rate primarily discounts the long-term impacts after the end of the aircraft's operational lifetime. This way, the long-term climate impacts are accounted for in the ATR, but do not dominate it. Figure 23 shows the temperature change over time for a devaluation rate of r = 3%. It can be observed that now especially the long-term climate impacts, $NO_{x\ cooling}$ and CO_2, decrease significantly faster after the end of the aircraft's operational lifetime of 30 years than in the reference mission in Figure 20 with r = 0%.

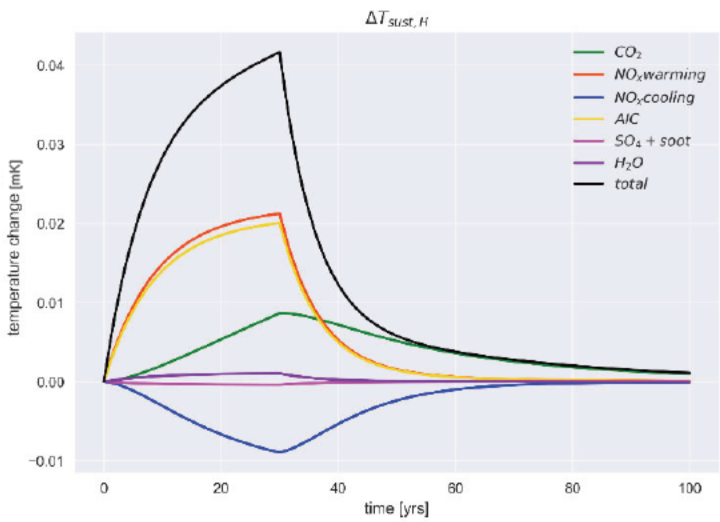

Figure 23: Temperature change for a devaluation rate r = 3%

The ATRs for a devaluation rate of r = 0%, r = 1% and r = 3% can be seen in Figure 24. The short-lived climate impacts, SO_4, soot, H_2O, $NO_{x\ warming}$ and AIC, which decline quite rapidly after the aircraft's operational lifetime, are reduced by 4.2% for a rate of 1% and by 9.7% for a rate of 3%

compared to the reference mission. $NO_{x\ cooling}$ which has a longer lifetime than the short-lived impacts, is reduced by 10.4% for a rate of 1% and by 21.8% for a rate of 3%. The ATR of CO_2, which remains in the atmosphere the longest, is reduced by 22.6% for a rate of 1% and by 47% for a rate of 3%. The total ATR is reduced by 10.7% for a rate of 1% and by 22.6% for a rate of 3%. Thus, the higher the devaluation rate, the more the short-term impacts dominate the total ATR.

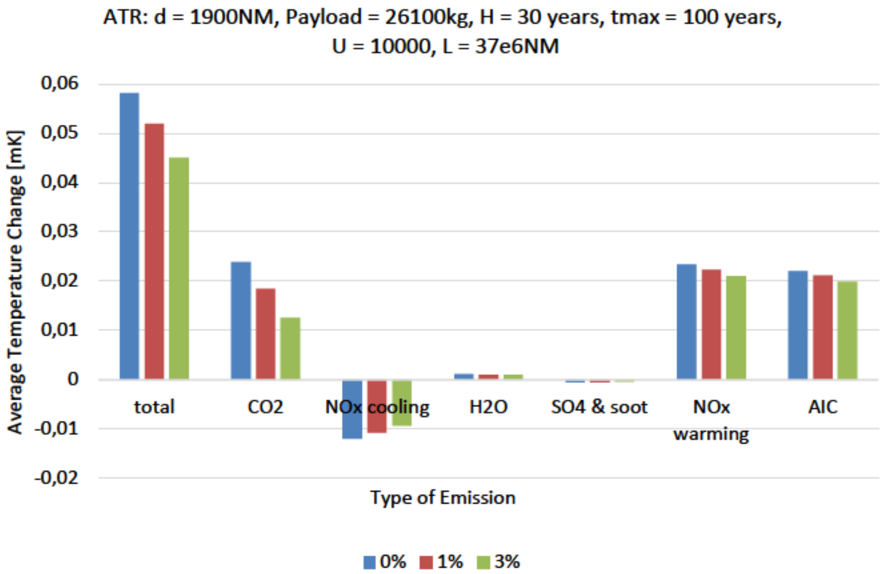

Figure 24: ATRs of different devaluation rates

The third parameter changed is the number of maximum observed years, t_{max}. In Figure 25, the temperature change over time for t_{max} = 300 years is shown. It can be observed that a significant fraction of the CO_2 emissions is still in the atmosphere after 300 years and is decreasing very slowly, while the other emissions have decreased to almost zero. This shows that especially the long-term impact, CO_2, becomes more important when the number of maximum observed years is increased. It also demonstrates the importance of a finite time window, defined by the maximum observed years, since a fraction of CO_2 emissions remains in the atmosphere for many thousands of years.

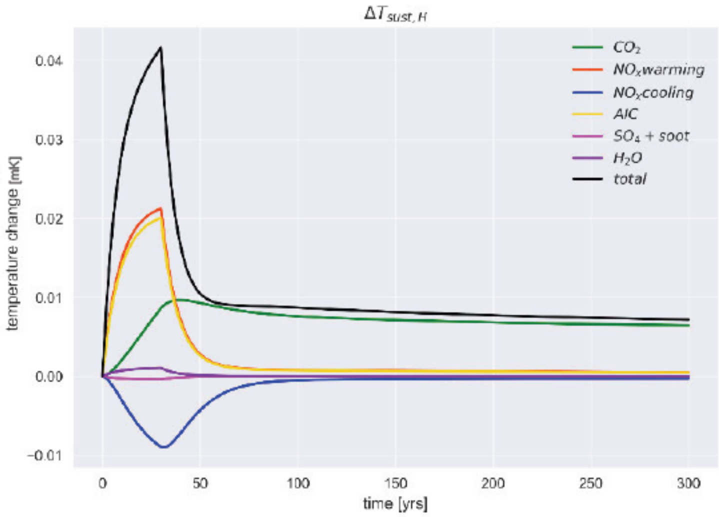

Figure 25: Temperature change for maximum considered years t_{max} = 300 years

Figure 26 shows the ATRs for t_{max} = 100 years, t_{max} = 300 years, and t_{max} = 500 years. The short-lived impacts, which decline quite rapidly after the end of the aircraft's operational lifetime, increase by 18% and 29%, for t_{max} = 300 years and t_{max} = 500 years, respectively. Similarly, $NO_{x\ cooling}$, which has a longer lifetime than the short-lived impacts but declines much faster than CO_2, is increased only by 19% for t_{max} = 300 years and by 31% for t_{max} = 500 years. CO_2, which remains in the atmosphere by far the longest, is increased by 192% for t_{max} = 300 years and by 367% for t_{max} = 500 years. The total ATR is increased by 89% for t_{max} = 300 years and by 167% for t_{max} = 500 years. Therefore, the larger the maximum years considered, the more the total ATR is dominated by the long-term impacts.

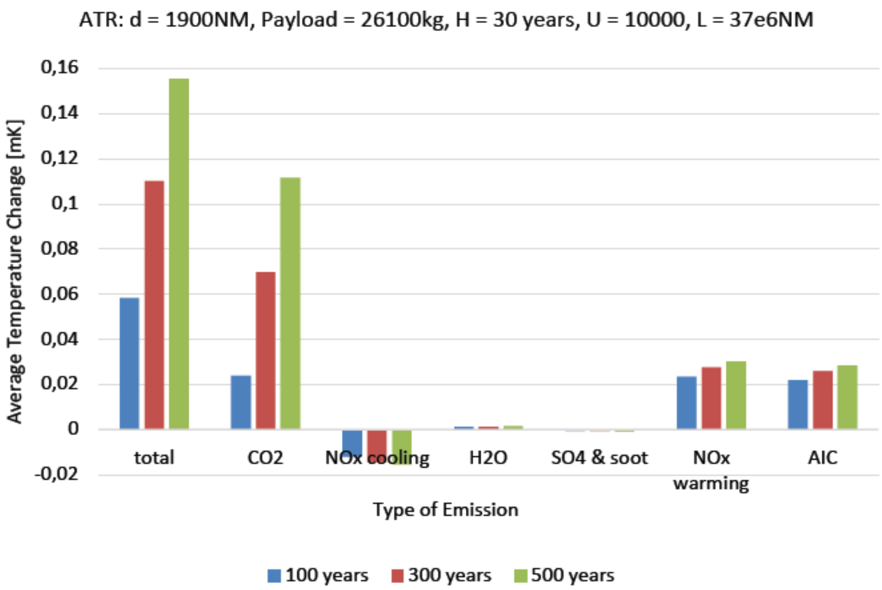

Figure 26: ATRs of different maximum considered years

Next, the operational lifetime is changed from H = 30 years to H = 20 years and H = 40 years. In Figure 27 the temperature change over time for H = 40 years can be seen. Since H = 40 years means that the aircraft will be operated for 40 years, after which no more emissions will be emitted, the peak temperature change of the different emissions shifts from 30 years to 40 years and then the emissions are dissipating again.

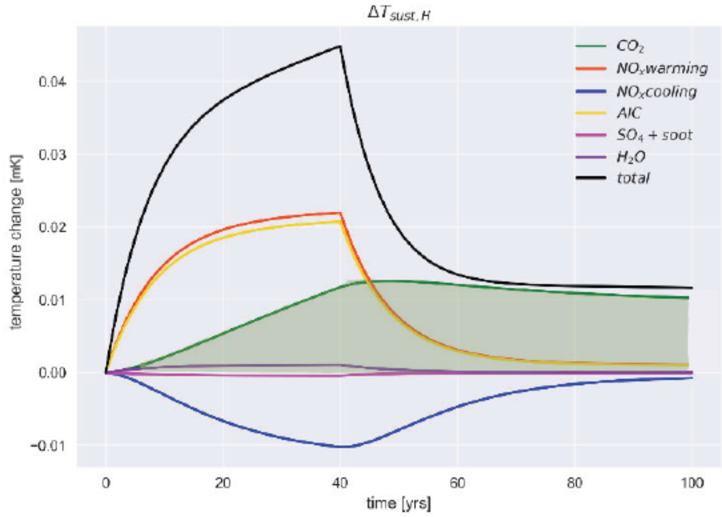

Figure 27: Temperature Change for an operational lifetime H = 40 years

In Figure 28, the ATRs for H = 30 years, H = 20 years and H = 40 years are shown. The ATR is calculated by integrating the weighted temperature change to determine the total lifetime impact in units of mK · yr, which for CO_2, for example, is represented by the green shaded area in Figure 27. This quantity is divided by the operational lifetime of the aircraft to find the ATR (see chapter 3.2.3). This way, an average temperature is determined, and therefore the ATR of the short-lived impacts and of $NO_{x\,cooling}$, which also decrease rapidly compared to CO_2, deviate from the reference mission by less than 1%. However, the ATR of CO_2 can be distinguished between the different operational lifetimes. A higher aircraft's operational lifetime of H = 40 years means that the peak temperature of CO_2 shown in Figure 27 is slightly higher than for the reference mission with H = 30 years (see Figure 20) (approximately 0.01mK for H = 30 years to 0.012mK for H = 40 years), because the aircraft is now emitting emissions continuously for 40 years, not just for 30 years. But, as the CO_2 emissions slowly decline, the percentage increase of the integrated temperature change in the fraction numerator is smaller than the percentage increase from 30 years to 40 years in the fraction denominator of the ATR calculation. Therefore, the ATR of CO_2 decreases by approximately 5% for H = 40 years. For H = 20 years, the ATR of CO_2 increases by approximately 5%. The total ATR is about 2.5% higher for H = 20 years and 2.5% lower for H = 40 years.

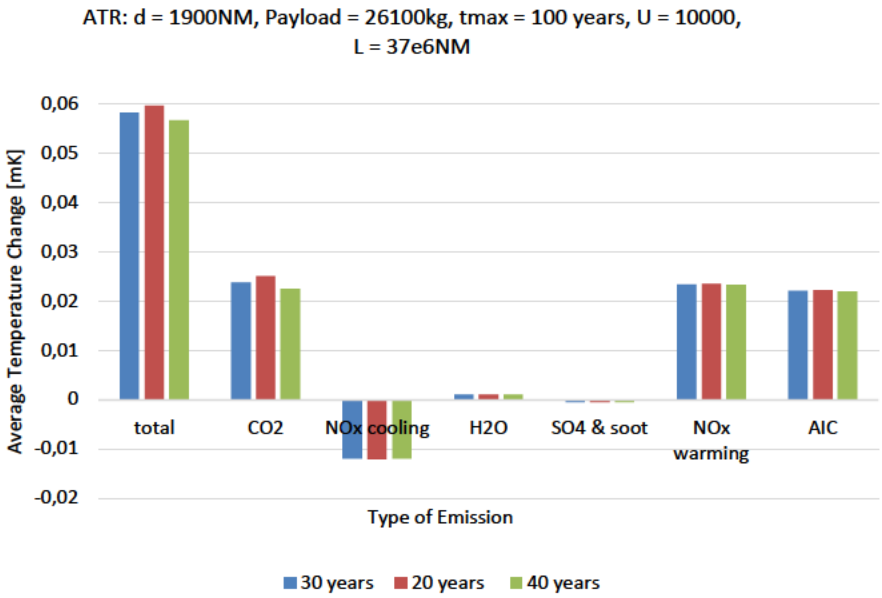

Figure 28: ATRs of different operational lifetimes

Next, the number of missions flown per year, U, is changed. If the number of missions flown per year is doubled, the ATRs of CO_2, $NO_{x\ cooling}$, H_2O, SO_4, soot, and $NO_{x\ warming}$ also double, because they are proportional to U, and if U is halved, these ATRs also halve, as shown in Figure 29. The ATR of AIC does not change with U because it is proportional to the total flight distance per year L and not to the number of missions per year U. The total ATR increases by 62% for U = 20000 missions and decreases by 31% for U = 5000 missions.

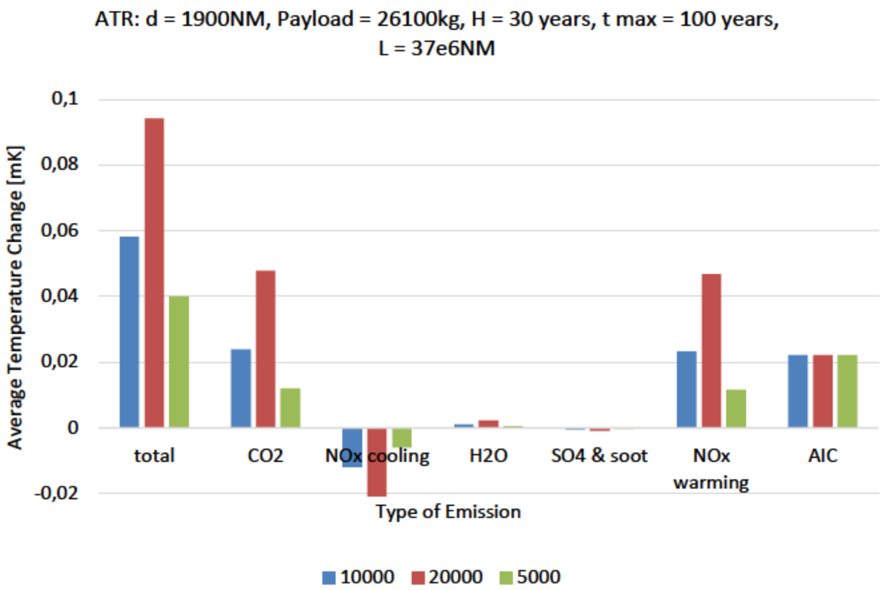

Figure 29: ATRs of different amounts of flown missions per year

The payload can also be changed. When the payload is changed to the next higher payload of 30000kg and the next lower payload of 20000kg, the most significant change is that more fuel is needed for the higher payload and less fuel is needed for the lower payload. Again, the ATRs of CO_2, H_2O, SO_4, and soot increase/ decrease in proportion to the fuel consumed. The ATRs of $NO_{x\ cooling}$, $NO_{x\ warming}$ and AIC do not change proportionally to the fuel consumed due to the forcing factors, as the step climb to 41000ft comes faster for the lower payload and slower for the higher payload than for the reference mission. The results of the different payloads can be seen in Figure 30.

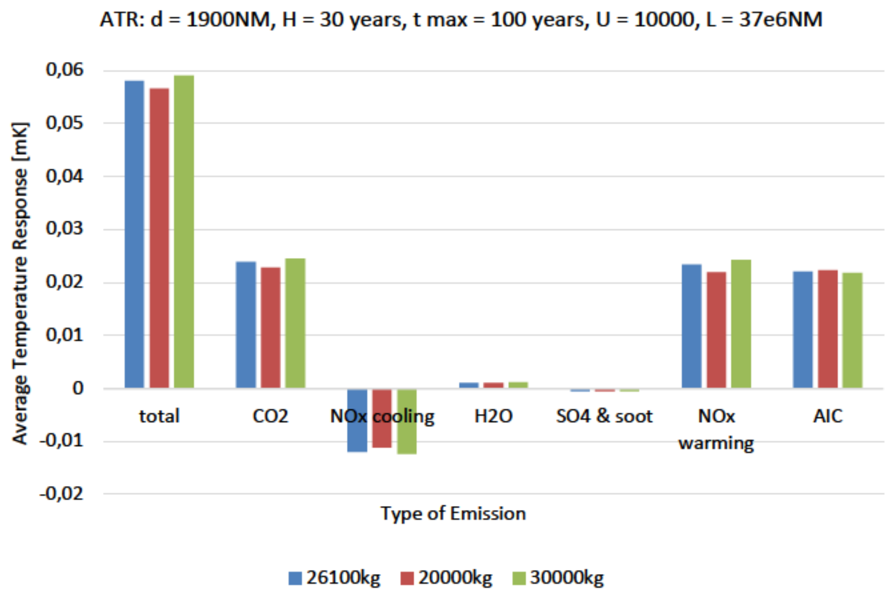

Figure 30: ATRs of different payloads

The last parameter that can be changed is the total distance flown per year L. Since this parameter is only proportional to the climate impact of AIC, the ATR of AIC changes proportionally to L.

As seen in Figure 22 through Figure 30, changing an input parameter can change which emission, short-term, long-term, or AIC, is focused on. This can significantly alter the results of the ATRs. Here, an operational lifetime of H = 30 years was chosen as this is considered the operational lifetime of a typical commercial aircraft (Dallara, 2011) However, other operational lifetimes could be considered for different aircraft design applications, with aircraft operational lifetimes typically ranging between 25 and 35 years. Furthermore, t_{max} = 100 years was chosen as the maximum considered years, as this time period was adopted by the United Nations Framework Convention on Climate Change for the Kyoto Protocol (Fuglestvedt, et al., 2010). However, setting a maximum time horizon for the inclusion of climate impacts also affects the balance between the short-lived and the long-lived impacts. Because the short-lived species decay quickly after the end of the aircraft's operational lifetime, but the long-lived impacts decay slowly, a long maximum time horizon favors the long-lived impacts, as shown in Figure 28. A short time horizon biases towards the short-lived species. Another value often taken as maximum considered years is t_{max} = 500 years, as this is the longest time horizon adopted by the IPCC (IPCC, 2007). The devaluation rate also affects the importance between the short-lived and the long-lived impacts. Here, a devaluation rate of r = 0% is used, so the short-term and long-term impacts are weighted equally. With larger devaluation rates, the temperature change of each year after the end of the aircraft's operation is less important than the temperature change experienced the previous year. In aircraft design studies, devaluation rates of r = 0% and r = 3% are usually considered (Dallara, 2011). For devaluation rates of r = 3% or greater, an infinite time horizon ($t_{max} = \infty$) is possible. Since the selection of the input parameters involves a value judgement of the relative importance of the short-lived and long-lived impacts, an aircraft design metric should be flexible and allow the user to specify it (Dallara, 2011). It should also be possible to represent the typical operation of a particular aircraft. This is achieved by being able to specify the reference mission, e.g. the payload or range, as well as the number of missions and the flight distance per year. However, it is important not to change the different input parameters when comparing two or more aircraft technologies or design options. Only then a fair comparison can be achieved.

6.3 Climate Impact of Jet A-1 Fuel, Drop-In Fuel Blend and SAF

For the comparison of the climate impacts of Jet A-1 fuel, drop-in fuel blend, and SAF, the combined ACT and the Emission Inventory Generation Methodology Tool based on a flight schedule was used. The input parameters used were an operational lifetime of H = 30 years, a maximum integration window of t_{max} = 100 years, and a devaluation rate of r = 3%. Since the climate impacts of the different input parameters, the payload and the range have already been analyzed in the last section, the focus is now on comparing the climate impacts of Jet A-1 fuel, drop-in fuel blend and SAF. Since very few studies calculate the climate impacts using the ATR, no total values for the ATRs for an entire fleet were available. However, the method used in the ACT was validated in Dallara's PhD (Dallara, 2011) and no changes were made to the formulas used therein.

First, the medium-range aircraft type is considered, for which a B767 similar aircraft type is used. In the medium-range, there are a total of 50033 mission and the total ATR for Jet A-1 fuel is 1.29mK, as can be seen in Figure 31. CO_2, AIC, and the total NO_x impacts ($NO_{x\ warming}$ and $NO_{x\ cooling}$ together) contribute about equally to the total ATR, with the climate impact of H_2O and SO_4, and soot being rather small. When the drop-in fuel blend is used, the ATR of CO_2 decreases by 50.505%, the ATR of soot decreases by 31%, and the ATR of H_2O increases by 6.315%. Soot leads to a small warming impact, while SO_4 leads to a cooling impact. Thus, when the impact of soot is reduced, the ATR of SO_4 and soot leads to a greater cooling impact. The total ATR of the drop-in fuel blend is reduced by 17.6% to 1.06mK. For 100% SAF, CO_2 emissions are reduced to zero, H_2O emissions are increased by 12.623%, and soot emissions are reduced by 62%. The total ATR of SAF is now 0.84mK, 34.9% lower than the total ATR of Jet A-1 and 21% lower than the total ATR of the drop-in fuel blend.

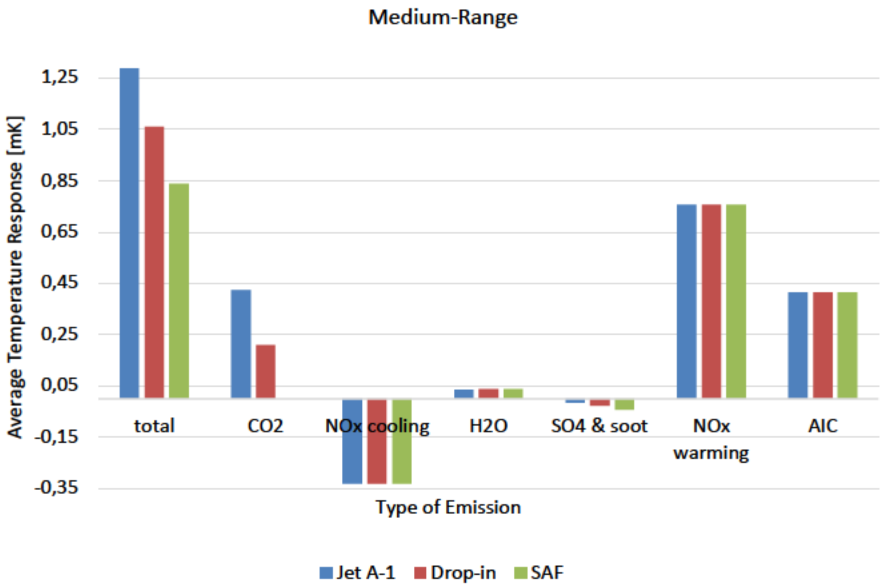

Figure 31: ATRs of medium-range aircraft types

In the short-range sector, for which an A320 similar aircraft is used, there are a total of 194428 missions and the total ATR for Jet A-1 fuel is 4.1mK, as shown in Figure 32. Here, the ATR of AIC has a larger share of the total ATR, which is mainly because the short-range aircraft fly shorter ranges and shorter flight times, and thus lower altitudes, where the impact of AIC is more significant (see Figure 7). If a drop-in fuel blend and 100% SAF is used instead of Jet A-1 fuel, the CO_2, H_2O, and soot emissions are reduced or increased by the same percentages as for the medium-range aircraft. The total ATR for the drop-in fuel blend is now 3.53mK, 13.9% lower than the total ATR of Jet A-1 fuel. The total ATR of SAF is 2.97mK, 27.5% lower than the total ATR of Jet A-1 and 15.8% lower than the total ATR of drop-in fuel blend.

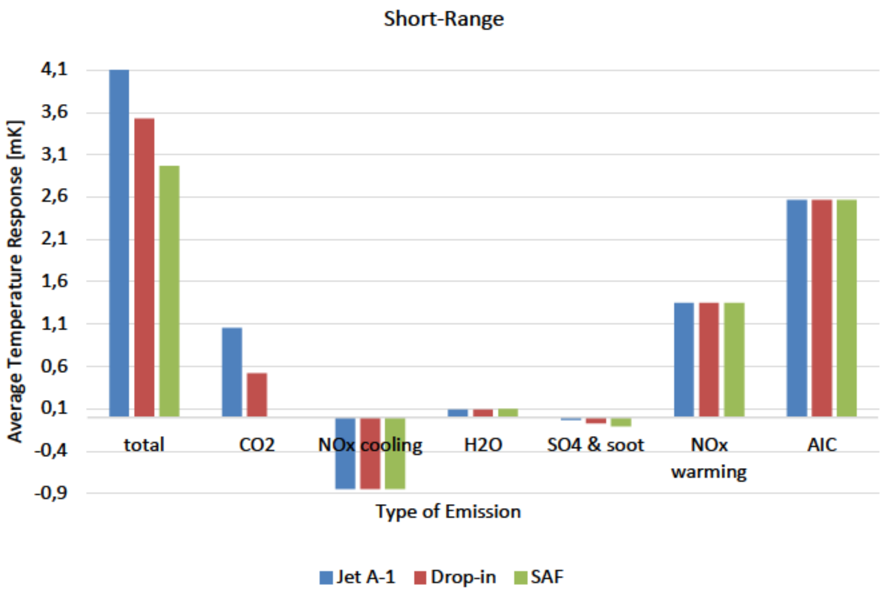

Figure 32: ATRs of short-range aircraft types

The long-range sector, for which an A350 similar aircraft was used, includes 17739 missions, and the total ATR is 1.91mK, as can be seen in Figure 33. Since most of the long-range aircraft types fly in the same altitude ranges as the medium-type aircraft, Figure 33 has a similar appearance to Figure 31, and the CO_2, the AIC, and the total NO_x emissions contribute about equally to the total ATR. Again, the CO_2, H_2O, and soot emissions for the drop-in fuel blend and the SAF change by the same percentage as for the medium-range aircraft type. The total ATR for the drop-in fuel blend is 1.61mK, 15.7% lower than the total ATR of Jet A-1 fuel, and the total ATR for SAF is 1.32mK, which is 31% lower than the total ATR of Jet A-1 fuel and 18.2% lower than the total ATR of the drop-in fuel blend.

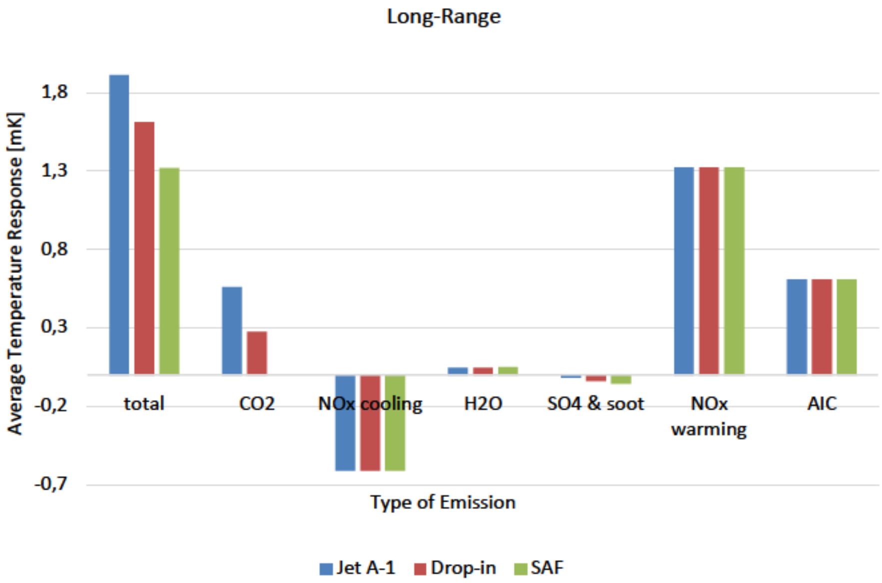

Figure 33: ATRs of long-range aircraft types

Overall, the flight schedule, which takes into account the major aircraft types of the short-, medium- and long-range sector, results in a total ATR of 7.3mK for the Jet A-1 fuel, 6.2mK for the drop-in fuel blend, which is 15% lower than the total ATR of Jet A-1 fuel, and 5.13mK for 100% SAF, which is 29.7% lower than the total ATR of Jet A-1 fuel and 17.3% lower than the total ATR of the drop-in fuel blend. This shows that significant reductions can be achieved with SAF for all three aircraft types, with the greatest reductions achieved for the medium-range aircraft of up to almost 35%. The main reason for the reduced climate impact are the reduced or even non-existing CO_2 emissions. A further reduction in climate impact is achieved by the reduced soot particle number by up to 62%. Practically, the reduced soot particle number also reduces the soot-cirrus clouds, which then reduce the climate impact of AIC. As the simple climate models do not link the soot particle number to the AIC, this further reduction potential is not considered here. Therefore, SAF offers even greater emission reduction potential than those shown in Figure 31 to Figure 33. Today, however, only 0.2% SAF is used. But the European Union and the United States in particular are trying to increase the SAF content in Jet A-1 fuel. For example, the European Commission published the ‘fit for 55’ package with legislative proposals to meet the targets agreed in the European Climate law in June 2021 (Soone, 2022). Since this report assumes that SAF has the greatest potential for short-term emission reductions, these proposals for aviation include, for example, the increased use of alternative fuels and the increased deployment of an infrastructure for alternative fuels. Therefore, fuel supplies are obliged to increase the share of SAFs in the fuel supplied at European Union airports according to a set timetable: 2% in 2025, 5% in 2030, 20% in 2035, 32% in 2040, 38% in 2045, and 63% in 2050 (Soone, 2022). Taking into account the emission reductions of the medium-range aircraft and this increase in the share of SAF in Jet A-1 fuel, emission reductions of up to 0.7% are possible for 2025, up to 1.75% in 2030, up to 7% in 2035, up to 11.2% in 2040, up to 13.3% in 2045 and up to 22% in 2050, with the climate impact of AIC being constant. To put these emissions reductions in relation to the emission savings from new technologies: The sharkskin technology, introduced in 2021, is expected to reduce CO_2 emissions by 3% by making aircraft more aerodynamic, which means they will consume less fuel and emit less CO_2. This 3% reduction is expected to result in potential savings of up to 11 million tons of CO_2 per year for commercial aviation (BASF). This once again illustrates the massive potential emission reductions of SAF and the importance of introducing this short-term option, as this is a promising contribution to achieving the set climate targets.

7 Conclusion

The objective of this thesis was to develop an approach to easily assess and compare the climate impacts of different aircraft designs, technologies, or fuel types for conceptual aircraft design and to enhance this approach by basing it on a flight schedule and by implementing the effects of SAF. Aircraft emit numerous emission species, which directly or indirectly change the concentration of greenhouse gases and particles over different time scales. Therefore, not only CO_2, but also non-CO_2 emissions were included in the methodology and different models for long-lived gases, such as CO_2 and $NO_{x\ cooling}$, short-lived pollutants, such as H_2O, $NO_{x\ warming}$, SO_4, and soot, and AIC had to be considered. The process for determining the climate impacts resulting from these aircraft emissions was divided into three sections: The Emission Modelling, the Climate Impacts Modelling, and the Climate Change Metric. In the Emission Modelling approach, a construct was developed that indicated the future emissions of a particular aircraft. Since the emission flows for different species were already given, the fuel proportional emissions approach was used, where the EIs are proportional to fuel consumption. In the Climate Impacts Modelling approach, the climate impacts of the computed annual emissions were calculated. LTR models that estimate global and annual averaged conditions were chosen for this purpose because they are computationally efficient and transparent, and new knowledge can be easily incorporated. RF and temperature change were selected as the LTR models, which also account for the altitude-varying impacts of NO_x emissions and AIC by implementing altitude-dependent forcing factors. For the Climate Change Metric, the metric ATR was used, which is appropriate for the initial aircraft design. It assesses the total integrated temperature change caused by the operation of a particular aircraft fleet and summarizes the climate impact into a meaningful quantity, which enables an easy comparison of the climate impacts. This metric was implemented in CPACS to easily change the input parameters and integrate it in the post-processing part of the aircraft design workflow. By changing the different input parameters, the user can specify on which impact, short-lived or long-lived, to focus on. However, to achieve a fair comparison, the input parameters must not be changed when comparing two or more aircraft technologies or design options. Since the described methodology is only based on one typical mission, the methodology was enhanced to base the lifetime climate impact of aircraft on more realistic data such as a flight schedule. For this purpose, a method had been implemented to calculate the great circle distance between two pairs of cities in the flight schedule and to interpolate each individual aircraft flight path between the existing ones. The interpolations were divided into the interpolation of the released emission species of CO_2, H_2O, NO_x, SO_4, and soot, the cruising distance and the amount of NO_x released during cruise, and in the interpolations of the cruising altitudes. Each of these parameters was interpolated for each mission of the flight schedule according to payload and range. Due to the limited calculation time, the aircraft types occurring in the flight schedule were divided into short-, medium-, and long-range aircraft according to their payload and range, and one aircraft type was defined for each range – an A320 similar aircraft for short-range, a B767 similar aircraft for medium-range and an A350 similar aircraft for long-range. Finally, to compare the climate impacts of conventional Jet A-1 fuel, drop-in fuel blend and 100% SAF, modifications to the emission calculation were made, since the SAF reduces the EI of CO_2, increases the EI of H_2O, and decreases the CO_2 and soot emissions. It was shown that the drop-in fuel blend and 100% SAF can result in significant emission reductions of up to 17.6% for the drop-in fuel blend and even up to 34.9% for 100% SAF and that the implementation of SAF is a promising contribution to reducing the climate impacts of aircraft emissions and to achieve the set climate targets.

8 Future Work

With this thesis, the climate impacts of Jet A-1 and SAFs can easily be assessed and compared. Nevertheless, there are still potential improvements and future opportunities related to the ACT and the Emission Inventory Generation Methodology, which can continue this project.

First, there are some advancements concerning the ACT. The Aircraft Climate Assessment Model programmed here is a LTR model, which means that the RF or temperature change is not calculated on a time-varying three-dimensional grid, but as globally and annually averaged values based on GCMs (see chapter 2.2.3). Therefore, to refine these LTR models, some optimizations could be made: More GCMs could be assessed to increase the knowledge of the NO_x and AIC RFs as a function of altitude and latitude. In particular, the accuracy of the climate impacts of AIC can be improved by better understanding these impacts and by incorporating sensitivities to engine exhaust gas temperature and water content. In addition, the seasonal and diurnal variations in the climate impacts could be taken into account. Once a more accurate GCM exists and a clearer picture of the climate impacts is achieved, the LTR model will also need to be updated.

Next, improvements in the Emission Inventory Generation Methodology can be made. The interpolations of the cruising altitudes are not as accurate if there is a step climb in the trajectory that is before or one after the current trajectory in the direction of payload or range. This can result in cruising altitudes that do not appear until after the interpolation, as well as an increased or decreased total number of cruising time steps. The total number of cruising time steps also affects the interpolations of the cruising distance and the released amount of NO_x during cruise. Therefore, in order to obtain more accurate interpolation results, the step climbs must be taken into account and a completely new interpolation function must be written. The trajectories where a step climb occurs for the first time must be defined and it must be programmed that before/ after this trajectory the corresponding step cruising altitude does not occur. This way more exact results for the interpolations could be obtained.

In order to limit the calculation time, the aircraft types that could be found in the given flight schedule were divided into short-, medium-, and long- range aircraft and one typically aircraft type was defined for each range. In addition, the General Aviation and propeller-driven aircraft types were neglected because the climate impact is rather small for such short flight times and ranges and low altitudes. However, to obtain more accurate results for the ATRs based on a flight schedule, each aircraft type could be calculated individually when such data are available.

Since the ACT includes the altitude variation for NO_X and AIC RF, mission optimizations could be considered. For example, it could be calculated whether climate impacts are reduced when a particular aircraft flies at lower altitudes, e.g., increasing CO_2 emissions due to higher fuel burn but reducing NO_x and AIC emissions due to lower altitude. Other ways to reduce the emissions, such as low NO_x combustion chambers, can also be implemented in the ACT, and the results can be compared and further mission optimizations considered.

The use of drop-in fuel blend and 100% SAF reduces CO_2 and soot emissions and increases H_2O emissions compared to Jet A-1. These effects were considered in the programmed tool. But the soot particles also play a role in the formation of contrail and cirrus clouds, so reduced soot emissions affect the contrail properties. If the number of soot particles is reduced, the AIC climate impact is also reduced. However, for the simplified climate assessment methods, such as the ACT, there is no direct dependence between soot and AIC, the thus the impact of AIC was not reduced for the drop-in fuel blend and for the 100% SAF. Also, the dependence of the reduced soot particles on the AIC is quite uncertain. However, in order to account for all the improvements in changing the energy carrier from Jet A-1 to SAF, a dependence between the soot particles and the AIC must be established. In this case, SAF would result in even more significant emission reductions.

9 References

Airbus: A320 - Aircraft Characteristics, Blagnac, Cedex: Airbus, 2022.

Airbus: A350 - Aircraft Characteristics, Blagnac Cedex: Airbus, 2022.

Airbus: Aircraft Families: Passenger Aircraft, in: Airbus, 2022, http://www.airbus.com/aircraftfamilies/passengeraircraft/ [12.10.2022]

Alder, M.; Skopnik, A.: Development of a software library for performant and consistent CPACS data processing.

Ariyan International Inc.: Aviation Jet Fuel A-1 & JP54, in: Ariyan International Inc, https://www.ariyancorp.com/aviation-jet-fuel/ [17.10.2022].

Arnot Mike: What is Jet Fuel, and How Does It Work?, in: The Points Guy, 2019, https://thepointsguy.com/news/what-is-jet-fuel/ [17.10.2022].

ATAG Air Transport Action Group: Beginner's Guide to Sustainable Aviation Fuel, Geneva: Air Transport Action Group, 2017.

Aviation Benefits beyond Borders: What is sustainable aviation fuel?, in: Aviation Benefits beyond Borders, https://aviationbenefits.org/faqs/what-is-sustainable-aviation-fuel/ [01.10.2022].

BASF: Von Haien lernen, in: BASF, https://www.basf.com/global/de/who-we-are/change-for-climate/Learning-from-sharks.html [20.12.2022].

Boeing: B767 - Airplane Chracteristics, Arlington: Boeing, 2021.

Boeing: The Boeing Company Official Website, in: Boeing, 2022, https://www.boeing.com/ [16.10.2022].

Boucher, O.; Reddy, M.S.: Climate trade-off between black carbon and carbon dioxide emissions, in: Energy Policy, 2008.

BP: What is sustainable aviation fuel (SAF)?, in: BP, 2022, https://www.bp.com/en/global/air-bp/news-and-views/views/what-is-sustainable-aviation-fuel-saf-and-why-is-it-important.html [01.10.2022].

BTS Bureau of Transportation Statistics: Bureau of Transportation Statistics, in: U.S. Departement of Transportation, 2019, https://www.bts.dot.gov/about-BTS [04.10.2022].

BTS Bureau of Transportation Statistics: Bureau of Transportation Statistics, in: U.S. Departement of Transportation, 2019, https://www.transtats.bts.gov/Tables.asp?QO_VQ=EEE&QO_anzr=Nv4%FDPn44vr4%FDf6n6v56vp5%FD%FLS14z%FDHE%FDg4nssvp%FM-%FDNyy%FDPn44vr45&QO_fu146_anzr=Nv4%FDPn44vr45 [05.10.2022].

Chandler, David: Greenhouse Gases, in: Massachusetts Institute of Technology (MIT), 2020, https://climate.mit.edu/explainers/greenhouse-gases [03.12.2022].

Dallara, Emily S.: Aircraft Desing for Reduced Climate Impact, Stanford, 2011.

Deidewig, F.; Dopelheuer, A.; Lecht, M.: Methods to assess aircraft engine emissions in flight, in: Proceedings of the 20th International Council of Aeronautical Science Congress, Sorrento, 1996.

Deutsches Zentrum für Luft- und Raumfahrt e.V.; Institute of System Architectures in Aeronautics: CPACS: a common language for aircraft design, in: Deutsches Zentrum für Luft- und Raumfahrt e.V, 2018, https://www.cpacs.de/ [29.10.2021].

Dopelheuer, A.; Lecht, M.: Influence of engine performance on emission chracteristics, in: RTO AVT, 1998.

DuBois, Doug; Paynter, Gerald C.: Fuel flow Method 2 for estimating aircraft emissions, in: SAE Technical Paper Series, 2006.

EPA, United States Environmental Protection Agency: Understanding Global Warming Potentials, in: EPA, 2020, https://www.epa.gov/ghgemissions/understanding-global-warming-potentials [13.10.2022].

Fuglestvedt, J.S.; Shine, K.P.; Bernsten, T.; Cook, J.; Lee, D.S.; Stenke, A.; Skeie, R.B.; Velders, G.J.M., Waitz, I.A.: Transport impacts on atmosphere and climate: Metrics, in: Atmospheric Environment, 2010.

Fuglestvedt, Jan S.; Berntsen, Terje K.; Godal, Odd; Sausen, Robert; Shine, Keith P.; Skodvin, Tora: Metrics of Climate Change: Assessing Radiative Forcing and Emission Indices, Netherlands: Kluwer Academic Publishers, 2003.

GFDL, Geophysical Fluid Dynamics Laboratory: Climate Modeling, Princeton : National Oceanic and Atmospheric Administration.

Grewe, V.; Lee, D.S.; Pitari, G.; Gierens, K.; Penner, J.E.; Petzold, A.; Prather, M.J.; Schumann, U.; Bais, A.; Berntsen, T.; Iachetti, D.; Lim, L.L.; Sausen, R.: Transport impacts on atmosphere and climate: Aviation, Atmospheric Environment, 2009.

Grewe, V.; Stenke, A.: AirClim: An efficient tool for climate evaluation of aircraft technology, Atmospheric Chemistry and Physics, 2008.

Hasselmann, K.; Hasselmann, S.; Giering, R.; Ocana, V.; Storch, H.V.: Sensitivity study of optimal CO2 emission paths using a simplified structural integrated assessment model, Climatic Change, 1997.

Heywood, John B.; Mikus, Thomas: Parameters controlling nitric oxide emissions from gas turbine combustors, in: 41st Meeting on Atmospheric Pollution by Aircraft Engines, London, 1973.

Hope, Chris; Anderson, John; Wenman, Paul: Policy analysis of the greenhouse effect: An application of the PAGE model, Energy Policy, 1993.

ICAO; UNDP; Facility Global Environment: Sustainable Aviation Fuels Guide, 2018.

IPCC; Penner, J.E.; D.H., Lister; Griggs, D.J.; Dokken, D.J.; McFarlands, M.: Aviation and the Global Atmosphere, Cambridge: Cambridge University Press, 1999.

IPCC, Intergovernmental Panel on Climate Change: Climate Change 2007: The Physical Science Basis, in: Contribution of Working Group I to the Fourth Assessment Report of the Intergovernmental Panel on Climate Change, Cambridge : Cambridge University Press, 2007.

IPCC, Intergovernmental Panel on Climate Change: Expert Meeting on the Science of Alternative Metrics, Cambridge: Cambridge University Press, 2009.

Kagan, Julia: Available Seat Miles (ASM), in: Investopedia, 2020, https://www.investopedia.com/terms/a/availableseatmiles.asp [06.11.2022].

Kareko, Joy: How to use the scipy.interpolate.interp1d() method, in: educative, https://www.educative.io/answers/how-to-use-the-scipyinterpolateinterp1d-method [20.11.2022].

Kohler, Marcus O.; Radel, Gaby; Dessens, Olivier; Shine, Keith P.; Rogers, Helen L.; Wild, Oliver; Pyle, John A.: Impact of pertubations to nitrogen oxide emissions from global aviation, Journal of Geophysical Research, 2008.

Kramer, Stephen; Andac, Gurhan; Heyne, Joshua; Ellsworth, Joseph; Herzig, Peter; Lewis, Kristin C.: Perspectives on Fully Synthesized Sustainable Aviation Fuels: Direction and Opportunities, frontiers in Energy Research, 2022.

Lee, D.S.; Fahey, D.W.; Skowron, A.; Allen, M.R.; Burkhardt, U.; Chen, Q.; Doherty, S.J.; Freeman, S.; Forster, P.M.; Fuglestvedt, J.; Gettelman, A.; Leon, R.R.; Lim, L.L.; Lund, M.T.; Millar, R.J., Owen, B. Penner, J.E.; Pitari, G.; Prather, M.J.: The contribution of global aviation to anthropogenic climate forcing for 2000 to 2018, Elsevier Ltd., 2020.

Lee, David S.; Fahey, David W.; Forster, Piers M.; Newton, Peter J.; Ron, C.N.: Aviation and global climate change in the 21st century, Atmospheric Environment, 2009.

Lefebvre A. H.: 20th Joint Propulsion Conference, Cincinatti, Ohio: AIAA/SAE/ASME, 1984.

Lim, L.; Lee, D.S.; Sausen, R.; Ponater, M.: Quantifying the effects of aviation on radiative forcing and temperature with a climate response model, in: Proceedings of an International Conference on Transport, Oxford : Athmosphere and Climate (TAC), 2006.

Lufthansa Aviation Training: General Navigation, Frankfurt: Lufthansa Aviation Training Germany GmbH, 2016.

Marais, Karen; Lukachko, Stephen P.; Jun, Mina; Mahashabde, Anuja; Ian, A.: Assessing the impact of aviation on climate, Meteorologische Zeitschrift, 2008.

Nordhaus, William D.: The 'Dice' Model: Background and Structure of a Dynamic Integrated Climate-Economy Model of the Economics of Global Warming, Cowles Foundation Discussion Papers, 1992.

Radel, Gaby; Shine, Keith P.: Radiative forcing by persistent contrails and its dependence on cruise altitudes, Journal of Geophysical Research, 2008.

Raymer, D.P.: Aircraft Design: A Conceptual Approach (AIAA Education Series), American Institute of Aeronautics & Astronautics, 2018.

Sausen, Robert; Schumann, Ulrich: Estimates of the climate response to aircraft CO2 and NOx emissions scenarios, Climatic Change, 2000.

Schaefer, Martin; Bartosch, Sebastian: Overview on fuel flow correlation methods for the calculation of NOx, CO and HC emissions and their implementation into aircraft performance software, Köln: Deutsches Zentrum für Luft- und Raumfahrt (DLR), 2013.

Schumann. Ulrich: Formation, properties and climatic effects of contrails, C. R. Physique, 2005.

Seider, D.; Fischer, P.M.; Litz, M.; Schreiber, A.; Gerndt, A.: Open source software framework for applications in aeronautics and space, in: IEEE Aerospace Conference, IEEE, 2012.

Shine, Keith P.; Fuglestvedt, Jan S.; Hailemariam, Kinfe; Stuber, Nicola: Alternatives to the global warming potential for comparing climate impacts of emissions of greenhouse gases, Climatic Change, 2005.

Silberhorn, Daniel; Dahlmann, Katrin; Görtz, Alexander; Linke, Florian; Zanger, Jan; Rauch, Bastian; Methling, Torsten; Janzer, Corina; Hartmann, Johannes: Climate Impact Reduction Potentials of Synthetic Kerosene and Green Hydrogen Powered Mid-Range Aircraft Concepts, MDPI, 2022.

Soone, Jan: ReFuelEU Aviation initiative: Sustainable aviation fuels and the 'fit for 55' package, European Parliamentary Research Service, 2022.

Stephen, Kramer; Andac, Gurhan; Heyne, Joshua; Ellsworth, Joseph; Herzig, Peter; Lewis, Kristin C.: Perspectives on fully synthesized sustainable aviation fuels: Direction and Opportunities, Frontiers in Energy Research, 2022.

Stordal, F.; Myhre, G.; Stordal, E.J.G.; Rossow, W.B.; Lee, D.S.; Arlander, D.W.; Svendby, T.: Is there a trend in cirrus cloud cover due to aircraft traffic?, Atmospheric Chemistry and Physics, 2005.

Stuber, Nicola; Forster, Piers; Rädel, Gaby; Shine, Keith: The importance of the diurnal and annual cycle of air traffic for contrail radiative forcing, Nature, 2006.

Tol, Richard S.J.: The climate framework for uncertainty, negotiation and distribution (FUND), technical describtion, Version 2.8, Hamburg, 2006.

Torenbeek, E.: Synthesis of Subsonic Airplane Design, Netherlands: Springer, 2013.

United States Government Interagency Working Group on Social Cost of Carbon: Social cost of carbon for regulatory impact analysis, in: Technical report, USG Executive Order 12866, 2010.

Wöhler, Sebastian; Atanasov, Georgi; Silberhorn, Daniel; Fröhler, Benjamin; Zill, Thomas: Preliminary Aircraft Design within a Multidisciplinary and Multifidelity Design Environment, 2020.

Wuebbles, Donald J.; Yang, Huiguang; Herman, Redina: Climate metrics and aviation: Analysis of current understanding and uncertainties, in: Technical Report Theme 8., FAA Aviation Climate Change Research Initiative (ACCRI), 2009.

Erklärung zur selbstständigen Bearbeitung einer Abschlussarbeit

Gemäß der Allgemeinen Prüfungs- und Studienordnung ist zusammen mit der Abschlussarbeit eine schriftliche Erklärung abzugeben, in der der Studierende bestätigt, dass die Abschlussarbeit „– bei einer Gruppenarbeit die entsprechend gekennzeichneten Teile der Arbeit [(§ 18 Abs. 1 APSO-TI-BM bzw. § 21 Abs. 1 APSO-INGI)] – ohne fremde Hilfe selbständig verfasst und nur die angegebenen Quellen und Hilfsmittel benutzt wurden. Wörtlich oder dem Sinn nach aus anderen Werken entnommene Stellen sind unter Angabe der Quellen kenntlich zu machen.“

Quelle: § 16 Abs. 5 APSO-TI-BM bzw. § 15 Abs. 6 APSO-INGI

Dieses Blatt, mit der folgenden Erklärung, ist nach Fertigstellung der Abschlussarbeit durch den Studierenden auszufüllen und jeweils mit Originalunterschrift als letztes Blatt in das Prüfungsexemplar der Abschlussarbeit einzubinden.
Eine unrichtig abgegebene Erklärung kann -auch nachträglich- zur Ungültigkeit des Studienabschlusses führen.

Erklärung zur selbstständigen Bearbeitung der Arbeit

Hiermit versichere ich,

Name: Neusser

Vorname: Anja

dass ich die vorliegende Masterarbeit bzw. bei einer Gruppenarbeit die entsprechend gekennzeichneten Teile der Arbeit – mit dem Thema:

Development of an emission inventory methodology for air traffic on the basis of a flight schedule scenario for a fast subsequent climate impact analysis

ohne fremde Hilfe selbständig verfasst und nur die angegebenen Quellen und Hilfsmittel benutzt habe. Wörtlich oder dem Sinn nach aus anderen Werken entnommene Stellen sind unter Angabe der Quellen kenntlich gemacht.

- die folgende Aussage ist bei Gruppenarbeiten auszufüllen und entfällt bei Einzelarbeiten -

Die Kennzeichnung der von mir erstellten und verantworteten Teile der -bitte auswählen- ist erfolgt durch:

Hamburg	02.01.2022	[redacted]
Ort	Datum	Unterschrift im Original